JOINTED PIPELINE RESPONSE TO LARGE GROUND MOVEMENTS

A Dissertation

Presented to the Faculty of the Graduate School

of Cornell University

In Partial Fulfillment of the Requirements for the Degree of

Doctor of Philosophy

by

Brad Parker Wham

February 2016

© 2016 Brad Parker Wham

JOINTED PIPELINE RESPONSE TO LARGE GROUND MOVEMENTS

Brad Parker Wham, Ph.D.

Cornell University 2016

This thesis addresses the performance of jointed pipelines subject to ground deformations triggered at a large scale by earthquakes and a construction-related scale by tunneling. Understanding and quantifying jointed pipeline response at these scales allows for better design, operational management, and risk assessment of underground infrastructure, where cast iron (CI) and ductile iron (DI) pipelines in the U.S. account for approximately 75% of water distribution systems. The thesis covers the response of DI and molecularly oriented polyvinyl chloride (PVCO) pipelines to earthquake-triggered soil movement as well as CI and DI pipeline response to tunneling.

A series of specially designed four-point bending experiments and 3D finite-element (FE) simulations were performed to characterize DI push-on joints commonly used in water distribution systems to develop a relationship between the rotation and axial pullout at both metal binding and first leakage. The results of uniaxial tension and one-dimensional compression tests on the elastomeric gaskets in DI push-on joints were implemented in numerical models that show joint leakage to be independent of load path, with a unique pressure boundary that predicts leakage for many combinations of axial pullout and rotation.

The increased circumferential strength, reduced pipe wall thickness, and enhanced cross-sectional flexibility of PVCO pipelines was evaluated through the characterization of PVCO material properties, axial joint tension and compression tests, four-point bending tests, and a full-scale fault rupture experiment. A nominal 150-mm (6-in.)-diameter PVCO pipeline is able to accommodate significant fault movement through axial tensile and bending strains in the pipe in combination with modest levels of axial slip at the restrained joints. Relatively large levels of axial strain in the low modulus PVCO material, which varies between 1% and 2% at pipeline failure, are able to sustain substantial extension and compression from ground movements.

Soil/pipeline interaction modeling was performed for vertical and horizontal ground movements caused by tunneling in jointed CI and DI pipelines perpendicular to the tunnel centerline that (1) extend beyond the width of the settlement profile and (2) connect through 90° tees with a pipeline parallel to the tunnel. The modeling incorporates the results of large-scale laboratory tests. Guidance is provided for design and the identification before tunneling of potential difficulties. In particular, CI tees are at high risk when subject to tunneling induced soil movement, whereas DI pipelines and tees have sufficient capacity to accommodate high levels of tunneling related ground deformation.

BIOGRAPHICAL SKETCH

Weighing in at 5.1 kg (11 lb 3 oz) Brad was born in Princeton, NJ on October 27, 1986 to loving parents, Liz and Barry. Brad grew up with two biological sisters, Amy and Christy, and two designated brothers, Ryan and Kevin. His youth was enriched through involvement in various communities including his church, the scouts, and various athletic teams. Brad is distinctly proud to have earned the rank of Eagle Scout on October 12, 2004. He credits his experiences teaching and leading Troop 79 for later confidence and success instructing students in the laboratory and classroom.

Brad has gained practical engineering and life experiences employed under a variety of titles including landscaper, construction equipment operator, land surveyor, and quality control inspector. Following a detrimental timing belt malfunction, Brad studied, disassembled, rebuilt, and timed his Jetta's 1.9L diesel engine. Over 12 years and 290,000 km (180,000 miles) later, the Jet continues to fly. Brad is proud of his adeptness for hands-on work and considers his practical experiences significant contributions to his engineering identity and education.

A product of central New Jersey public schools, Brad attended Virginia Tech where he fought through early struggles to graduate Cum Laude with a Bachelor of Science in Civil Engineering (Lets Go Hokies!). His desire to work in the field of forensic engineering lead him to earn a Masters of Engineering in Structural Engineering at Cornell (Lets Go Red!). His interest in the full-scale testing performed at the Bovay

Civil Infrastructure Laboratory inspired him to continue his graduate studies with the geotechnical engineering group and, eventually, prepare the enclosed dissertation.

To my natural and honorary families

“Never delegate understanding.”

- Charles Eames

ACKNOWLEDGEMENTS

First and foremost, I would like to thank my advisors, Professors Thomas D. O'Rourke and Harry E. Stewart, for the opportunity to continue my education at Cornell and the afforded experiences.

I am exceedingly grateful for Professor O'Rourke's invaluable training and continuous guidance during my studies, without which this dissertation would not have been possible.

I thank sincerely Professor Stewart for his council and countless contributions to my laboratory work, research, and teaching as well as his gamesmanship on the course.

I extend appreciation to Professor Anthony Ingraffea for his advice and teachings on and off the softball field.

I am grateful to have shared this leg of the journey with fellow Geotech graduate students Dimitra Bouziou, Christina Argyrou, and Chalermpat (Pat) Pariya-Ekkasut. I am especially thankful for Christina's optimism and expertise down the home stretch, and for her significant contributions to Chapter 4 of this dissertation.

I am grateful to have shared many hours of head scratching, soil slinging, guacamole-ing, and experimenting with the staff and students of the Bovay (Civil Infrastructure) Laboratory; including Joe Chipalowski, Michael Wickham, Nicholas Chmelev, Dakota Price, Addie Lederman, Blake Burger, Andrew Shakalis, Nathaniel Lyon, Kim Buhl,

Han Wei Chew, Alex Teeter, Karina Estrada, and the many others. I also thank the CEE staff for their support and friendship as well as all the sustaining coffee and snacks.

I thank Tim Bond for… being Tim Bond, and all that requires.

From the M.Eng. Crew and the Germans, on through to the softball, trivia, and ice hockey teams, I thank all of my past and present Cornell/Ithaca friends for fond memories and necessary contributions to my sanity.

I acknowledge the folks who believed in me long before adequate data was available, including Goldie Applegate, Jeff Sikora, and those listed below.

I save my most sincere thanks for my family: Mom, Dad, Amy, Christy, and Marty, for their constant presence and the many forms of support expressed over the years. I am also thankful for my extended family, especially Pop-Pop and Gran (Dr. George and Beth Wham) for their support and many words of encouragement, including the ethos "keep your eye on the prize".

I am appreciative of the financial support provided by Cornell University and the School of Civil and Environmental Engineering through seven teaching assistantships and an instructorship, as well as funding from research sponsors IPEX, Inc., U.S. Pipe, Inc., NYSEARCH, the Northeast Gas Association (NGA), and the U.S. Department of Transportation and Hazardous Materials Safety Administration (PHMSA).

TABLE OF CONTENTS

LIST OF FIGURES

LIST OF TABLES

CHAPTER 1

INTRODUCTION

1.1 Overview

It is well recognized that ground movements can impose severe deformation on underground infrastructure disrupting critical services (O'Rourke, 2010; Hamada, 2014). Evidence of water distribution system vulnerability to earthquake-induced permanent ground deformation (PGD) is well documented for the 1906 San Francisco (O'Rourke et al., 2006), 1971 San Fernando (O'Rourke et al., 1992), and 1999 Kocaeli, Turkey (Tang, 2000) events, as well as the more recent 2010-2011 Canterbury earthquake sequence (O'Rourke et al., 2014), among many others. Ground and pipeline deformations are also generated by landslides, floods, construction activities including tunneling and deep excavations, and subsidence caused by dewatering or withdrawal of minerals and fluids during mining and petroleum production (O'Rourke, 1998; O'Rourke & Bonneau, 2007). The physical attributes of the buried system, ground failure pattern, and soil properties each contribute to pipeline deformation and potential failure.

Pipeline response to ground deformation is an important concern for water supply pipelines, especially segmented pipelines linked by joints vulnerable to pullout and rotation. Ductile iron (DI) pipelines with push-on joints are widely used in current practice for new installations and replacements in water distribution systems, whereas cast iron (CI) pipelines were used extensively in the past, and represent a large fraction

of the current pipeline inventory of many water and some gas distribution networks.

There are over 2.1 million km (1.3 million mi.) of pipelines in water and wastewater systems throughout the U.S. (Congressional Budget Office, 2002). Approximately 60% of the 1.3 million km (800,000 mi.) of U.S. water distribution system are composed of CI pipelines, with an average age exceeding 90 years (Taki & O'Rourke, 1984). Ductile iron pipelines with bell and spigot joints account for nearly 20% of the over 1.6 million km (1,000,000 mi.) of water distribution pipelines in the U.S. and nearly 50% of new installations (AWWA, 2007). Distribution lines with diameters of 200 mm (8 in.) or less account for 66% of the U.S. pipeline network (Folkman, 2012). Pipelines with diameters ≤ 300 mm (12 in.) comprise 99% of gas distribution pipelines in the U.S. (PHMSA, 2015) and a large portion of water distribution systems. For example, approximately 90% of the water distribution system operated by the Los Angeles Department of Water and Power involves pipe diameters ≤ 300 mm (12 in.) (Davis, 2015).

Technological advances have improved pipeline capacity to accommodate large ground deformation associated with earthquakes, floods, landslides, tunneling, deep excavations, mining, and subsidence. The fabrication of polyvinyl chloride (PVC) piping, for example, can be modified by expanding PVC pipe stock to approximately twice its original diameter, thus causing PVC molecular chains to realign in the circumferential direction. This process yields biaxially oriented polyvinyl chloride (PVCO) pipe with increased circumferential strength, reduced pipe wall thickness, and enhanced cross-sectional flexibility.

Among the sources of ground deformation affecting underground infrastructure are deep excavations and tunneling. Substantial research has been performed on the characterization of ground movements caused by tunneling (e.g., Peck, 1969; O'Reilly & New, 1982; Mair & Taylor, 1997) and the influence of such movements on the response of underground pipelines (e.g., Attewell et al., 1986; Klar et al., 2005; Vorster et al., 2005; Klar et al., 2008). Previous research has concentrated on model development and relatively simple characterizations of pipe and joint response. There is the need for a more rigorous and detailed characterization of jointed pipeline performance, using the most recent research findings and large-scale test results for DI and CI pipelines. Improved modeling, validated by large-scale testing, is needed to understand the sensitivity of jointed pipeline response to different soil conditions and variations in the ground movement modeling parameters. Improved modeling is also required for design and the identification before tunneling of potential difficulties regarding pipeline response.

1.2 Objectives

The objectives of this research are to improve the characterization of jointed pipeline response to ground deformation caused by extreme events, such as earthquakes, and by adjacent underground construction with emphasis on tunneling. The results of large-scale laboratory tests are used to understand in detail jointed pipeline limits states with respect to joint pullout and rotation as well as allowable tensile strains. This thesis involves three separate, but interrelated, research investigations to evaluate the (1)

response of jointed DI pipelines commonly used in practice to the effects of large permanent ground movements, (2) performance of biaxially oriented PVCO pipelines under earthquake-induced ground deformation, and (3) performance of CI and DI pipelines subjected to tunneling induced ground movements. Each of these objectives is discussed briefly under the subheadings that follow.

1.2.1 Ductile Iron Pipeline Response to Large Ground Deformation

The earthquake performance of segmental pipelines is strongly influenced by the axial pullout and compressive load capacity of their joints, as well as by the limits on joint rotation during permanent ground deformation. Although DI pipelines with push-on joints are commonly used in water distribution systems, experimental data and numerical simulation related to their performance under large ground movements are lacking. While most segmented pipelines have limited axial pullout capacity, they may be able to accommodate substantial rotation without leakage. Full-scale tests to characterize joint performance under combined axial and rotational deformation were performed as part of the research at the Cornell Large-Scale Lifelines Testing Laboratory and 3D finite element modeling, calibrated by the test results, was performed to quantify joint behavior under extreme rotational deformation combined with axial pullout.

1.2.2 PVCO Pipeline Performance under Large Ground Deformation

Experiments performed at the Cornell Large-Scale Lifelines Testing Laboratory were used to characterize PVCO pipeline performance in response to large ground

deformation. The evaluation was performed on 150-mm (6-in.)-diameter PVCO pipelines with bell-and-spigot joints. The testing procedure included determination of fundamental PVCO material properties, axial joint tension and compression tests, four-point bending tests, and a full-scale fault rupture simulation. The PVCO pipeline performance is quantified in terms of its capacity to accommodate pullout, axial compression, and joint rotation in response to earthquake-induced ground deformation. The PVCO pipeline limit states are compared with a statistical characterization of liquefaction-induced ground deformation measured with high resolution LiDAR (O'Rourke et al., 2014) during the Canterbury Earthquake Sequence in New Zealand.

1.2.3 Jointed Pipeline Response to Tunneling Induced Ground Deformation

Finite element modeling was performed for soil/pipeline interaction in response to vertical and horizontal ground movements caused by tunneling involving CI and DI pipelines perpendicular to the tunnel centerline that (1) extend beyond the width of the settlement profile and (2) connect through 90° tees with a pipeline parallel to the tunnel. The modeling incorporates the results of large-scale laboratory tests to characterize the axial force vs. displacement and moment vs. rotation relationships of DI and CI joints commonly encountered in practice. Limit states for joint pullout and rotation at various leakage levels as well as allowable tensile strain for pit cast iron pipe are discussed and used in the modeling. The evaluation of pipeline response on this basis allows for generalizations that guide design and risk assessment and help to identify potential difficulties regarding pipeline integrity.

1.3 Scope and Organization

This thesis consists of five chapters, the first of which provides introductory and background information, explains the thesis objectives, and describes the scope and organization of the work. Chapters 2 to 4 are organized in the format of four individual research papers. Chapter 2 deals with characterization of leakage in DI push-on joints as a function of combined pullout and rotation through full-scale experimental testing and 3D FE simulations. Chapter 3 involves the evaluation of PVCO pipeline capacity to accommodate large deformations through a series of large-scale laboratory tests designed to simulate earthquake-induced ground rupture conditions. Chapter 4 describes soil-pipeline interaction simulations for CI and DI pipelines affected by tunneling induced soil settlement and lateral displacements, and provides generalizations of pipeline response that guide design and risk assessment related to pipeline performance. Chapter 5 presents the conclusions of this work, and provides recommendations for future research.

REFERENCES

Attewell, P. B., Yeates, J., & Selby, A. R. (1986). *Soil movements induced by tunnelling and their effects on pipelines and structures*, Chapman & Hall, New York.

AWWA. (2007). "Distribution system inventory, integrity and water quality." U. S. Environmental Protection Agency, Washington DC.

Davis, C. (2015). Resilience Manager, Los Angeles Department of Water and Power, personal communication.

Folkman, S. (2012). “Water main break rates in the USA and Canada: A comprehensive study.” *Utah State University Buried Structures Laboratory,* Logan, UT.

Congressional Budget Office. (2002). “Future investment in drinking water and wastewater infrastructure.” United States Congress, Washington, DC.

Hamada, M. (2014). *Engineering for earthquake disaster mitigation*, Springer, Tokyo.

Klar, A., Vorster, T. E. B., Soga, K. & Mair, R. J. (2005). “Soil–pipe interaction due to tunnelling: comparison between Winkler and elastic continuum solutions.” *Géotechnique.* **55**(6), 461–466.

Klar, A., Marshall, A. M., Soga, K. & Mair, R. J. (2008). “Tunneling effects on jointed pipelines.” *Can. Geotech. J*., **45**(1) 131–139.

Mair, R. J. & Taylor, R. N. (1997). Bored tunnelling in the urban environment. *Proc. 14th Int. Conf. Soil Mech. Found. Engng, Hamburg*, **4**, 2353–2385.

O’Reilly, M. P. & New, B. M. (1982). Settlements above tunnels in the United Kingdom: their magnitude and prediction. *Proc. Tunnelling ’82, Brighton*, 173–181.

O’Rourke, T. D. (2010). “Geohazards and large, geographically distributed systems.” *Géotechnique,* **60**(7), 505–543.

O'Rourke, T. D., Jeon, S.-S., Toprak, S., Cubrinovski, M., Hughes, M., Ballegooy, S., and Bouziou, D. (2014). “Earthquake response of underground pipeline networks in Christchurch, NZ.” *Earthquake Spectra,* **30**(1), 183-204.

O’Rourke, T. D., and Bonneau, A. (2007). “Lifeline performance under extreme loading during earthquakes.” *Earthquake geotechnical engineering*, K. D. Pitilakis, ed., Springer, Dordrecht, The Netherlands, 407–432.

O'Rourke, T. D., Bonneau, A. L., Pease, J. W., Shi, P., and Wang, Y. (2006). "Liquefaction and ground failures in San Francisco." *Earthquake Spectra*. 22(S2) 91-112.

O'Rourke, T. D. (1998). "An overview of geotechnical and lifeline earthquake engineering." *Geotechnical earthquake engineering and soil dynamics III*, ASCE, 1392-1426.

O'Rourke, T. D., Roth, B.L., and Hamada, M., (1992) "Large ground deformations and their effects on lifeline facilities; 1971 San Fernando earthquake." *NCEER-92-0002*, 3:1-85.

Peck, R. B. (1969). Deep excavations and tunnelling in soft ground. *Proc. 7th Int. Conf. Soil Mech. Found. Engng, Mexico City*, 225–290.

Pipeline Safety and Hazardous Materials Administration [PHMSA]. (2015). Data and Statistics http://www.phmsa.dot.gov/pipeline/library/data-stats (accessed 30 Nov. 2015).

Taki, H., & O'Rourke, T. D. (1984). "Factors affecting the performance of cast iron pipe." *Geotechnical Engineering Rep. 84-1*, School of Civil and Environmental Engineering, Cornell Univ., Ithaca, N.Y.

Tang, A. (2000). "Izmit (Kocaeli), Turkey, earthquake of August 17, 1999, including Duzce Earthquake of November 12, 1999-Lifeline performance." *ASCE, Technical Council on Lifeline Earthquake Engineering*, Monograph No.17, Reston, VA.

Vorster, T. E. B., Klar, A., Soga, K. & Mair, R. J. (2005). "Estimating the effects of tunneling on existing pipelines." *J. Geotech. Geoenviron. Engng* **131(**11), 1399–1410.

CHAPTER 2

DUCTILE IRON PIPELINE RESPONSE TO LARGE GROUND DEFORMATION

ABSTRACT

The performance of segmental pipelines under large ground deformation is strongly influenced by the axial pullout and compressive load capacity of their joints, as well as by the limits on joint rotation during permanent and transient ground deformation. Although ductile iron (DI) pipelines with push-on joints are commonly used in water distribution systems, experimental data and numerical simulation related to their performance under large ground movements are lacking. This paper reports on a series of specially designed four-point bending experiments and finite-element (FE) simulations to characterize 150-mm-(6-in.) diameter DI push-on joints. The results were used to develop a relationship between rotation and metal binding as a function of axial pullout, as well as to determine the magnitudes of rotation and moment that initiate joint leakage. Finite-element simulations were performed using the software ABAQUS 6.13 to investigate the deformation associated with joint leakage. Uniaxial tension and one-dimensional compression tests were performed on the elastomeric gasket and fitted with hyperelastic strain energy approximations to characterize behavior under extreme loading. Numerical models demonstrate joint leakage to be independent of load path, and that a unique pressure boundary predicts leakage for many combinations of deformation.

2.1 Introduction

It is well recognized that ground movements can impose severe deformation on underground infrastructure disrupting critical services (Hamada, 2014). Evidence of water distribution system vulnerability to earthquake-induced permanent ground deformation (PGD) is well documented for the 1906 San Francisco (O'Rourke et al., 2006), 1971 San Fernando (O'Rourke et al., 1992), and 1999 Kocaeli, Turkey (Tang, 2000) events, as well as the more recent 2010-2011 Canterbury earthquake sequence (O'Rourke et al., 2014), among many others. Ground and pipeline deformations are also generated by landslides, floods, construction activities including tunneling and deep excavations, and subsidence caused by dewatering or withdrawal of minerals and fluids during mining and petroleum production (O'Rourke & Bonneau, 2007). The physical attributes of the buried system, ground failure pattern, and soil properties each contribute to pipeline deformation and potential failure.

Pipeline response to ground deformation is an important concern for water supply networks, especially segmented pipelines linked by joints vulnerable to pullout and rotation. Ductile iron (DI) pipelines with bell and spigot joints account for nearly 20% of the over 1,600,000 km (1,000,000 mi.) of water distribution pipes in the U.S. (AWWA, 2007) and, according to one study, nearly 50% of new installations (Kirmeyer et al., 1994). Distribution lines with diameters of 200 mm (8 in.) or less account for 66% of the U.S. pipeline network (Folkman, 2012).

This paper focuses on the performance of DI water distribution pipelines under large ground deformation. It presents the results of research to determine the leakage

threshold of 150-mm (6-in.) DI push-on joints when subjected to various combinations of axial displacement and joint rotation. DI pipe and rubber gasket material testing results are presented and discussed. Numerical modeling validated by large-scale testing is used to characterize joint leakage behavior for ground deformation effects causing pullout and rotation at the joints.

2.2 Test Specimens

Test specimens of nominal 150-mm (6-in.) diameter DI pipes, manufactured by U.S. Pipe and Foundry Company, were used in this investigation. Commercially available TYTON JOINT® pipes were provided by the Los Angeles Department of Water and Power (LADWP), and represent a type of DI pipe frequently used in water distribution systems. Figure 2.1(a) shows a longitudinal cross-section of the 150-mm (6-in.) diameter DI push-on joint used in the study.

ANSI/AWWA C151/A21.51-09 (AWWA 2009) requires the DI pipe grade tested to have minimum strength parameters of 60/42/10 (414 MPa ultimate tensile strength, 290 MPa yield strength, 10% elongation). Figure 2.1(b) shows the stress versus strain data from three tensile tests, performed according to ASTM E8/E8M - 13a (ASTM 2013a), on coupons cut from the test pipe specimens. The DI exceeded specifications with an average ultimate strength of 460 MPa (66.7 ksi), 0.2% offset yield strength of 311 MPa (45.1 ksi), and strain at failure of 10.4%. The coupons had an average elastic modulus of 186,000 MPa (27,000 ksi). The pipe specimens were lined with a 3.3-mm (0.13-in.)

thick cement-mortar liner, which reduces the pipe's susceptibility to corrosion and tuberculation (Bonds, 2005).

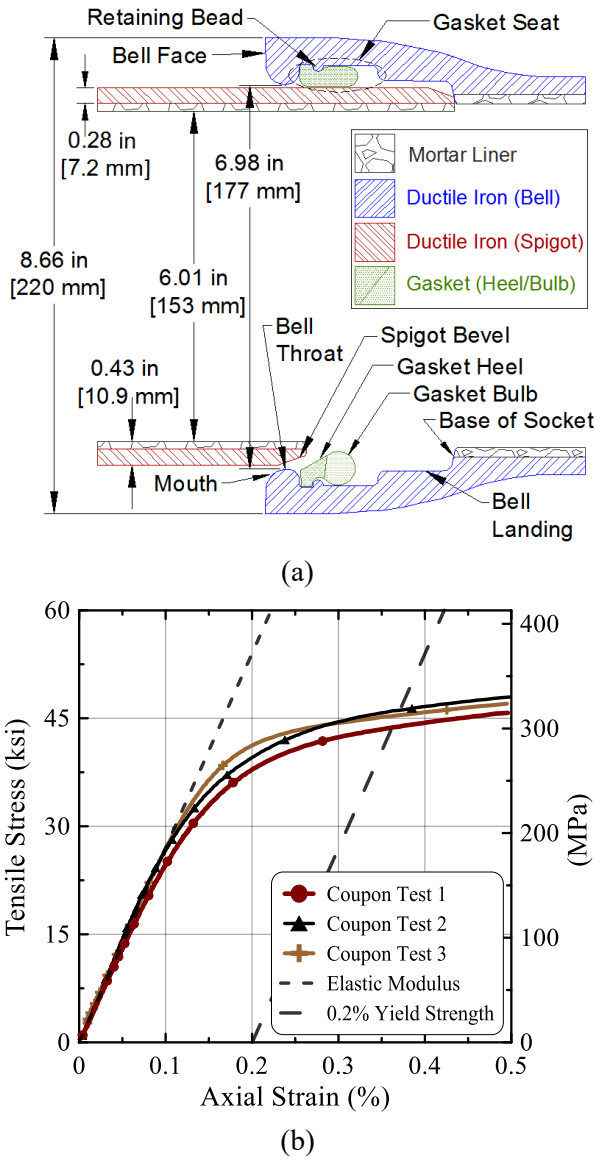

Figure 2.1. (a) Cross-section of typical 150-mm (6-in.) DI joint including key nomenclature; (b) DI stress-strain curves from tensile coupon tests

Each joint was equipped with an elastomeric seal, commercially referred to as a TYTON® Gasket, composed of styrene butadiene rubber (SBR) and manufactured in

accordance with ANSI/AWWA C111/A21.11 and National Sanitation Foundation ANSI/NSF-61 standards (U.S. Pipe, 2013a). Before assembling the joint, a thin film of lubricant is applied to the inside surface of the gasket and end of the spigot, per the manufacturer's installation instructions. Although this material exhibits time-dependent behavior and will experience relaxation under constant compressive loading, this study does not directly address changes in gasket properties due to long-term creep behavior or ageing effects and is strictly valid for the conditions that exist in the short term after large ground deformation.

2.3 Geometrical Pipe Joint Limits

2.3.1 Axial Joint Displacement

Jointed pipelines are especially susceptible to joint pullout resulting from PGD. Singhal (1984) reports that a standard 150-mm (6-in.) DI joint provides 0.31 kN (69 lb) of tensile pullout resistance.

Wham et al. (2014) presents experimental results that show how axial joint displacement and rotation at leakage are interrelated. A test sequence was developed to verify the axial force and displacement required to insert and pull out these joints. Shown in Fig. 2.2(a), a peak insertion force of 1.25 kN (280 lb) is required to insert the spigot into the bell. At an insertion of 6.35 mm (0.25 in.), after the spigot has fully compressed the gasket, the axial insertion force reduces to an approximate constant value of 0.44 kN (100 lb). The pull-out force, shown in Fig. 2.2(b), is less than the insertion force and has a maximum value of 0.90 kN (200 lb). While variations will

result from standard casting tolerances of the pipe including initial out of roundness and the use of different joint lubricants, even at minimum burial depths the joint pullout resistance is substantially less than the axial soil friction force mobilized along a typical pipe length.

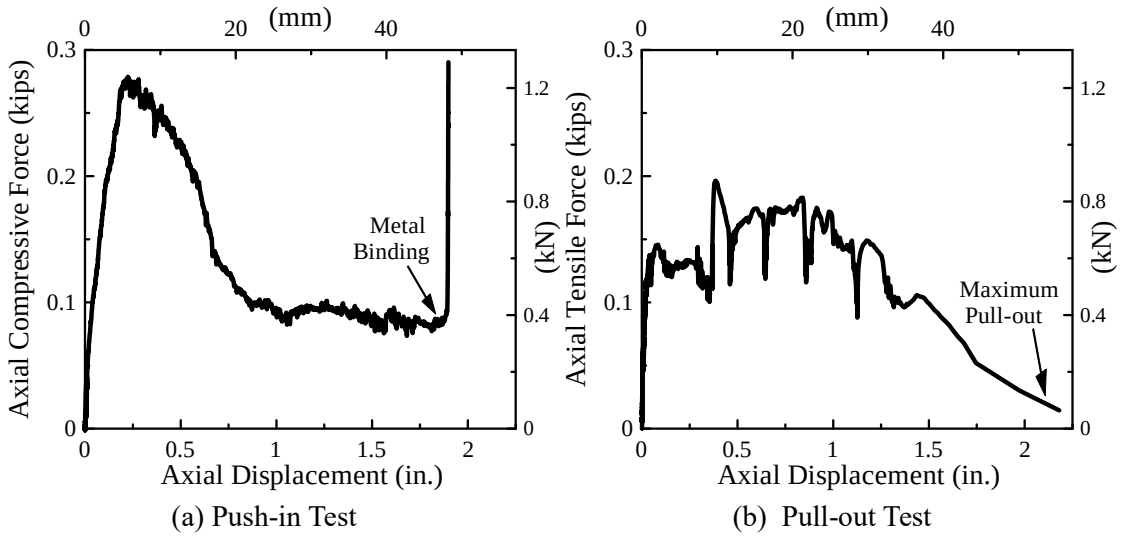

Figure 2.2. Results from (a) axial insertion and (b) axial retraction tests performed on 150-mm (6-in.) DI push-on joints

DI joints have much greater capacity to resist compressive loads. Maragakis et al. (1999) conducted axial compression experiments on DI pipe joints of various diameters and showed that 150 mm (6 in.) DI joints have a peak compressive load capacity of approximately 1070 kN (240 kips) at 7 mm (0.28 in.) of displacement from a fully seated position. At a compressive load of 934 kN (210 kips) and 8.6 mm (0.34 in.) of axial displacement the test was discontinued due to damage of the specimen. While performance is dependent on pipe diameter and thickness class, these tests demonstrate

the significant compressive capacity of typical DI joints, and provide evidence that DI push-on joints are far more vulnerable to pullout than compressive deformation.

2.3.2 Joint Rotation

Manufacturer guidelines permit 5° of allowable joint deflection, referred to herein as joint rotation, during installation of 150-mm (6-in.) DI push-on joints (U.S. Pipe, 2013b). This rotational tolerance provides the installer some freedom to moderately curve the pipelines during installation. Beyond 5° of rotation, the spigot makes internal contact with the bell landing [Fig. 2.1(a)], constraining further rotation. Metal-to-metal contact like this is referred to herein as metal binding, and results in a significant increase in rotational joint stiffness.

In assessing a pipeline's vulnerability to imposed deformation, it is important to characterize the joint response to rotation beyond the manufacturers maximum deflection limit so that an accurate limit state of pipeline deflection can be established. For brittle pipe materials, such as cast iron (CI), there is limited additional joint rotation capacity beyond installation tolerances because stress concentrations from metal binding will promote fracture of the pipe bell or spigot and subsequent leakage. In contrast, the DI material is significantly more ductile and has the capacity to accommodate substantially more rotational deformation beyond the onset of metal binding.

2.3.3 Combined Joint Deformation

Joint deflection design capacity assumes the joint is installed properly, i.e. the spigot is fully inserted axially into the bell. However, during PGD events, ground movement will cause various combinations of axial, transverse and rotational joint deformation depending on the orientation of the pipe with respect to the ground motion. Due to the irregular internal features of the bell, metal binding will occur at varying degrees of joint distortion depending on the position of the spigot inside the bell, which requires a more robust method for modeling the joint response to deformation.

Becerril Garcia & Moore (2014) performed tests on buried 600-mm (24-in.) diameter and 1200-mm (48-in.) diameter reinforced concrete pipes in which surface loading was shown to impose shear deformation across bell and spigot joints. Wang & Moore (2014) developed a simplified design model for these types of rigid pipelines and suggest that shear forces are likely to influence the leakage resistance of gasketed joints. Preliminary testing of fully-seated 150-mm (6-in.) diameter DI joints show that under typical loading conditions transverse deformation results in metal binding without leakage. While it is recognized that shear loading imposed by large transverse deformations provides an additional degree of joint distortion, this loading condition is beyond the scope of the present study, which focuses on axial and rotational deformation.

A series of preliminary tests was performed to investigate how joint leakage and metal binding are related to levels of imposed axial pullout and free rotation (Wham et al., 2014). While monitoring and manually adjusting internal water pressure, a pressurized joint was first displaced axially, then rotated by lifting the bell at the center

of the 5.5-m (18-ft) long test specimen. Figure 2.3 shows the joint rotation imposed at various levels of initial axial displacement or pullout. Joint rotation was determined by importing high resolution, profile view photos of the specimen at leakage into CAD and measuring the relative angle between lines drawn along the crown, springline and invert of the bell and spigot. Although some additional axial movement occurred because of geometric lengthening during rotation, such displacement was generally small at the level of rotation required for metal binding.

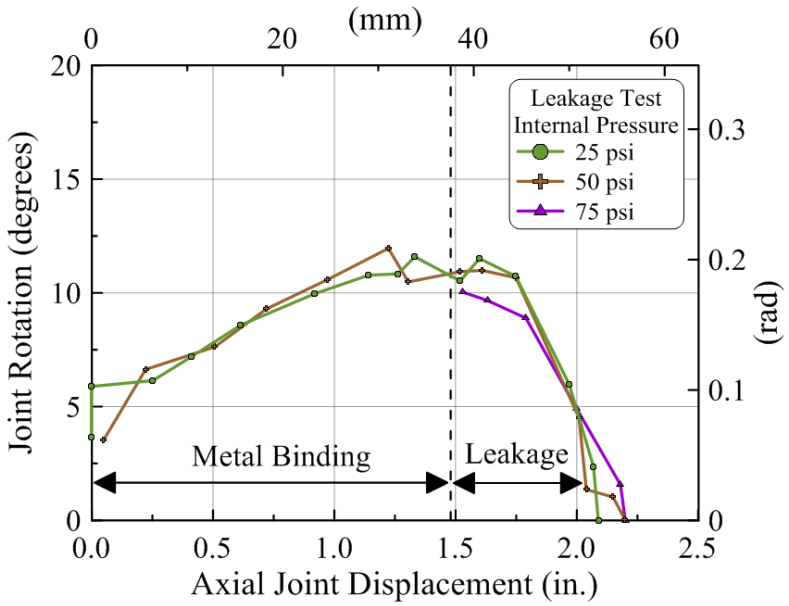

Figure 2.3. Pressurized joint deflection tests addressing metal binding and leakage of 150-mm (6-in.) DI pipe joints relative to combinations of axial pullout and free rotation

In Fig. 2.3 zero axial displacement represents a fully inserted spigot. The left side of the figure shows that deflecting joints with initial axial displacement from 0 to 36 mm (0 to 1.4 in.) results in metal binding without leakage. Joint leakage, conservatively defined by visually observing a flow rate of 1 drop/sec (0.05 mL/sec or 4.32 L/day) or greater, occurred at various levels of rotation in tests with axial displacements greater

than 38 mm (1.5 in.). Experience acquired during testing shows that only a small increment in rotation above this level was needed to generate substantially larger leakage. Similar results for tests performed at internal water pressures of 170, 345, and 520 kPa (25, 50, and 75 psi) suggest that leakage is relatively independent of variations in internal pressure within the range of typical operating levels.

2.4 Experimental Testing

The mechanics of the joint during metal binding and subsequent yielding are complex. Four-point bending tests were performed to apply constant moment at the joint positioned at the center of the test setup. Two pipes, Specimen A and Specimen B, were used to conduct the pressurized bending tests shown in Figure 2.4. For each specimen, two 1.83-m (6-ft.) long sections of pipe were cut from 5.5 m (18 ft) standard-length pipes and joined with a factory spigot and bell, providing the 3.7-m (12-ft) long bending test specimen.

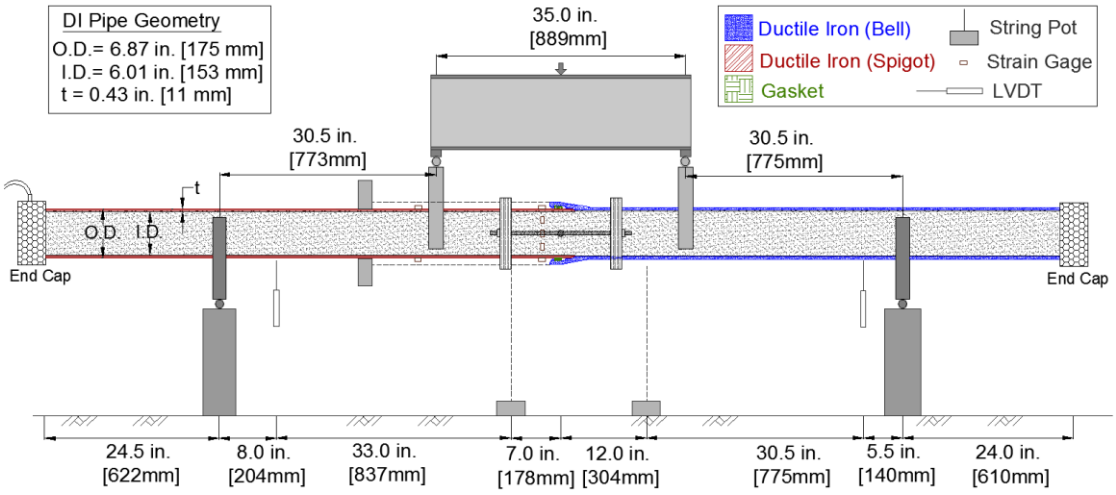

Figure 2.4. Schematic of four-point bending test setup

2.4.1 Test Equipment and Instrumentation

A 1800 kN (400 kip) Baldwin Test Frame was used to perform pressurized leakage tests on the DI pipe specimens at an approximately constant load rate of 0.44 kN/sec (0.1 kip/sec). As shown in Figure 2.4, load was applied through a spreader beam and transferred to the pipe via loading saddles. Vertical displacement was measured along the bottom of the specimen by a combination of two linearly varying differential transformers (LVDTs) and two string potentiometers. Two string potentiometers were also installed at the top and bottom of the joint to record axial joint displacement between bell and spigot. These axial measurements were used to calculate the relative rotation of the joint while the vertical measurements provided verification of specimen deflection and associated curvature. Each test was performed at an internal pressure of 380 ± 35 kPa (55 ± 5 psi), which was visually monitored with an analogue pressure gauge and digitally recorded with a pressure transducer. Approximately 380 kPa (55 psi) was introduced into the closed system at the beginning of each trial. As fluctuations in pressure occurred during rotation due to internal volume changes, the pressure was manually adjusted such that it remained within 35 kPa (5 psi) of its initial value.

A flexible restraint was used to stabilize the joint against thrust-induced axial pullout generated by internal pressure. The restraint, shown in Figure 2.5, was equipped with pin connections to limit resistance to rotation. Pipe clamps were attached to the specimen on either side of the joint; each spaced approximately 180 mm (7 in.) from the center of rotation. The clamps were joined by two 13 mm (½ in.) fine threaded rods with a hinge, positioned at the center of rotation, to allow free rotation of the joint.

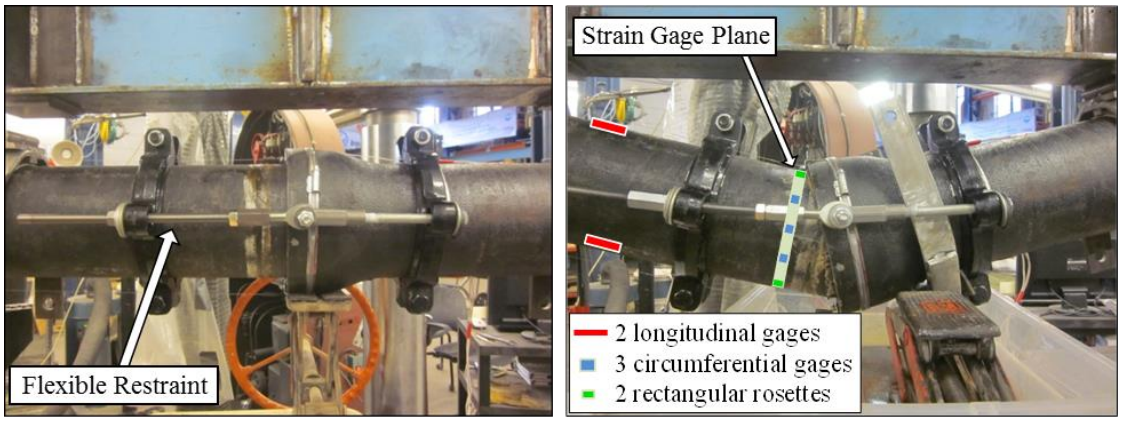

(a) (b)

Figure 2.5. (a) Profile view of pipe joint at 33 mm (1.3 in.) axial displacement prior to imposed deflection. (b) 6.4 mm (0.25 in.) initial axial displacement test at maximum rotation of 26.6°

Specimen A included three strain gages, two at the crown and one at the invert, which provided data regarding imposed bending strains to correlate with applied force. Specimen B was fitted with strain gages at 9 locations. A plane of 5 circumferential gages, shown in Figure 2.5(b), was located 102 mm (4.5 in.) from the end of the spigot to obtain measurements at the crown, invert, springline, and eighth points. Longitudinal gages were installed along the crown and invert of the spigot at locations 102 mm (4.5 in.) and 510 mm (20 in.) from the end of the spigot.

2.4.2 Experimental Procedure

Each four-point bending trial began by assembling the joint. With the spigot fully seated in the bell and flexible restraint in place, water was introduced into the specimen and the system was purged of air. Using the axial force provided by internal pressure, the restraint was adjusted axially allowing the joint to open to the prescribed initial axial

displacement of a particular trial. Once adjustments to horizontal and vertical positioning were made to ensure consistent initial positioning among trials, initial internal pressure was adjusted. Supporting jacks were removed and vertical displacement was imposed at the loading points shown in Figure 2.4.

During deflection the internal pressure was monitored and adjusted to account for fluctuations due to changes in internal volume. As with the preliminary tests previously discussed, the combined joint rotation/axial displacement threshold for leakage was set at a constant flow rate of 1 drop/sec (0.05 mL/sec or 4.32 L/day). Joint leakage was visually monitored throughout the procedure. Loading was paused at the first sign of water and flow rate was assessed. If a constant rate of 1 drop/sec or greater was not achieved, loading was continued until the leakage criterion was met for a duration greater than 60 seconds. Once the leakage threshold was reached, the specimen was unloaded and returned to its initial position.

2.4.3 Joint Rotation Experimental Results

A total of 22 pressurized joint rotation tests were performed. Initial axial displacements ranged from 6.4 mm (0.25 in.) to direct pullout at 56 mm (2.3 in.). Each data point designated as “Forced Joint Leakage” in Fig. 6(a) represents a combination of axial displacement and rotation at which joint leakage occurred. Due to geometric lengthening of the test specimen at large rotations, some additional axial displacement occurs during each trial. For example, the 6.4-mm (0.25-in.) initial axial displacement trial, represented by a red cross in Figure 2.6(a), is plotted at 20 mm (0.80 in) of joint displacement, the maximum pullout reached during the test sequence. Leakage of the

joint was observed during all tests which terminated at axial displacements greater than or equal to 21 mm (0.83 in.). The 6.4-mm (0.25-in.) initial displacement test did not leak despite the application of significantly greater load and rotation than any other test. For each test with axial displacements from 21 mm (0.83 in.) to 41 mm (1.6 in.), the rotation angle at leakage was approximately 16°. In the absence of rotation the joint leaked at a pullout of approximately 58 mm (2.3 in.).

Also shown in Figure 2.6(a) are the range of rotations and initial axial displacements previously plotted in Figure 2.3. For axial displacements greater than 43 mm (1.7 in.), the test results are quite consistent with those of the preliminary rotation tests. The four-point bending test rotations plot slightly higher than those for the preliminary rotation test results for axial pullout between 38 mm (1.5 in.) and 43 mm (1.7 in.). Due to the greater precision in the four-point bending test measurements, these results should be considered the most reliable and representative of pipe performance. For axial displacements of 21 mm (0.83 in.) and greater, the *Forced Joint Leakage* plot defines the experimental pressure boundary for 150-mm (6-in.) DI pipe joints at any combination of rotation and axial displacement.

Figure 2.6(b) shows the moment applied to the joint at the onset of leakage. Moment was calculated for each trial under the simplified assumptions of beam theory for four-point loading. Because the non-linear conditions at large deformations, as well as the effects of axial joint restraint, are not accounted for in the calculation of moment, the plotted moments are approximate at rotations above 10º to 12º. At axial displacements greater than approximately 42 mm (1.65 in.) very small to negligible moment is required

to induce leakage. At these displacements the pipe deflected under its own weight until leakage occurred due to loss of contact between spigot bevel and gasket. Beyond 42 mm (1.65 in.) of pullout, therefore, the joint behaves as a pinned connection. The figure also illustrates the significant level of applied moment the joint accommodates at 20 mm (0.8 in.) of pullout without leaking.

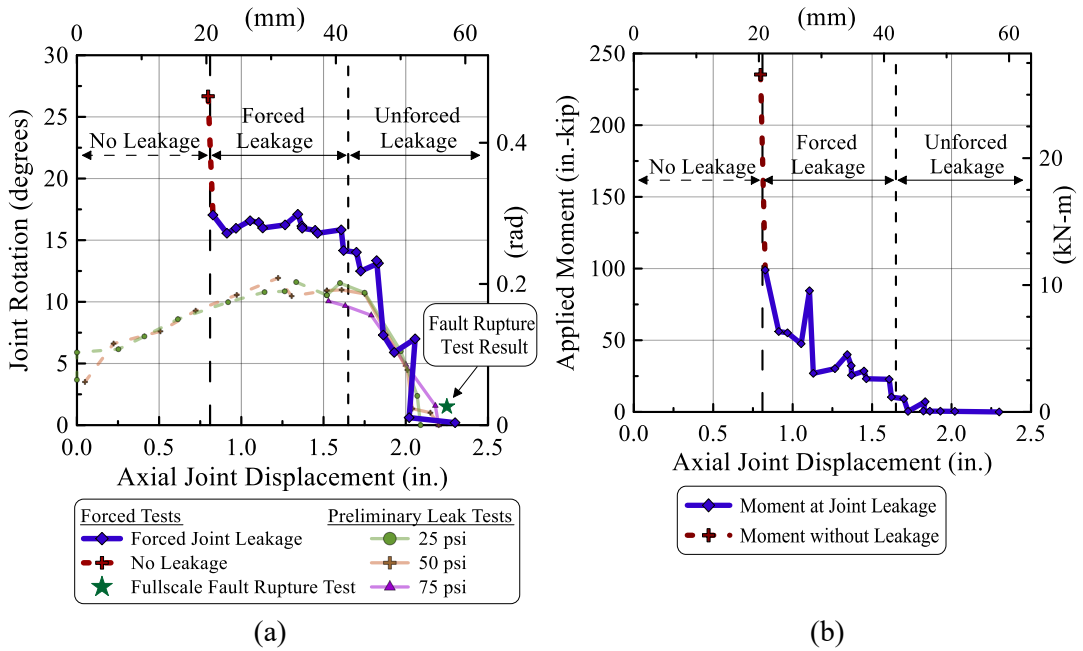

Figure 2.6. (a) 150-mm (6-in.) DI joint pressure boundary for combined axial pullout and rotation; (b) applied moment, calculated from beam theory, at leakage versus axial displacement for imposed deformation tests

2.4.4 Full-Scale Ground Rupture Experiment

A large-scale soil-structure interaction test on a 150-mm (6-in.) DI pipeline with push-on joints was performed at the Cornell University NEES equipment site. The pipeline was buried in partially saturated sand at a depth of 760 mm (30 in.), and oriented at a 50° crossing angle with respect to fault displacement. The properties of

the test sand are described by O'Rourke (2010), which shows that the sand has low suction on the order of 3-5 kPa (0.4-0.7 psi). The pipeline was initially pressurized to 517 kPa (75 psi) and manually adjusted during the test to compensate for pressure fluctuations caused by changes in internal volume. The data for this large-scale test, designated as Cornell - Unlined Pressurized Test with Soil, is available online in the NEES repository (Stewart et al., 2014).

During this large-scale test, the fault displacement was accompanied by axial displacement and rotation of the joints. Three LVDTs, installed under a protective shield at the crown and springlines of the joint, measured differential movement between bell and spigot during the test. At a fault displacement of 137 mm (5.4 in.) the pipeline experienced a complete loss of pressure. Visual evidence and recorded data confirm that pressure loss occurred at the south joint when it reached an axial displacement of 57 mm (2.25 in.) and rotation of 1.5°. This combination of displacement and rotation is labeled and shown in Figure 2.6(a). While this test only provides one additional data point, it represents full-scale soil-pipeline interaction and is consistent with the results of the experimental four-point loading tests.

2.4.5 Experimental Discussion

The test results suggest that leakage of the joint is largely a result of contact with, and deformation of, the elastomeric gasket. When the spigot is positioned within the gasket seat during rotation, as is the case in Figure 2.7(a), leakage occurs. Fluid typically breaches the pressure boundary at the crown where reduction in contact pressure occurs as the spigot rotates away from the gasket. Tests at axial displacements

of 21 mm (0.83 in.) and greater resulted in this condition. As shown in Figure 2.8(a) and 1.8(b), many of these tests resulted in significant damage to the gasket at the invert of the joint.

During the 6.4-mm (0.25-in.) initial axial displacement test, the spigot made contact with the bell landing resulting in significant circumferential deformation of the spigot and failure of the internal mortar liner [Figure 2.8(c)]. Circumferential yielding occurred to a lesser extent in the bell because of its thicker geometry. Metal binding between the bell landing and spigot, as shown in Figure 2.7(b), caused significant deformation to the spigot crown and invert [Figure 2.8(d)]. Even at a substantial imposed rotation of 26.7° the spigot did not lose contact with the gasket and the joint remained sealed. These experimental results show that leakage is highly dependent on local joint deformation and gasket contact pressure.

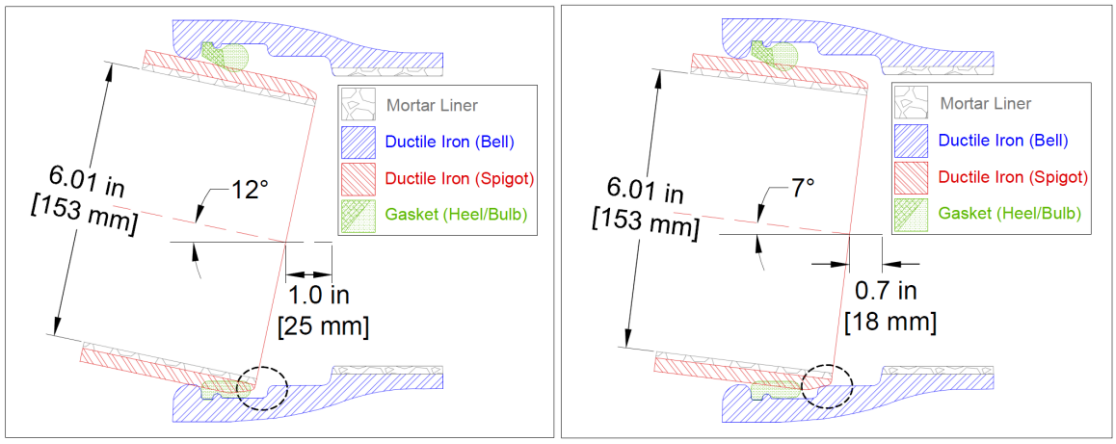

(a) (b)

Figure 2.7. Joint cross-sections depicting internal geometry during bending: (a) 25-mm (1.0-in.) axially displaced joint at 12° of free rotation; (b) 18-mm (0.7-in.) axially displaced joint at 7° of free rotation

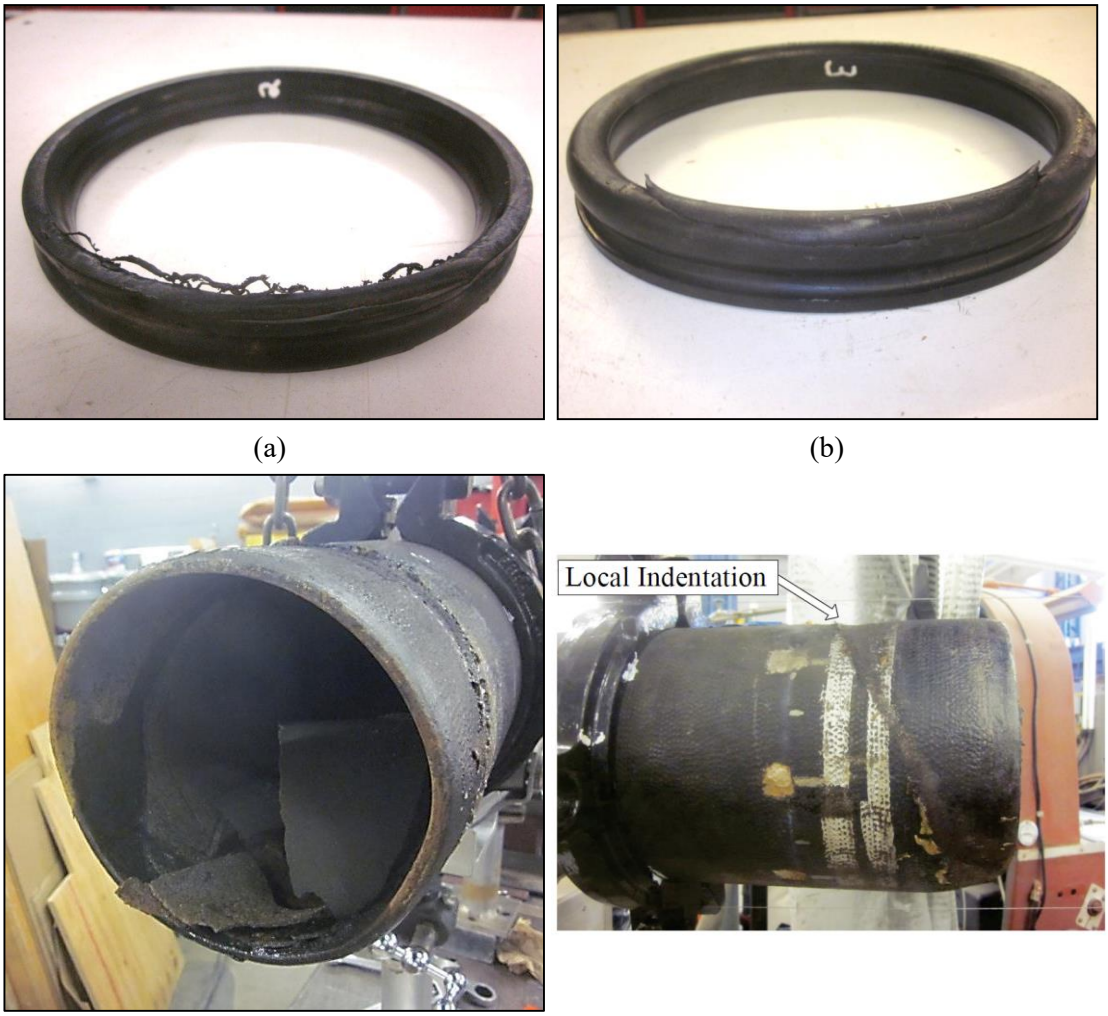

(a) (b)

(c) (d)

Figure 2.8. Gasket damage after: (a) 18-mm (0.7-in.); (b) 13-mm (0.5-in.) initial displacement tests; (c) deformed spigot after application of 26.7° of rotation at axial displacement of 20.3 mm (0.8 in.); (d) Specimen B showing bending of spigot at both crown and invert

2.5 Numerical Modeling

Finite-element (FE) simulations were performed using the software ABAQUS 6.13 to evaluate the deformation associated with leakage of the joint. The 3D model

replicated the overall geometry and boundary conditions of the experimental setup. Figure 2.9 shows a rendering of the pipe joint model composed of over 320,000 3D solid elements and 1.2 million degrees of freedom. Symmetric boundary conditions were used to model one-half of the axially symmetric pipe geometry.

2.5.1 Elements and Materials

The DI spigot and bell were modeled as an elastic-plastic, isotropic solid material using C3D8R type 8-noded (linear), reduced integration brick elements. The gasket components were represented with C3D8RH type, 8-node (1^{st} order), reduced integration, hybrid brick elements with isotropic, hyperelastic material properties. The hybrid elements interpolate the displacement and pressure stress solutions independently, providing a robust numerical simulation of materials that are nearly incompressible with Poisson's ratios greater than 0.48 (ABAQUS 6.13).

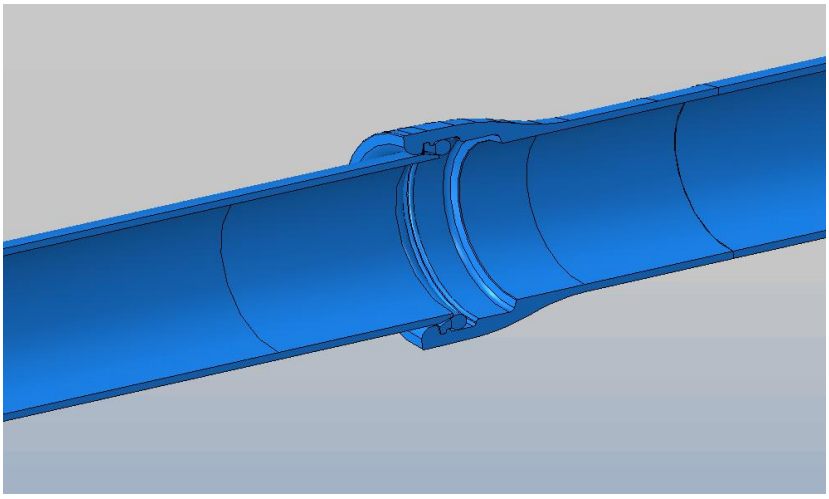

Figure 2.9. 3D rendering of ABAQUS model

The DI material was represented by an elastic-plastic curve derived from the tensile coupon tests previously discussed [Figure 2.1(b)]. The bottom of Figure 2.1(a) shows an undeformed cross-section of the rubber gasket, which is composed of two SBR materials. The softer bulb material is designed to compress between the bell and spigot during joint assembly, providing a water tight seal. The stiffer heel component serves as a retainer, securing the gasket in place by limiting translation during spigot insertion. The characterization of the rubber gasket components was derived from laboratory test samples provided by a pipe manufacturer approved vendor.

Uniaxial tension and one-dimensional (1D) compression tests were performed on specimens of each type of SBR in accordance with ASTM D412-06a (ASTM, 2013b) and ASTM D575-91 (ASTM, 2012), respectfully. The specimens were specially prepared to conform to the aforementioned standards by Specification Rubber Products Inc., Alabaster, Al. Representative data from the tension and compression tests are plotted in Fig. 10 as solid lines. The rubbers are characterized on the basis of Shore A hardness (ASTM, 2010), with the heel and bulb of the gasket having durometer values of 83 ± 5 and 53 ± 5, respectively. Both materials exceeded the pipe manufacture's specifications for minimum tensile strength and elongation.

Results from the uniaxial tensile and 1D compression tests were implemented in ABAQUS simulations as user-defined test data and fit with hyperelastic strain energy approximations. The 1st order Ogden strain energy function (Ogden, 1972; Ogden et al., 2004) was used to define the hyperelastic curve for the harder heel material because it provided a good fit to experimental data at relatively low computational cost

compared to other hyperelastic models investigated. The gasket bulb was fitted with a 2nd order polynomial function (Rivlin & Saunders, 1952). This hyperelastic strain energy approximation provided a robust model that accommodated large gasket deformations while providing a reasonable fit to the experimental data at low strain levels. Both elastomeric material models were assigned Poisson ratios of 0.495 to represent nearly incompressible behavior.

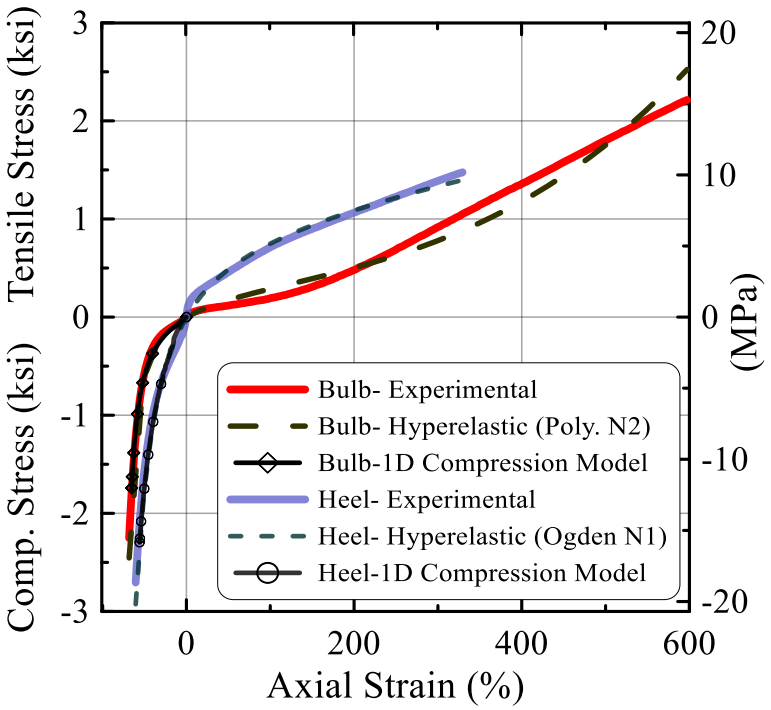

Figure 2.10. Stress-strain relationships of the gasket bulb and heel generated from material testing, hyperelastic curve fitting, and ABAQUS 1D compression test simulation.

Figure 2.10 shows the tensile and compression test results compared with the hyperelastic strain energy curves fitted to the data in ABAQUS and used to characterize the hyperelastic material properties. To confirm that the hyperelastic properties provide an accurate representation of behavior, they were used in a 1D compression ABAQUS

model to generate numerical test results (black lines) for each rubber material. Figure 2.10 shows that there is excellent agreement between the numerical and laboratory compression test results for 1D strains in excess of 0.55 (55%) and 0.65 (65%) for the gasket heel and bulb, respectively.

2.5.2 Simulation Procedure

The analysis was performed in four discrete steps. The first focused on providing the gasket a realistic initial state of compression. Since the gasket was modeled on the basis of its undeformed geometry, gasket compression was achieved in the first step by numerically inserting the spigot into the bell.

The second step accounts for internal water pressure, which imposes very little strain on the DI pipe. However, the much softer gasket bulb material deforms appreciably under typical operating pressures, reaching strain levels on the order of 11% for an internal pressure of 380 kPa (55 psi). Therefore, a constant pressure was imposed on the surface of gasket exposed to internal pressure.

The third step represents the initial axial pullout of the joint. The prescribed axial displacement was imposed on the spigot, pulling it from its fully seated position. This displacement was varied between 0 and 58 mm (2.3 in.), depending on the level of pullout under investigation.

The fourth and final final step was to duplicate the 4-point loading process by applying two identical vertical displacements at the loading points, 445 mm (17.5 in.) on either side of joint center. Vertical boundary conditions were assigned at the location

of experimental supports shown in Figure 2.4. Axial boundary conditions were applied to the pipe springline at locations where the flexible restraints were positioned during laboratory tests.

2.5.3 FE Modeling Results

To examine in detail how the numerical simulation results compare with the experimental evidence, the simulated and measured strains at key locations on the test pipe are plotted as a function of rotation under 4-pt loading in Fig. 11. The 4-pt loading was modeled as described above in step four. The numerical simulations and test results, at a cross-section located 114 mm (4.5 in.) from the end of the spigot [Figure 2.5(b)], are compared for initial axial spigot displacements of 23 mm (0.91 in.) and 33 mm (1.3 in.) from the fully seated position. Figure 2.11(a) and 1.11(b), 1.11(c) and 1.11(d), and 1.11(e) and 1.11(f) compare measured and simulated axial and hoop strains at the pipe crown, invert, and springlines, respectively.

In general there is favorable comparison between the experimental and modeling results. Although there are local variations, the measured and simulated strains are comparable at approximately the same level of rotation within ±3 degrees, especially at the crown and invert. The least favorable comparisons are at the springline where distortion is complicated by 3D effects as stresses are distributed from crown and invert contact points around the circumference of the pipe. Nevertheless, even at these locations, the trends in strain as a function of rotation are similar with comparable maximum strains.

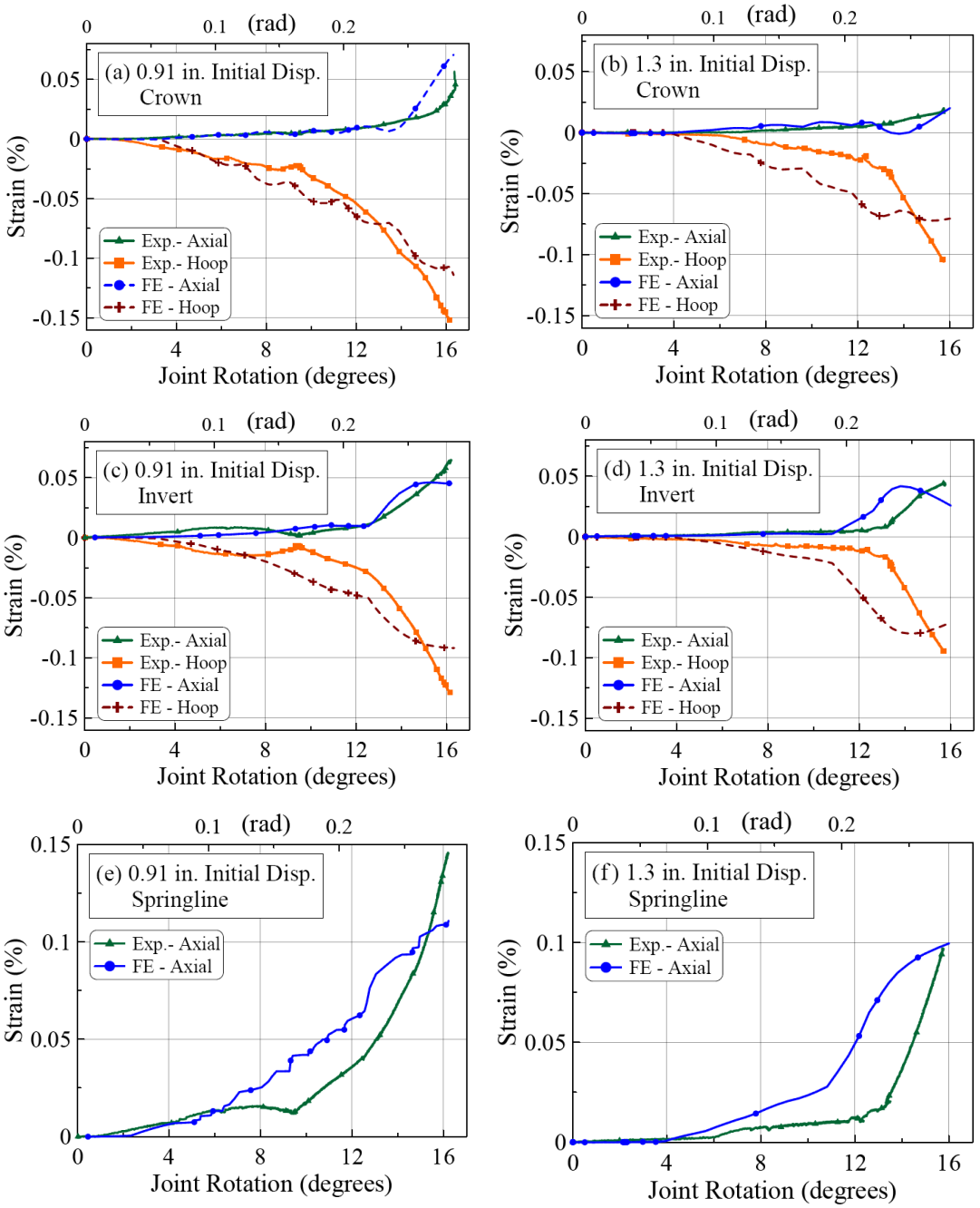

Figure 2.11. Correlations between axial and circumferential strain gage measurements and FE results

To develop a predictive model it is necessary to identify a numerical indication of joint leakage. This study assumes that water will penetrate the DI/gasket interface if the

stress normal to the interface (referred to numerically as contact stress) is less than the internal water pressure. Initially, when the joint is fully inserted, there is an axisymmetric contact stress of approximately 1030 kPa (150 psi) between the spigot and gasket. As the joint deflects for a given axial displacement the contact stresses at the DI/gasket interface change and, in many instances, reduce to a value less than the internal pressure. Applying this numerical representation of leakage, simulations that varied only by their internal water pressure were found to reach leakage at nearly the same geometric deformation, an observation previously noted during experimental testing.

Figure 2.12 shows combinations of axial joint displacement and joint rotation that caused leakage during experimental tests and numerical simulations. The blue line represents the pressure boundary from experimental trials previously presented in Figure 2.6(a). Shown in red are FE modeling results when contact pressure at the DI/gasket interface is less than the internal water pressure, triggering leakage. At axial displacements between 23 mm (0.9 in.) and 40 mm (1.6 in.) leakage conditions occur consistently in both the experiments and FE simulations at about 16° of joint rotation. Both the experimental and FE simulation results show that progressively less rotation is required to initiate joint leakage at axial displacements greater than 40 mm (1.6 in.). At axial displacements less than 23 mm (0.9 in.) and rotations greater than 16° significant deformation of the gasket occurs at the invert of the joint, resulting in compressive strain levels exceeding 80%. This level of deformation led to numerical instabilities in the analysis, and thus numerical results for a pressure boundary at small axial displacements

less than 23 mm (0.9 in.) cannot be presented. As described previously, no leakage was observed in the full-scale tests at an axial displacement of 20 mm (0.8 in.), and the test terminated because of large, irrecoverable deformation in the pipe.

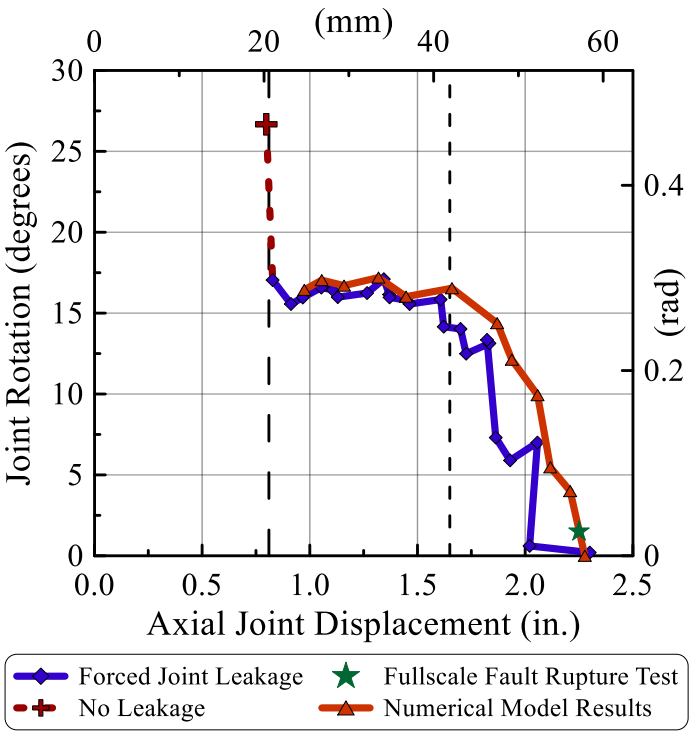

Figure 2.12. DI joint pressure boundary as determined from experimental and analytical results

2.5.4 Load Paths

In this paper load path refers to the combination of changing joint rotation and axial displacement leading to leakage or large irrecoverable deformation of the pipe. During ground rupture the imposed load path depends on the orientation of the rupture plane with respect to the pipe. In other cases of soil deformation imposed by underground construction and subsidence, the load paths will depend on the pipeline joint location in the ground strain field.

Both the experiments and the FE simulations of the experiments involve similar combinations of rotation and axial displacement until leakage. To investigate the effect of different load paths on the initiation of leakage, FE simulations were performed for various combinations of rotation and axial displacement that differed significantly from those associated with the experiments. Four of these load paths are plotted in Figure 2.13 with respect to the pressure boundary determined by the actual measurements and FE simulations of the experiments. The pressure boundary is shown as a cross-hatched zone in the figure. It can be seen that the results for load paths that differed from those followed in the experiments define a similar pressure boundary. In other words, the load path does not affect the combination of rotation and axial displacement at which leakage occurs. Regardless of the evolution of gasket strain related to load path, leakage appears to be controlled by unique geometric conditions associated with axial slip and rotation of the spigot with respect to the bell.

The reason for this behavior appears to be related to the significant difference in compressibility of the gasket with respect to DI pipe. The gasket compresses and distorts to sustain sufficiently high DI/gasket contact pressure independent of load path until the relative positioning of the spigot inside the bell causes a relaxation in DI/gasket contact stress below the internal water pressure. The onset of leakage is therefore controlled by a specific locus of axial movements and joint rotations that defines the pressure boundary for many different load paths. This finding has important implications with respect to modeling and behavior in the field because the same

pressure boundary will determine the onset of leakage irrespective of different ground failure and distributed ground movement patterns.

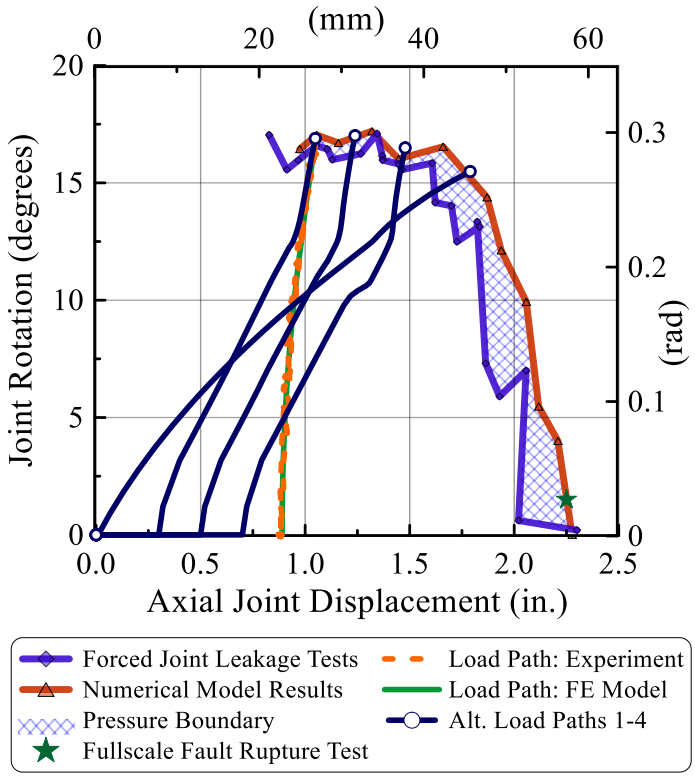

Figure 2.13. Experimental and FE model pressure boundaries with load paths from various numerical trials

2.5.5 3D Deformation

Figure 2.14 compares the simulated joint deformation for conditions of large rotation with and without leakage. Figure 2.14(a) shows the 3D distribution of maximum principal strain for a simulation displaced axially 25 mm (0.97 in.) and rotated 16.4°, representing the initiation of leakage. Narrow zones of concentrated maximum principal strains, exceeding 2%, are located immediately beneath the bell mouth contact

with the crown and invert of the spigot. Leakage occurs at the crown of the joint due to loss of contact stress between the spigot and gasket.

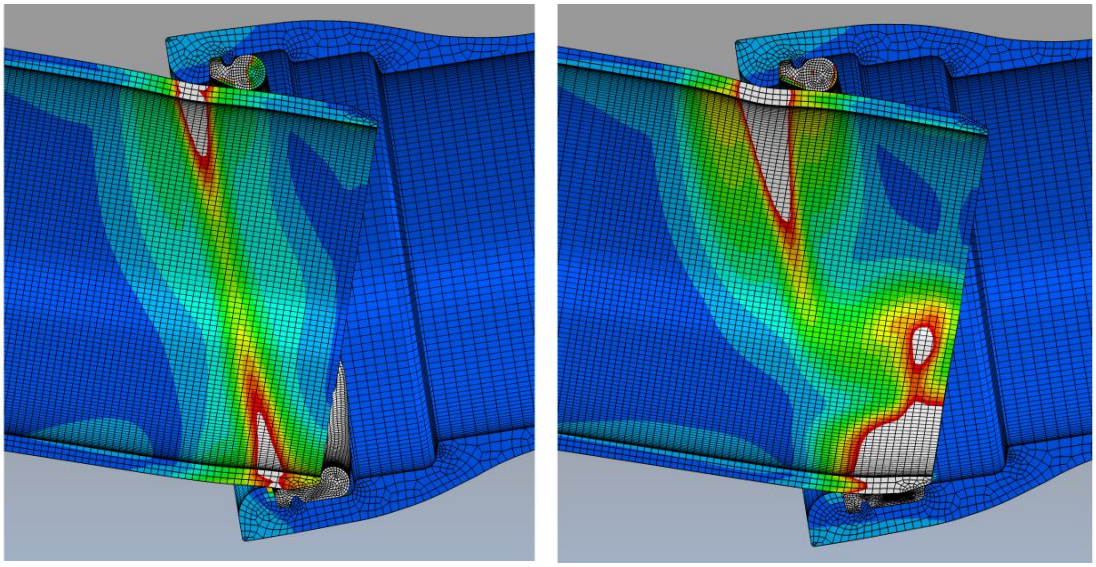

(a) (b)

Figure 2.14. Numerical simulations showing maximum principal strains (white) exceeding 10 times the 0.2% yield strain of DI at (a) 25 mm (0.97 in.) of axial displacement and 16.4° of rotation, the initiation of leakage, and (b) 7.6 mm (0.3 in.) of axial displacement and 18.0° of rotation, without reaching leakage.

Figure 2.14(b) shows the FE model at 7.6 mm (0.3 in.) of axial displacement and 18° of rotation. Maximum principal strains exceeding 2% strain are shown in white, identifying areas of significant irrecoverable deformation. These numerical results are consistent with experimental findings that show axial displacements less than about 21 mm (0.83 in.) lead to contact between the end of the spigot and the bell landing, substantially increasing rotational stiffness of the joint. As the joint continues to rotate, local irrecoverable deformation occurs at the spigot invert, and causes an indentation where the throat of the bell is in contact with the top of the spigot. At this level of

deformation the bell throat acted as a fulcrum about which the spigot crown deforms and the gasket/DI contact stress remains greater than the internal water pressure.

Although leakage at large rotations was not shown in either the experiments or FE simulations for axial pullout less than 21 mm (0.83 in.), large local deformation of the spigot, as described above and shown in Figs. 2.8(d) and 2.1(b), was observed at rotations greater than 16°. The development of a prominent local indentation illustrated in Fig. 2.1(b) promotes uncertainly with respect to the joint's long-term ability to prevent leakage. As a practical limit for levels of axial displacement less than 21 mm (0.83 in.), an upper bound rotation of 16° is recommended.

2.6 Concluding Remarks and Practical Applications

Results from 22 joint rotation tests on 150-mm (6-in.) diameter DI pipeline specimens with push-on joints at internal water pressures of about 380 kPa (55 psi) show the relationship among joint leakage, rotation, and applied moment at various levels of axial displacement. This relationship establishes a pressure boundary for the onset of leakage in DI pipe joints. The pressure boundary provides an upper bound on mechanical joint behavior in response to faulting, liquefaction, landslides, mining, dewatering, and construction activities. It is useful in practice for the design and risk assessment of pipelines subjected to large ground deformation.

The test program shows that the mechanical behavior of even a simple push-on joint requires resolution of leakage as a function of both axial pullout and rotation to characterize performance under extreme deformation. In the past, joint behavior has

been characterized simply as rotation until metal binding, independent of axial pullout. This type of characterization is overly simplistic, and will yield markedly conservative results.

Although DI push-on joints have limited capacity to accommodate pull-out, they have considerable capacity for rotation without leakage, even for axial displacements as high as 70% of the maximum insertion depth. The DI joint is expected to leak at rotations greater than approximately 16° when displaced axially 21 (0.83) to 41 mm (1.62 in.), providing three times more rotational capacity than the manufacturer's guidelines. Beyond 38 mm (1.62 in.), the DI joint becomes increasingly more susceptible to deflection-induced leakage, with straight axial pullout occurring at 58 mm (2.3 in.).

When the spigot is fully seated in the bell, the DI push-on joint has substantial capacity to accommodate rotation without leaking. For joint rotation exceeding 16°, however, experimental and FE results show high levels of irrecoverable local deformation of the spigot. Therefore, a rotational limit of 16° is recommended for joint pullouts between 0 and 20 mm (0.8 in.) to reduce the risk of additional degradation and future leakage.

This study shows that the pressure boundary is independent of load path. This finding has important practical ramifications because one pressure boundary can be used for many different conditions of ground deformation, thus reducing analytical demand and computational requirements when modeling soil-pipeline interaction.

2.7 Acknowledgments

The work described in this paper was supported by the George E. Brown, Jr. Network for Earthquake Engineering Simulation (NEES) Program of the National Science Foundation (NSF), under award No. CMMI-1041498. Any opinions, findings and conclusions or recommendations expressed in this material are those of the authors and do not necessarily reflect the views of the NSF. Thanks are extended to the Los Angeles Department of Water and Power for providing the pipeline specimens, Specification Rubber Products Inc., Alabaster, Al., for supplying rubber gasket test samples, and to US Pipe Inc. for providing information regarding the joint characteristics.

REFERENCES

ABAQUS. (2013). *Theory manual of ABAQUS.* ABAQUS Inc., Providence, RI.

AWWA. (2007). "distribution system inventory, integrity and water quality." U. S. Environmental Protection Agency, Washington DC.

AWWA. (2009). "Ductile iron pipe, centrifugally cast, for water." *AWWA Standard: ANSI/AWWA C151/A21.51-09,* Denver, CO.

ASTM. (2010). "Standard test method for rubber property- durometer hardness." *D2240-05*, West Conshohocken, PA.

ASTM. (2012). "Standard test methods for rubber properties in compression." *D575-91*, West Conshohocken, PA.

ASTM. (2013a). "Standard test methods for tension testing of metallic material." *E8/E8M-13a,* West Conshohocken, PA.

ASTM. (2013b). “Standard test methods for vulcanized rubber and thermoplastic elastomers- tension.” *D412-06a*, West Conshohocken, PA.

Becerril Garcia, D. and Moore, I. D. (2015) “Behaviour of bell and spigot joints in buried reinforced concrete pipelines.” *Can. Geotech. J.*, **52**(1), 1-17. dx.doi.org/10.1139/cgj-2013-0072

Bonds, R. W. (2005). “Cement-mortar linings for ductile iron pipe.” *Ductile Iron Pipe Research Association*. Birmingham, AL.

Folkman, S. (2012). “Water main break rates in the USA and Canada: A comprehensive study.” *Utah State University Buried Structures Laboratory*, Logan, UT.

Hamada, M. (2014). *Engineering for Earthquake Disaster Mitigation*. Springer, Tokyo.

Kirmeyer, G. J., Richards, W., and Smith, C. D. (1994). “An assessment of water distribution systems and associated research needs.” *AWWA Research Foundation and American Water Works Association*. Denver.

Maragakis, E., Siddharthan, R., and Meis, R. (1999). “Axial behavior characteristics of pipe joints under static loading.” *Multidisciplinary Center for Earthquake Engineering Research*. Buffalo.

Ogden, R. W. (1972). “Large deformation isotropic elasticity - on the correlation of theory and experiment for incompressible rubberlike solids.” *Proc. of the Royal Society of London. Series A, Mathematical and Physical Sciences*, 326(1567) 565-584.

Ogden, R. W., Saccomandi, G., and Sgura, I. (2004) “Fitting hyperelastic models to experimental data,” *Comput. Mech.*, 34(6), 484–502.

O’Rourke, T. D. (2010). “Geohazards and large, geographically distributed systems.” *Géotechnique*, **60**(7), 505–543.

O'Rourke, T. D., Jeon, S.-S., Toprak, S., Cubrinovski, M., Hughes, M., Ballegooy, S., and Bouziou, D. (2014). “Earthquake response of underground pipeline networks in Christchurch, NZ.” *Earthquake Spectra,* **30**(1), 183-204.

O’Rourke, T. D., and Bonneau, A. (2007). “Lifeline performance under extreme loading during earthquakes.” *Earthquake geotechnical engineering*, K. D. Pitilakis, ed., Springer, Dordrecht, The Netherlands, 407–432.

O’Rourke, T. D., Bonneau, A. L., Pease, J. W., Shi, P., and Wang, Y. (2006). “Liquefaction and ground failures in San Francisco.” *Earthquake Spectra*. 22(S2) 91-112.

O'Rourke, T. D., Roth, B.L., and Hamada, M., (1992) “Large ground deformations and their effects on lifeline facilities; 1971 San Fernando earthquake.” *NCEER-92-0002*, 3:1-85.

Rivlin, R. S. and Saunders, D. W. (1951). “Large elastic deformations of isotropic materials. VII. Experiments on the deformation of rubber.” *Phil. Trans. R. Soc. Lond. A*, 243(865) 251–288.

Singhal, A. C. (1984) “Behavior of jointed ductile iron pipelines.” *J. of Transp. Eng.*, 110(2), 235-250.

Stewart, H., Argyrou, C., Bond, T., O’Rourke, T. D. and Wham, B. P. (2014). "Cornell - unlined pressurized di test with soil", Network for Earthquake Engineering Simulation (distributor), Dataset, 10.4231/D3930NW1Z.

Tang, A. (2000). “Izmit (Kocaeli), Turkey, Earthquake of August 17, 1999, including Duzce Earthquake of November 12, 1999-lifeline performance.” *ASCE, Technical Council on Lifeline Earthquake Engineering*, Monograph No.17, Reston, VA.

U. S. Pipe. (2013a) “TYTON® Gasket.” *U.S. Pipe and Foundry Co.*, Birmingham, AL.

U. S. Pipe. (2013b) “TYTON JOINT® Pipe- Ductile Iron.” *U.S. Pipe and Foundry Co.,* Birmingham, AL.

Wang, Y. and Moore, I. D. (2014). “Simplified design model for rigid pipe joints based on the two-pipe approximation.” *Can. Geotech. J.,* **52**(1), 1-12.

Wham B.P., Argyrou C., Bouziou D., O’Rourke T.D., Stewart H.E., and Bond T.K. (2014) “Jointed pipeline response to earthquake induced ground deformation,” *Proc.,10th National Conf. on Earthquake Engineering*, Earthquake Engineering Research Institute, Anchorage, AK.

CHAPTER 3

PVCO PIPELINE PERFORMANCE UNDER LARGE GROUND DEFORMATION

ABSTRACT

Technological advances have improved pipeline capacity to accommodate large ground deformation associated with earthquakes, floods, landslides, tunneling, deep excavations, mining, and subsidence. The fabrication of polyvinyl chloride (PVC) piping, for example, can be modified by expanding PVC pipe stock to approximately twice its original diameter, thus causing PVC molecular chains to realign in the circumferential direction. This process yields biaxially oriented polyvinyl chloride (PVCO) pipe with increased circumferential strength, reduced pipe wall thickness, and enhanced cross-sectional flexibility.

This paper reports on experiments performed at the Cornell University Large-Scale Lifelines Testing Facility characterizing PVCO pipeline performance in response to large ground deformation. The evaluation was performed on 150-mm (6-in.)-diameter PVCO pipelines with bell-and-spigot joints. The testing procedure included determination of fundamental PVCO material properties, axial joint tension and compression tests, four-point bending tests, and a full-scale fault rupture simulation. The test results show the performance of segmental PVCO pipelines under large ground deformation is strongly influenced by the axial pullout and compressive load capacity of the joints, as well as their ability to accommodate deflection and joint rotation. The

PVCO pipeline performance is quantified in terms of its capacity to accommodate horizontal ground strain, and compared with a statistical characterization of lateral ground strains caused by soil liquefaction during the Canterbury earthquake sequence in New Zealand.

3.1 Introduction

The capacity of lifelines to provide continuous transportation of services and resources is vital for commerce, communication, and security. Pipelines used for water distribution are classified as lifelines because their disruption can threaten life and property, and lead to significant economic and social impacts. Failure of these critical systems leaves communities without the capacity for firefighting, water for drinking and sanitary services, and supply necessary for industrial and domestic operations.

One of the greatest threats to lifeline systems is ground deformation generated by geohazards such as earthquakes and landslides. The vulnerability of water distribution systems to earthquake-induced permanent ground deformation (PGD) is well known. Liquefaction-induced soil movements damaged the water distribution systems in San Francisco in 1906 and 1989, with serious consequences with respect to firefighting and fire losses (O'Rourke et al., 2006). The 2010-2011 Canterbury earthquake sequence caused severe disruption of the Christchurch, NZ water distribution system in three main seismic events, necessitating repairs at thousands of locations throughout the pipeline network (O'Rourke et al., 2014). Construction activities including tunneling and deep excavations, floods, and subsidence caused by withdrawal of minerals and fluids during

mining and petroleum production are additional sources of significant ground deformation that result to pipeline damage (O'Rourke, 2010).

The use of polyvinyl chloride (PVC) pipe for water distribution systems has increased steadily since its introduction to North America in 1951 due to its corrosion resistance, light weight, and flexibility. Molecularly oriented polyvinyl chloride (MOPVC or PVCO) is composed of the same material as conventional PVC. However, after the stock pipe is extruded, it is drawn over a mandrel expanding the pipe to approximately twice its original diameter (PVC Pipe Association 2012). The stretching process realigns the long PVC molecular chains circumferentially, producing a lighter product with greater strength, ductility, and impact resistance than standard PVC, and allows PVCO to be manufactured with a relatively thin wall (Michel & Akkerman, 2012).

This paper focuses on the mechanical characterization of PVCO pipe. It presents the results of a series of experiments designed to evaluate the performance of PVCO pipelines with mechanical joint restraints under large PGD, including a full-scale test of soil-pipeline interaction in response to surface faulting, using the Cornell Large-Scale Lifelines Facility. Fault rupture simulated in the large-scale test is also representative of the most severe ground deformation that occurs along the margins of landslides and liquefaction-induced lateral spreads.

3.2 Test Specimens

The pipes used in this study were Bionax 150 mm (6 in.) CIOD (cast iron outside diameter) PVCO pipes manufactured by IPEX Inc., Montreal, Quebec. The pipe outer diameter and wall thickness were 175 mm (6.9 in.) and 6.2 mm (0.245 in.), respectively. The pipeline joints were standard C909 bell-and-spigot connections, compliant with AWWA C909 (2009), ASTM D3139 (2011), and CSA B137.3.1 (2013). An elastomeric gasket, fixed within each bell, provides the joint with a water tight seal. The gaskets conform to the requirements of ASTM F477 (2010) for high-head applications (PVC Pipe Association 2012). Before assembling the joint, a thin film of lubricant is applied to the inside surface of the gasket and end of the spigot, per the manufacturer's installation instructions.

The pipeline was fitted with commercially available Uni-Flange® Pipe Restraints (UFR1559-C-6-U style), manufactured by The Ford Meter Box Company Inc., Wabash, IN. The Series 1559 Restraint Device is available for 100- to 400- mm (4- to 16- in.)-diameter C909 PVC bell joints. Constructed of ductile iron, the 150 mm (6 in.) restraint design incorporates a series of 6 individually torqued iron segments, spaced circumferentially around the pipe, which evenly distribute the restraining force to the pipe body (Ford Meter Company 2014). Restraints on either side of the joint were joined by six 15.8 mm (5/8in.) threaded steel rods.

The primary objective of the joint restraint is to increase the axial force capacity at the bell-and-spigot push-on joint. Common applications for this type of restraint include anchoring pressurization end caps as well as resisting unburied pipe joint opening during

pressure checks. When applied in soil subject to PGD effects, the mechanical joint restraint prevents pullout under tensile ground strains. It also affects the joint response to compressive ground strains and differential settlement.

3.3 PVCO Material Properties

Standard performance requirements for thermoplastic pressure pipes, such as PVCO, are based largely on hydrostatic pressure testing. The 150-mm (6-in.)-diameter pipes in this study had a Hydrostatic Design Basis (HDB) of 49 MPa (7100 psi), as defined by ASTM D2837 (2013a), and pressure rating of 1.62 MPa (235 psi). Requirements include burst testing to internal pressures of 5.21 MPa (755 psi) and sustained pressure testing at 3.45 MPa (500 psi) for 1000 hours (ASTM 2013b). These tests provide minimum pipe performance limits under pressure. A more detailed resolution of material properties, however, is needed in characterizing upper bound pipeline response under irrecoverable strain levels imposed by external loading sources such as PGD.

The continuous on-line process used during manufacturing to expand the material results in significant molecular realignment in the circumferential direction, as well as reorientation to a lesser extent in the axial direction. The process results in an anisotropic material with different strength and deformation characteristics in the axial and circumference directions of the pipe.

To characterize the axial properties a series of dogbone samples were machined from 150-mm (6-in.) and 200-mm (8-in.)-diameter pipes and tested in uniaxial tension following guidelines set by ASTM E8/E8M (2013c). The tensile coupons were fitted

with both axial and lateral strain gages and reflective tape to record high strain values with a laser extensometer. Figure 3.1(a) shows representative stress-strain curves from select tensile coupon tests. Estimates of longitudinal elastic modulus, 3.10 GPa (450 ksi), and Poisson's ratio, 0.37, were determined from the linear portion of the coupon test results. At axial strains of about 0.05, tensile coupons consistently reached peak stresses between 54 and 59 MPa (7.8 and 8.5 ksi). Beyond peak some softening occurred, followed by failure at large strain values ranging from 0.60 to 1.3 and stresses of 43 to 48 MPa (6.2 to 7.0 ksi). Some temperature and rate dependent variations in viscoelastic material response are expected for thermoplastics (Rahman & Watkins, 2005), but beyond the scope of the present study.

Circumferential properties could not be determined from standard tensile coupons because pipe curvature in the circumferential direction was too severe for machining tensile specimens sufficiently straight for accurate measurements. To evaluate circumferential properties, a 2.4 m (8 ft) long section of 150-mm- (6-in.)-diameter pipe was instrumented with strain gages, fitted with end caps and pressurized with water to a maximum internal pressure of 2.76 MPa (400 psi), imposing stress levels exceeding the elastic range of the material.

The PVCO created by stretching molecular chains in the circumferential direction best matches a transversely isotropic material with its plane of symmetry oriented in the radial and longitudinal directions. Hooke's law for these conditions yields

$$\varepsilon_l = \frac{\sigma_l}{E_l} - \frac{\nu_{\theta l}}{E_\theta}(\sigma_\theta + \sigma_r) \qquad (3.1)$$

$$\varepsilon_\theta = \frac{\sigma_\theta}{E_\theta} - \frac{\nu_{l\theta}}{E_l}(\sigma_l + \sigma_r) \qquad (3.2)$$

for which ε_l and ε_θ are the longitudinal and circumferential pipe strains, respectively; E_l and E_θ are Young's moduli in the longitudinal and circumferential directions, respectively; $\nu_{\theta l}$ and $\nu_{l\theta}$ are the circumferential and longitudinal Poisson's ratios, respectively; and σ_r, σ_θ, and σ_l are the radial, circumferential, and longitudinal stresses, respectively.

For the pressurization test with internal pressure, p_i, the principal stresses are $\sigma_r = p_i/2$, $\sigma_\theta = p_i r/t$, and $\sigma_l = p_i r/2t$, for which r = internal pipe radius, t = pipe wall thickness, and σ_r is approximated as the average radial stress across t.

Combing Eqn. 3.2 with the expressions for principal stresses results in

$$E_\theta = [\varepsilon_\theta t/p_i r + (\nu_{l\theta}/2E_l)(1 + t/r)]^{-1} \qquad (3.3)$$

Using $E_l = 3.10$ GPa (450 ksi) and $\nu_{l\theta} = 0.37$ from the direct tension tests, E_θ is plotted with respect to p_i in Fig. 3.1(b), showing that $E_\theta = 3.71$ GPa (538 ksi) fits the data in the linear elastic range of response. Substituting this E_θ into Eqn. 3.1 yields $\nu_{\theta l} = 0.44$ for representative measurements of σ_l and ε_l in the linear elastic range.

For a transversely isotropic material, $\nu_{l\theta}/E_l = \nu_{\theta l}/E_\theta$. Using the values of E_l, E_θ, $\nu_{\theta l}$ and $\nu_{l\theta}$ reported above satisfies this equality within ±1%, thus providing validation of the material property evaluation.

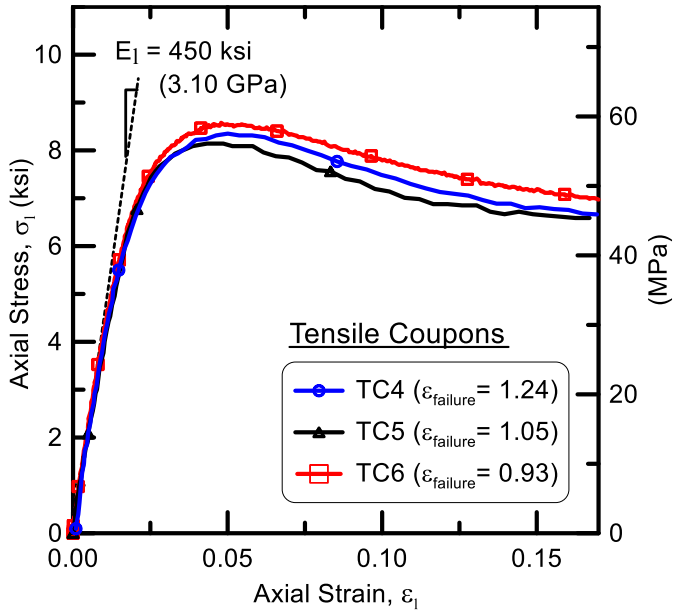

(a) Tensile Coupons

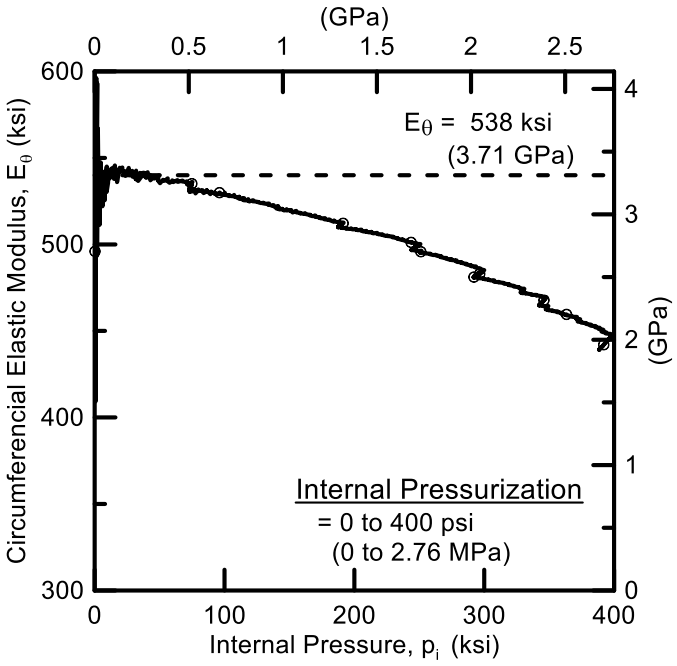

(b) Internal Pressurization

Figure 3.1. PVCO stress-strain characterization of (a) longitudinal properties from tensile coupon tests and (b) circumferential properties from internal pressurization

Table 3.1 summarizes the elastic modulus and Poisson's ratio for the PVCO material in both the longitudinal and circumferential directions. The circumferential elastic modulus is about 16% greater than the modulus measured in the axial direction, reflecting the stiffening effects of molecular alignment around the circumference. The table also presents average stress and strain values recorded at the proportionality limit and maximum loading of the longitudinal tensile coupon tests.

Table 3.1. Summary of PVCO anisotropic properties from material testing

PVCO Material Properties	Young's Modulus [GPa(ksi)]	Poisson's Ratio	Proportional Limit [MPa (ksi)]	Proportional Limit Strain	Average Maximum Stress [MPa (ksi)]	Average Strain at Maximum Stress
Longitudinal	3.10 (450)	0.37	24.8 (3.6)	0.008	57.5 (8.34)	0.0502
Circumferential	3.71 (538)	0.44	NA	NA	NA	NA

3.4 Full-scale Tests

The full-scale tests included axial joint tension and compression tests, four-point bending tests, and a full-scale fault rupture simulation. The axial joint tests were designed to investigate the longitudinal force-displacement behavior of the pipeline and its joints, with and without mechanical restraints. The bending tests provide a measure of the moment-rotation characteristics of both the pipe body and mechanically restrained joints. These test results are used to characterize pipeline response for various orientations and magnitudes of ground rupture.

The full-scale fault rupture test provides detailed measurements of soil-pipeline interaction at various levels of fault rupture so that the performance of the pipe, joints, and restraints can be validated under actual ground failure conditions. The test provides confirmation of the pipeline failure mechanism as well as the level of ground deformation that can be accommodated by the pipeline. The large-scale test results are also used to develop and verify analytical models of soil-pipeline interaction and the mechanical response of the pipe, joints, and restraints.

3.4.1 Axial Tension Tests

Push-on joints are susceptible to pullout. Two axial tension tests were performed to characterize the pullout capacity of the PVCO C909 bell-and-spigot joints. Each 2.4-m (8-ft)-long test specimen was constructed of two 1.22-m (4-ft)-long segments with a joint at its center. Each specimen was fitted with end caps and pressurized with water to an approximately constant 586 MPa (85 psi) of internal water pressure. The specimen was secured at its ends to the load frame and tension was applied through a 222 kN (50 kip) actuator.

The first test, TT1, was performed on an unrestrained joint. Two sections of pipe were joined by inserting the spigot 150 mm (6 in.) into the bell, consistent with pipeline installation in the field. Axial force was then applied to the joint as axial joint opening was measured. As shown in Fig. 3.2, at 63.5 mm (2.5 in.) of joint displacement the unrestrained joint required a maximum tensile force of 2.93 kN (0.66 kips) to open. Disengagement of the joint, and subsequent leakage, occurred at 98.3 mm (3.87 in.) of axial displacement. Studies have shown that variation in axial pullout force will occur

depending on initial pipe out of roundness and the application of different joint lubricants and methods (Balkaya et al., 2012). While the pullout displacement provides some capacity for the pipeline to elongate under axial deformations, even at shallow burial depths, the joint pullout resistance provided by the rubber gasket is substantially less than the soil friction force mobilized axially along a typical pipe length.

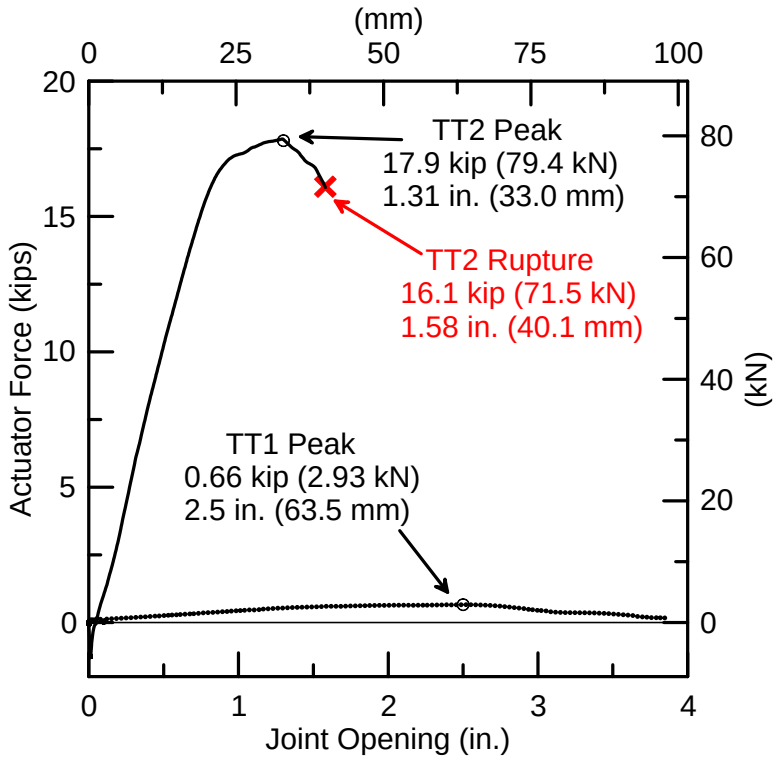

Figure 3.2. Axial force-displacement results of joint tension test

Specimen TT2 was fitted with mechanical restraints on either side of the joint, connected with threaded rods. As shown in Fig. 3.3 the mechanical joint restraint spans the bell and provides a rigid link between two sections of pipe. The figure also shows some of the string potentiometers used to measure joint opening and relative movement between pipe and either restraint. Figure 3.2 includes the actuator force vs. joint

displacement for Specimen TT2. Note that the actuator force starts at a negative value to reflect the axial load induced by internal pressurization. Joint displacement is calculated by subtracting the longitudinal elastic shortening of the pipe barrel, derived from strain gage measurements, from the total actuator movement to capture the axial deformation occurring within the immediate vicinity of the restrained joint.

Figure 3.3. Specimen TT2 joint with restraint prior to tension test

Specimen TT2 sustained a maximum force of 79.6 kN (17.9 kips) at 33.0 mm (1.30 in.) of joint opening. After peak load, softening occurred until rupture at a maximum joint displacement of 40.1 mm (1.58 in.) and axial load of 71.6 kN (16.1 kips). As shown in Fig. 3.4(a), the pipe bell ruptures at the location where the restraint is clamped closet to the bell. To secure the joint restraint to the pipe, the iron segments of the restraint are torqued circumferentially around the pipe. Ribs on the face of the segments create indentations on the pipe surface. Post-failure investigation of Specimen TT2 shows that fractures propagated circumferentially from these stress concentrations, resulting in a circumferential rupture perpendicular to the direction of loading [Fig. 3.4(b)]. Video recordings of the test indicate that some differential racking of the

restraints occurred just before failure, which may have further indented the pipe at the location of restraint segments and contributed to the initiation of rupture.

(a)

(b)

Figure 3.4. Rupture of restrained joint Specimen TT2 (a) at failure and (b) after specimen failure

3.4.2 Axial Compression Tests

Two compression tests were performed on nominal 150-mm (6-in.)-diameter PVCO piping. For each test two 145-cm (57-in.)-long sections were assembled with a joint at their center and internally pressurized to approximately 586 kPa (85 psi). Restraints at either end were designed to secure the pipe to the load frame and provide axial compression via a 220 kN (50 kip) actuator. Specimen CT1 had a standard joint without mechanical restraint. Similar to Specimen TT2 shown in Fig. 3.3(b), Specimen CT2 had pipe restraints on either side of the joint connected with threaded steel rods.

The axial force vs. joint displacement plots for both compression tests, as well as the plots for the previously discussed tensile tests, are shown in Fig. 3.5. Both compressive tests achieved greater than 127 mm (5 in.) of displacement from a fully-inserted position without leaking. At the beginning of each test approximately 17.8 kN (4 kips) of compressive force was required to initiate joint closure. For Specimen CT1 the compressive force increases in an approximately linear relationship with joint displacement at forces greater than 17.8 kN (4 kips). Shown in Fig. 3.6(a) the spigot of Specimen CT1 was pushed into the bell resulting in some reduction in spigot diameter and an observable budging of the bell's base. The linear increase in force is likely a result of increased frictional surface area between the spigot exterior and bell interior as the spigot is forced into the bell.

The addition of the mechanical restraints for Specimen CT2 increased the compressive force required to push the spigot into the bell. As shown in Fig. 3.6(b), even with the restraint in place, the spigot was sufficiently ductile to reduce in size by

circumferential wrinkling. This deformation did not compromise the pressure boundary of the joint. Neither leakage nor rupture of the specimen occurred during the test. A relatively constant 80 kN (18 kips) of compressive force was measured at displacements (joint closure) greater than 50 mm (2 in.).

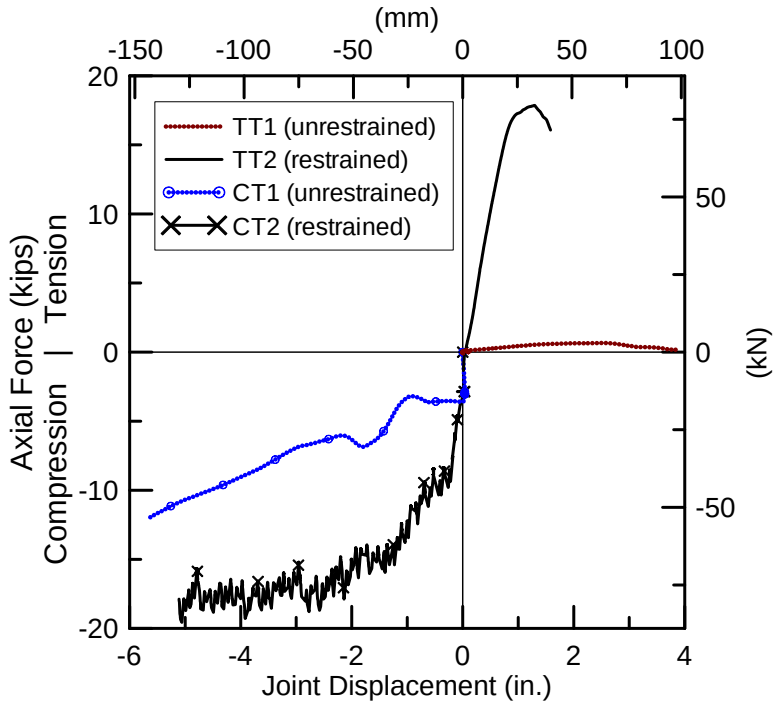

Figure 3.5. Axial tensile and compressive test results for restrained and unrestrained PVCO joints

The axial tensile and compressive test results are summarized in Table 3.2. The tests indicate that the PVCO joint can accommodate significant compressive displacements without structural or serviceability failure. The results also show that while the mechanical restraint provides about 3 times more compressive force resistance during the first 50 mm (2 in.) of joint closure, the unrestrained joint's axial stiffness continues to increase at large compressive displacements, providing additional resistance during

deformation. When considered with the axial tension tests, these experimental results suggest that, while the restraint does provide additional resistance to axial loading, the pipeline remains more vulnerable to axial extension than compressive deformation, irrespective of the joint restraint.

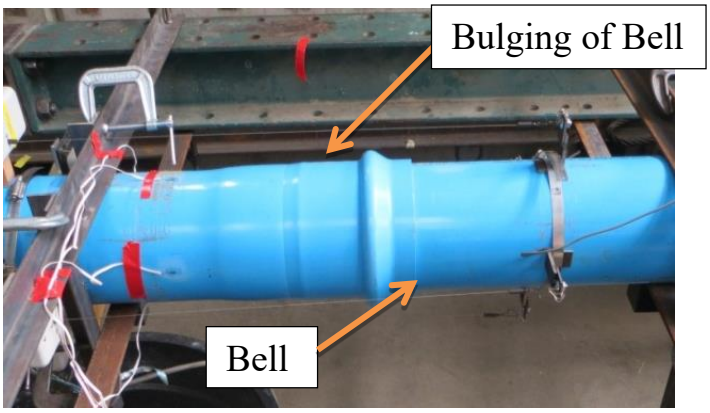

(a) Specimen CT1 bell bulging

(b) Wrinkling of Specimen CT2 spigot

Figure 3.6. Axial compression tests

Table 3.2. Summary of axial displacement tests

Test Specimen	Joint Restraint	Maximum Force [kN (kips)]	Maximum Joint Displacement [mm (in.)]	Failure (Joint leakage)
TT1	No	2.93 (0.66)	98.3 (3.87)	Yes
TT2	Yes	79.6 (17.9)	40.1 (1.58)	Yes
CT1	No	-54.2 (-12.1)	-144.8 (-5.7)	No
CT2	Yes	-86.7 (-19.4)	-129.5 (-5.1)	No

3.4.3 Four-point Bending Tests

Installation guidelines (Extrusion Technologies, 2003) for nominal 150-mm (6-in.) PVCO joints permit 2° of allowable joint rotation, or deflection, after which the spigot makes internal contact with the bell. The joints have considerable capacity under large ground deformation to deflect beyond the installation limit of 2º, and this aspect of their behavior was explored with two four-point bending tests.

The first test, RT2, was performed on a straight section of PVCO pipe without a joint. Figure 3.7 shows the four-point bending test setup for the second test, RT3, which included a joint restraint. Both specimens were supplied with a water pressure of approximately 517 kPa (75 psi) during the tests. The test specimens were supported vertically on rollers and loaded at the one-third points using a load spreader beam. As shown in Fig. 3.7, the distances between end supports and pipe loading points were each 711 mm (28 in.). Thus, the moment arms for uniform bending to the central portion of the pipe sections were both 711 mm (28 in.).

Figure 3.7 also shows typical instrumentation for both tests including string potentiometers to measure vertical displacements along the specimen and strain gages

at key locations along the specimen. The jointed specimen, RT3, was also fitted with linearly varying displacement transducers (LVDTs) and string potentiometers at the crown and invert of the joint to measure joint opening and relative displacements between the pipe and restraints.

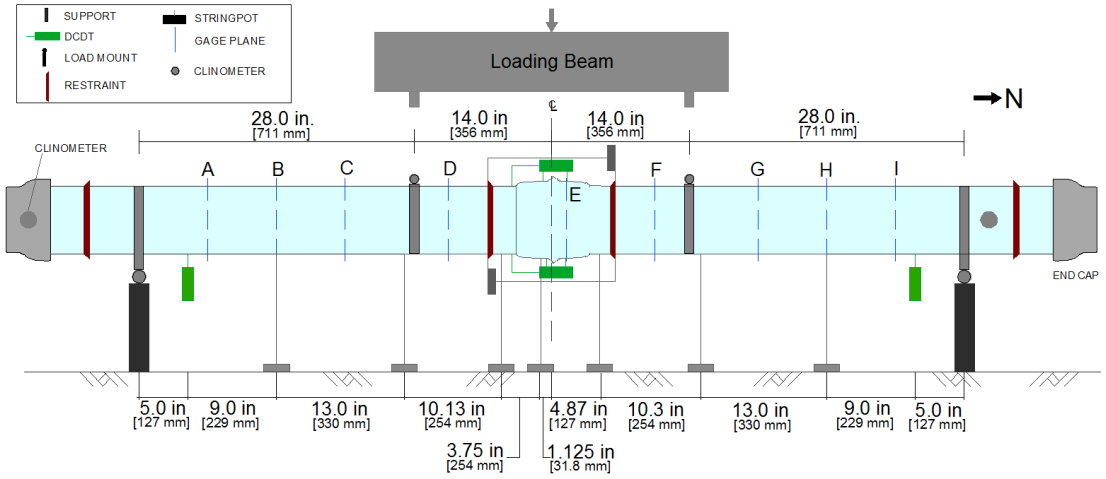

Figure 3.7. Four-point bending test setup for rotation test RT3

Figure 3.8 compares the moment-rotation relationships derived from the experimental results for Specimens RT2 and RT3. The secant rotation angle, θ_s, for Specimen RT2 is calculated as

$$\theta_s = \tan^{-1}\left(\Delta_r / l_r\right) + \tan^{-1}\left(\Delta_l / l_l\right) \qquad (3.4)$$

for which Δ_r and Δ_l are the relative displacements between the center of the pipe and the locations of applied force from the load spreader beam on the right and left sides of the pipe center, respectively, and l_r and l_l are the corresponding distances between the locations of applied force and pipe center. Because there is constant moment and curvature in the pipe between the applied loads, θ_s is uniquely related to curvature in the

center section of the pipe. It is, however, an index value, which provides the relative rotation of secant lines between the locations of driving force and pipe center.

A maximum moment of 4.44 kN-m (39.3 kip-in.) was measured in Specimen RT2 by strain gages at the crown and invert of the pipe at a vertical displacement of 88.9 mm (3.5 in.) and $\theta_s = 3.7°$. At this bending level, the axial strain gages at the pipe center peaked at 1.5%, indicating the onset of plastic yielding, and the test was discontinued.

The test setup for Specimen RT3 was similar to that for Specimen RT2 except that it included a restrained joint centered between loading points. In the moment-rotation plot for Specimen RT3, the joint rotation was measured directly using the LVDT measurements at the pipe crown and invert. It represents a true measure of rotation in comparison to the relative rotation metric for Specimen RT2.

Specimen RT3 was loaded to a maximum moment of 3.31 kN-m (29.3 kip-in.) and 6.8° of joint rotation without failure. At an imposed actuator displacement of 114.3 mm (4.5 in.) the test was discontinued. At gage planes located 267 mm (10.5 in.) on either side of joint center (planes D and F in Fig. 3.7) maximum compressive strains of 1.5% and maximum tensile strains of 1.7% were measured at the crown and invert of the pipe, respectively. These strain levels indicated the onset of plastic yielding of the pipe between load points and provided justification to discontinue the test before progressive strain softening occurred.

Figure 3.8 shows that the restrained joint exhibits substantial nonlinear behavior, with increasing rate of rotation in response to increased moment. The relatively flexible response of the restrained joint allowed the PVCO pipe to accommodate deformation

with relatively large rotation at low to moderate levels of moment. This type of response helps the jointed pipe adjust to ground deformation perpendicular to the longitudinal axis of the pipeline while imposing relatively low levels of bending stress in the pipe.

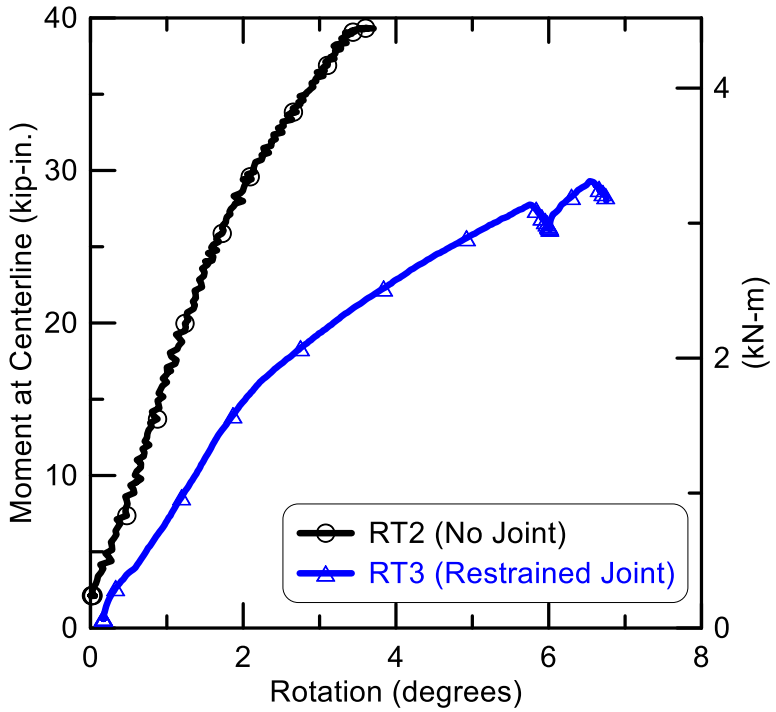

Figure 3.8. Moment-rotation of four-point bending tests RT2 and RT3.

Following the testing of Specimen RT3 the pipe restraints were removed from the specimen and observations were made at the location where the pipe clamps were fastened to the pipe. The presence of indentations in the pipe wall and localized plastic deformation around the segments at both the crown and invert of the pipe suggest that Specimen RT3 was nearing its maximum sustainable deformation at a rotation of about 6.8°.

3.4.4 Full-Scale Fault Rupture Test

The performance of PVCO bell-and-spigot pipes and restrained joints was evaluated in a full-scale soil-interaction simulation performed at the Cornell University Large-Scale Lifelines Testing Facility. The facility is capable of simulating fault rupture effects with as much as 1.8 m (70 in.) of strike-slip fault offset on pipelines as large as 600 mm (24 in.) in diameter.

Figure 3.9 shows a plan view of the test layout. The pipeline consisted of three pipe segments connected with bell-and-spigot joints and the pipe joint restraints previously described. A typical 6.1-m (20-ft)-long PVCO pipe section was centered over the fault and oriented at a 50° crossing angle with respect to the rupture plane. The total length of the pipeline buried in soil was approximately 39 ft (11.9 m). The pipeline was rigidly fixed to each end of the test basin. The direction and orientation of fault movement imposed a combination of axial tensile and lateral loading to the pipeline during the test.

The specimen was buried in partially saturated, glacio-fluvial sand that was compacted to have an average friction angle of approximately 42°, equivalent in strength to that of a typical medium dense to dense granular backfill. The pipeline was placed on 200 mm (8 in.) of soil and covered in approximately 200 mm (8 in.) lifts with a depth of burial to the pipe crown of 760 mm (30 in.). The soil dry unit weight was measured in situ using a nuclear density gage in accordance with ASTM D6938 (2010b). Soil moisture content was measured by direct sampling in accordance with ASTM D2216 (2010a). Measurements taken at 40 locations during soil placement showed an average dry unit weight of 16.4 kN/m^3 (105.9 lb/ft^3) and an average moisture content of

4.0%. Further descriptions of the RMS sand properties and strength characteristics are provided by O'Rourke (2010).

During the test the south part of the basin remained stationary while the north part was displaced, as illustrated in Fig. 3.9, by four displacement controlled large-stroke actuators to cause soil rupture and slip at the interface between the two sections of the test basin. The imposed displacement is characteristic of left lateral strike slip fault rupture, and is representative of the most severe ground deformation that occurs along the margins of liquefaction-induced lateral spreads and landslides.

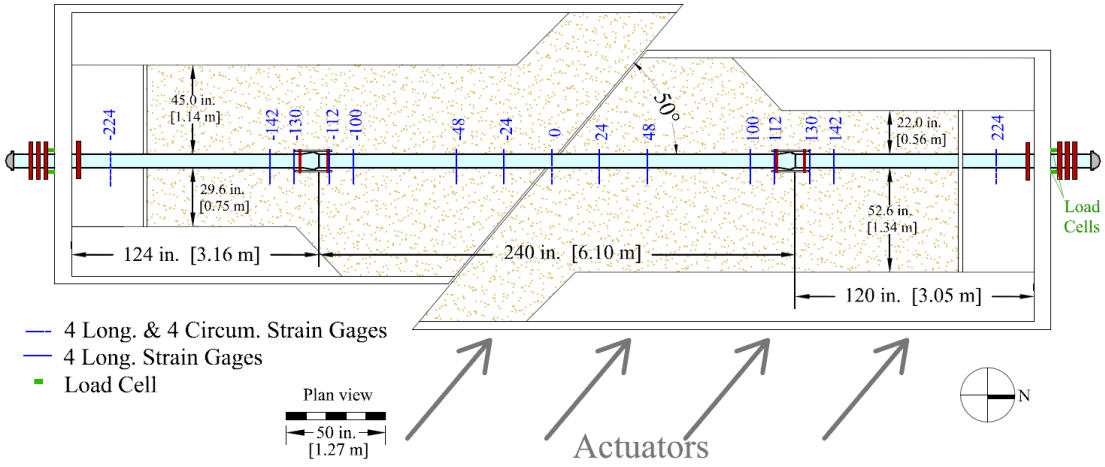

Figure 3.9. Plan view of PVCO pipeline centered specimen in test basin

Extensive instrumentation was used to measure pipeline response. The pipeline was fitted with seventy-two strain gages installed at fifteen locations along the specimen to measure axial and circumferential strains and evaluate axial forces and bending moments. Strain gages were positioned at the crown (C), invert (I), east (E) springline, and west (W) springline of the pipe. Strain gage locations were chosen on the basis of the expected deformed shape and axial behavior of the pipeline as determined from the

axial pull and bending tests, as well as the results of preliminary 2D finite element analyses of the test. There were four LVDTs at each joint to measure relative joint and restraint movements and to evaluate joint rotation. Four load cells were placed outside the pipe basin at each end, reacting between the test basin structural frame and pipe end restraint to measure axial force. The pipe was pressurized with an approximately constant 552 kPa (80 psi) of water pressure during the test.

3.4.5 Full-Scale Fault Rupture Results

The north box was displaced at a rate of 50 mm/minute (2 in./minute). At a fault displacement of roughly 320 mm (12.6 in.) there was an audible "pop", the pipeline depressurized, and the test was stopped. The 320 mm (12.6 in.) of fault displacement corresponds to 206 mm (8.1 in.) of axial extension of the test basin and pipeline. Following excavation, a full circumferential fracture of the center pipe was observed just north of the north restraint at the south joint. As observed during the restrained joint tensile test, the fracture pattern propagated from indentations in the pipe wall caused by the joint restraint clamps.

Strains increased steadily as fault displacement increased from 0 to 320 mm (0 to 12.6 in.). Figure 3.10 shows the maximum average axial and bending strains along the pipeline at failure. A maximum axial strain of 2.0% occurred at the fault rupture plane just before failure of the pipeline. Abrupt changes in axial and bending strains occurred at the joints, reflecting the resistance to axial movement mobilized by the restraints as well as the reduced flexural stiffness at the joints. Large axial strains near the rupture

plane coincide with the initiation of plastic pipe elongation at fault displacements greater than 305 mm (12 in.). A localized peak in axial strain was observed at the gage station just north of the south joint (gage plane -112), where pipeline rupture initiated at the pipe restraint clamp fastened near the spigot end of the pipe joint.

Bending strains, calculated as one half the difference between the west and east springline strains, were generated in the center section of the pipeline, within 254 mm (100 in.) either side of the fault. Bending strains were near zero at the fault, indicating an inflection point. Maximum bending strains of ±1.0% were measured at a distance of 610 mm (24 in.) south and north of the fault. The distribution of both the axial and bending strains reflect the anti-symmetric conditions of pipeline deformation.

The end forces measured by load cells at the south and north ends of the test basin were about 71 and 80 kN (16 and 18 kips) at failure, respectively. Axial force was also determined from longitudinal strains at gage stations closest to the ends of the pipeline (gage planes ±224 shown in Fig. 3.9). Because axial strains were beyond the linear range of stress-strain behavior it was necessary to consider a reduced modulus at higher strain levels. A strain-dependent longitudinal modulus was defined from the tensile coupon data previously presented. Axial pipeline force calculated from longitudinal strains, cross-sectional pipe area, and the strain-dependent modulus were within 5% of the values measured by the load cells. The axial force along the pipe was similarly calculated and found to be largest at the fault crossing, equal to roughly 110 kN (25 kips).

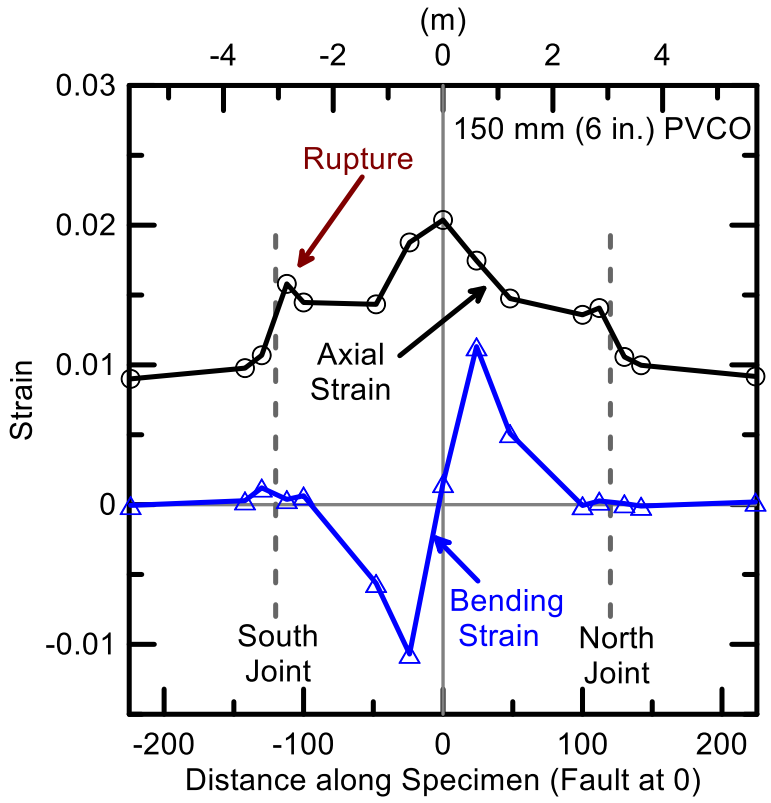

Figure 3.10. Average axial and bending strains at failure during split-basin test

3.5 Concluding Remarks

This paper presents results from an experimental program evaluating material properties and mechanical characteristics of 150-mm (6-in.)-diameter Bionax PVCO water distribution pipelines fitted with mechanical pipe joint restraints and provides information regarding the pipeline's ability to accommodate deformation. Stress-strain characteristics of the PVCO pipe were derived from tensile coupon and internal pressure tests. Estimates of longitudinal elastic modulus, $E_l = 3.10$ GPa (450 ksi), and Poisson's ratio, $\nu_{l\theta} = 0.37$, were determined from uniaxial tensile coupon tests while the circumferential elastic modulus and Poisson's ratio were estimated as $E_\theta = 3.71$ GPa

(538 ksi) and $\nu_{\theta l} = 0.44$, respectively. Axial tensile and compression tests for joints with and without mechanical joint restraints provide axial force-displacement relationships for the joints and predictions of joint failure under extreme loading conditions. Moment-rotation relationships are derived from four-point bending test results offering a characterization of the bending behavior of the pipe and restrained joint.

The PVCO pipeline was able to accommodate significant fault movement through axial tensile and bending strains in the pipe in combination with modest levels of axial slip at the restrained joints. Although the pipeline failed because of stress concentration where the pipe restraint clamps were fastened to the pipe, the axial stress in the pipeline was sufficient to induce relatively large levels of strain in the low modulus PVCO material. The level of axial tensile strain mobilized in the pipeline varied between 1% and 2% at failure.

Overall the pipeline was able to accommodate 206 mm (8.1 in.) of axial extension, corresponding to an average tensile strain of 1.67% along the pipeline. Such extension is large enough to accommodate the great majority of liquefaction-induced lateral ground strains measured by high resolution LiDAR after each of four major earthquakes during the recent Canterbury Earthquake Sequence in Christchurch, NZ (O'Rourke et al., 2012).

The testing provides a characterization of restrained joint behavior in response to deformations imposed by faulting, liquefaction, landslides, mining, dewatering, and construction activities. The findings are useful in practice for the design and risk assessment of PVCO pipelines subjected to large ground deformation.

3.6 Acknowledgments

Appreciation is extended to IPEX Inc. and their professional staff for providing the pipe specimens and support for this testing program. In particular, the assistance of Jeff Phillips of IPEX Inc. is gratefully acknowledged.

REFERENCES

ASTM. (2010a). "Standard specifications for elastomeric seals (gaskets) for joining plastic pipe." *F477*, West Conshohocken, PA.

ASTM. (2010b). "Standard test method for in-place density and water content of soil and soil-aggregate by nuclear methods (shallow depth), *D6938*, West Conshohocken, PA.

ASTM. (2010c). "Standard test methods for laboratory determination of water (moisture) content of soil and rock mass." *D2216*, West Conshohocken, PA.

ASTM. (2011). "Standard specification for joints for plastic pressure pipes using flexible elastomeric seals." *D3139 − 98*, West Conshohocken, PA.

ASTM. (2013a). "Standard test method for obtaining hydrostatic design basis for thermoplastic pipe materials or pressure design basis for thermoplastic pipe products," *D2837*, West Conshohocken, PA.

ASTM. (2013b). "Specification for oriented polyvinyl chloride PVCO pressure pipe." *F1483*, West Conshohocken, PA.

ASTM. (2013c). "Standard test methods for tension testing of metallic material." *E8/E8M-13a*, West Conshohocken, PA.

AWWA (American Water Works Association). (2009). “Standard for oriented polyvinyl chloride (PVCO) pressure pipe, 4 in. through 24 in. (100 mm through 600 mm) for water, wastewater, and reclaimed water service.” *C909*, Denver, CO.

Balkaya, M., Sağlamer, A. & Moore, I. D. (2012). “Conta bağlantılı PVC boruların deformasyon davranışının laboratuvar deneyleri ile belirlenmesi (Laboratory experiments to determine the deformation behavior associated with gasketed PVC),” İTÜDERGİSİ/d, 10 (4).

CSA (Canadian Standards Association). (2013). “Molecularly oriented polyvinylchloride (PVCO) pipe for pressure applications.” *B137.3.1*. Mississauga, Ontario.

Extrusion Technologies Inc. (2003). “Ultra-BlueTM CIOD molecularly oriented PVC pressue pipe: pressure class 200 psi – AWWA C-909.” http://www.pwpipe.com/literature/w/ubciodcl200short.pdf.

Ford Meter Company Inc. (2014). “Pipe restraints and adapter flanges for PVC, ductile iron and steel pipe.” Wabash IN, http://www.fordmeterbox.com/catalog/u/ujpeg.pdf.

Michel, C., and Akkerman, J. (2012). “A study assessing the performance of O-PVC in pressure pipes,” *Proc. Plastic Pipes Conf. Assoc*., Barcelona.

O’Rourke, T.D., Jeon, S-S., Toprak, S., Cubrinovski, M., & Jeon, J.K. (2012). “Underground lifeline system performance during the Canterbury earthquake sequence*,” Proc. 15th World Conference on Earthquake Engineering*, Lisbon.

O’Rourke, T.D., Bonneau, A., Pease, J., Shi, P., and Wang, Y. (2006). “Liquefaction ground failures in San Francisco.” *Earthquake Spectra, EERI Special 1906 San Francisco Earthquake*, **22**(52), 691-6112.

O'Rourke, T. D., Jeon, S.-S., Toprak, S., Cubrinovski, M., Hughes, M., Ballegooy, S., and Bouziou, D. (2014). "Earthquake response of underground pipeline networks in Christchurch, NZ," *Earthquake Spectra*, **30**(1), 183-204.

O'Rourke, T. D. (2010). "Geohazards and large, geographically distributed systems," *Géotechnique*, **60**(7), 505–543.

Carleo, J., ed. (2012). "Handbook of PVC pipe design and construction." *PVC Pipe Association*. New York, NY. 5th Ed.

Rahman, S., and Watkins, R. (2005). "Longitudinal mechanics of buried thermoplastic pipe: analysis of PVC pipes of various joint types." *American Society of Civil Engineers (ASCE) Pipelines Conf*, Houston, TX.

CHAPTER 4

JOINTED PIPELINES RESPONSE TO TUNNELING INDUCED GROUND DEFORMATION

ABSTRACT

This paper presents the results of soil/pipeline interaction modeling for vertical and horizontal ground movements caused by tunneling, involving jointed cast iron (CI) and ductile iron (DI) pipelines perpendicular to the tunnel centerline that (1) extend beyond the width of the settlement profile and (2) connect through 90° tees with a pipeline parallel to the tunnel. The latter case is important because it can result in pullout and leakage at the tee in response to lateral soil movements. The modeling incorporates the results of large-scale laboratory tests to characterize the axial force vs. displacement and moment vs. rotation relationships of DI and CI joints, and focuses on soil displacements induced by a 6.1-m (20-ft) diameter tunnel in clay and another in sand, both with cover to depth ratios of 1.15. Limit states for joint pullout and rotation at various leakage levels, as well as allowable tensile strain for pit cast iron pipe, are discussed and used in the modeling. The analytical results show that the response to tunneling in sand for condition (1) is accompanied by joint rotations and maximum tensile strains that exceed those for tunneling in clay by a factor as high as two to three for the same centerline settlement and pipe diameter. Ductile iron joint rotations are well below the limits for metal binding and far less than the rotational capacity at first leakage. Moreover, DI

joint pullout is minimal, and maximum tensile strains are below yield conditions. The maximum tunnel settlement associated with the initiation of leakage at a CI tee for condition (2) is sufficiently low that CI tee locations within the width of the settlement trough should be regarded as a potentially high risk situation. In contrast to CI tees, pullout at DI tees is not a major risk, although pullout at push-on joints connected to tees should always be checked when encountered during tunneling. Observations and conclusions are presented that provide guidance for design, operational management, and risk assessment.

4.1 Introduction

Substantial research has been performed on the characterization of ground movements caused by tunneling (e.g., Peck, 1969; O'Reilly & New, 1982; Mair & Taylor, 1997; Cooper et al., 2002) and the influence of such movements on the response of underground pipelines (e.g., Attewell et al., 1986; Bracegirdle et al., 1996; Klar et al., 2005; Vorster et al., 2005; Klar et al., 2008). This paper expands on previous research by examining how jointed pipelines respond to tunneling induced vertical and horizontal soil movements, using the most recent research findings on the performance of DI and CI pipelines. Ductile iron pipelines with push-on joints are widely used in current practice for new installations and replacements in water distribution systems, whereas CI pipelines were used extensively in the past, and represent a large fraction of the current pipeline inventory of many water and some gas distribution networks. Focusing on DI and CI pipelines not only covers a large fraction of the piping in current use, but

covers a wide range of performance in the existing pipeline inventory, thus bracketing the response to ground deformation that can be anticipated in jointed pipeline systems. By concentrating on a rigorous and detailed characterization of pipeline performance, this study is able to show what aspects of the ground movement modeling are most important for assessing the risk of pipeline failure as well as the sensitivity of jointed pipeline response to different soil conditions and variations in the ground movement modeling parameters.

This paper begins with a summary of DI and CI pipeline performance, with emphasis on the characterization of axial force vs. displacement and moment vs. rotation relationships for DI and CI joints that are consistent with the results of large-scale laboratory tests. Limit states for the onset of leakage in DI and CI joints are selected and justified on the basis of the large-scale test data. The finite element (FE) modeling for soil/pipeline interaction is described next, with a discussion of how soil reaction normal and frictional force parallel to the longitudinal pipe axis are simulated and coupled with rotation and pullout of the pipeline joints and axial compression/tension and bending in the pipe segments. The models selected for distributed vertical and horizontal soil movements caused by tunneling in clay and sand are described. The analytical results from FE soil/pipeline interaction simulations are presented and discussed for two cases involving jointed pipelines perpendicular to the tunnel centerline axis that (1) extend well beyond the width of the settlement profile and (2) connect through 90° tees with a pipeline parallel to the tunnel centerline axis. The latter case is important because it can result in pullout and leakage at the tee in response to lateral soil movements. The analytical results are summarized and discussed for

nominal 150-mm and 300-mm (6 and 12 in.)-diameter pipelines. Pipelines with diameters ≤ 300 mm (12 in.) comprise 99% of gas distribution pipelines in the U.S. (PHMSA, 2015) and a large portion of water distribution systems. For example, approximately 90% of the water distribution system operated by the Los Angeles Department of Water and Power involves pipe diameters ≤ 300 mm (12 in.) (Davis 2015). Recommendations are made for the identification of pipeline conditions at highest risk of leakage, governing modes of pipeline failure, and sensitivity of pipeline response to movements in clay vs. sand as well as changes in the parameters for modeling distributed ground movements.

4.2 Cast Iron Pipelines

The characterization of CI pipeline response to tunneling induced ground deformation is drawn from various investigations of CI pipeline properties (e.g., Prior, 1935; Taki & O'Rourke, 1984; Rajani, 2012) and pipeline performance under differential ground movement (e.g., Attewell et al., 1986; Harris & O'Rourke, 1983; Rajani & Abdel-Akher, 2013), with only the salient features of these investigations summarized herein. Characterization involved the evaluation of relevant CI pipe properties and the development of axial force vs. pullout and moment vs. rotation relationships for CI joints.

4.2.1 Cast Iron Pipe

Cast iron pipelines currently used in U.S. gas and water distribution systems were installed primarily between 1870 and 1960 (Taki & O'Rourke, 1984). Pipe installed

between 1870 and 1930 was predominantly manufactured by vertical pit casting to produce nominal 3.66-m pipe lengths. After 1930 most CI pipe was manufactured by centrifugal casting and installed in nominal 5.50-m lengths. This study focuses on the majority of CI pipelines in current service, which are composed of older pit cast iron.

Extensive investigations of pit cast iron pipe (Harris & O'Rourke, 1983; Taki & O'Rourke, 1984) indicate that an allowable incremental tensile strain of 0.0006, or 600 microstrain (600 με), provides in general a suitable margin of confidence against pipe failure, provided that significant corrosion and defects are absent. This allowable strain takes account of residual strain that may already be present in the pipe. Using the results of extensive full-scale field tests to measure bending strains induced during pipeline installation, backfilling, and subsequent traffic loads (e.g., O'Rourke & Kumbhojkar, 1984; Stewart et al., 1989), a tensile bending strain of 250 με was selected to represent residual strain conditions. When the allowable incremental and residual strains are added, the resulting strain is less than one-fourth the average failure strain measured in tensile tests performed on pit cast iron specimens from pipelines removed from service (Taki and O'Rourke, 1984).

A secant modulus, E, of 75.8 GPa (11,000 ksi) was found to be strain compatible with the allowable tensile strain (Taki & O'Rourke, 1984) and was selected for use in this study. Soil-pipeline interaction sensitivity analyses were performed with E = 75.8 GPa (11,000 ksi) and E modeled with the hyperbolic constitutive law proposed by Rajani (2012). Consistent with recommendations by Attewell et al. (1986), little to negligible difference in the results was found at the low levels of residual and allowable

incremental strain discussed above. Considering tensile test data for pit and centrifugally cast iron from Johnson (1889), Schlick & Moore (1936), and Taki & O'Rourke (1984), a range of E was identified from 75.8 to 128 GPa (11,000 to 18,500 ksi) to use in FE simulations.

4.2.2 Axial Force vs. Displacement of CI Joints

Figure 4.1 shows a profile view of a typical CI joint, which connects the spigot and bell ends of adjoining pipes. The annular space between the spigot and bell is packed with hemp or jute yarn and caulking. Lead and cement are the caulking materials in the great majority of CI joints, with lead used substantially more often than cement. Prior (1935) indicates that the lead caulking depth is typically 57 mm (2.25 in.), while Attewell et al. (1986) suggest depths of 44 to 57 mm (1.75 to 2.5 in.), depending on diameter.

This work focuses on CI joints with lead caulking and soft hemp or jute, typical of most water and some gas distribution pipelines. Such joints are less resistant to pullout and more flexible in rotation than cement-caulked joints and joints in gas mains where the yarn is impregnated with hardened hydrocarbons (Harris & O'Rourke, 1983). Since the onset of leakage is related to the amount of pullout and/or rotation, joints with lead and soft yarn are most susceptible to the effects of differential ground movement. They provide for a conservative estimate of performance for pipelines with stiffer and stronger packing materials.

The relationship between joint pullout force at first slip, $F_{j,slip}$; CI-lead adhesion, C_A; and joint geometry is

$$F_{J,slip} = \pi D_{os} d_L C_A \qquad (4.1)$$

where D_{os} is the outer spigot diameter and d_L is the lead caulking depth as illustrated in Figure 4.1.

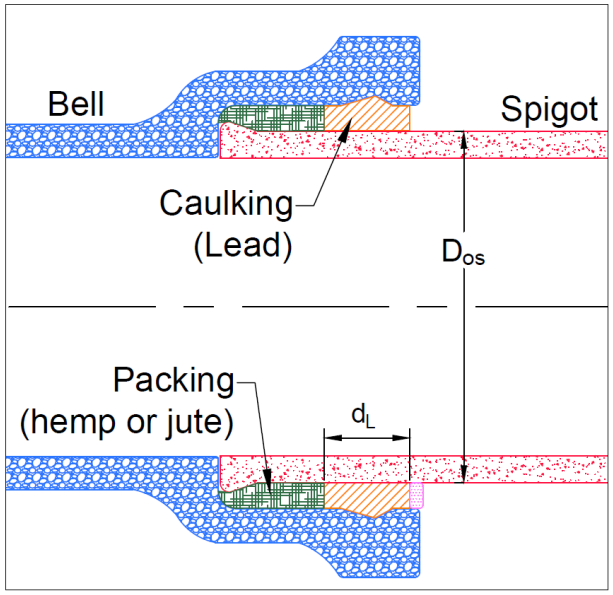

Figure 4.1. Cross-section of a typical CI joint

Through Eqn. 4.1 the C_A corresponding to first leakage was calculated from the results of pullout tests under internal water pressure ranging from 140 to 2500 kPa (20 to 360 psi) on 15 specimens of lead caulked CI joints ranging from 150 to 1500 mm (6 to 60 in.) in nominal diameter (Prior, 1935), and two similar specimens of nominal 300-mm (12-in.)-diameter CI joints tested under nitrogen pressure of 2.0 kPa (0.29 psi) (O'Rourke et al., 1996), to develop the cumulative frequency plot in Figure 4.2. All tests were conducted with CI joints having a lead caulking depth of approximately 57 mm (2.25 in.). Detailed information about the joint pullout tests and tabulation of experimental data are provided in Appendix A.

A normal cumulative probability curve, developed from the mean and standard deviation of the data, is shown in Figure 4.2. The Lilliefors (1967) goodness of fit test shows that a normal distribution is verified at the 5% significance level, and thus represents a good fit of the data.

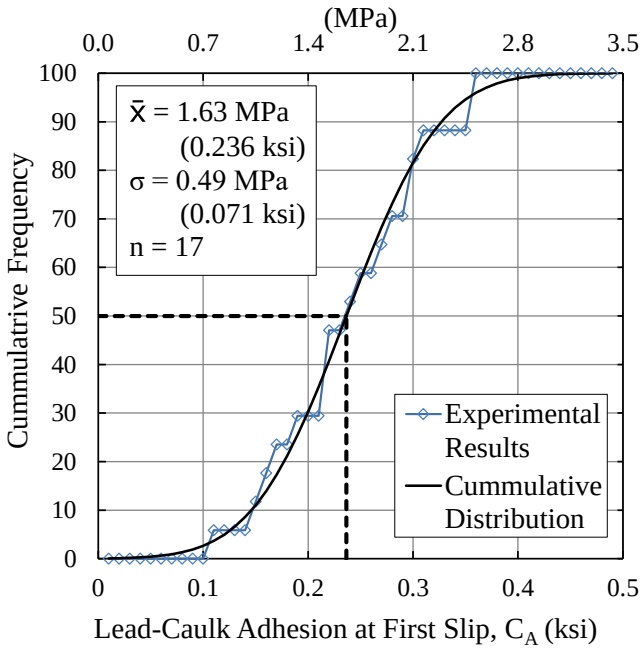

Figure 4.2. Cumulative frequency plot of CI-lead adhesion at first leakage in CI joints

Figure 4.3 shows the normalized force vs. displacement plots for five typical pullout tests, including two with internal gas pressure and three with internal water pressure. The measured axial force is normalized with respect to the pullout force at first leakage. Due to limitations of measuring methods used by Prior (1935), initial joint stiffness data at displacements less than 0.79 mm (0.031 in.) are not reliable. The O'Rourke et al. (1996) pull-out tests offer the most detailed data available for assessing initial joint stiffness and provide the basis for the idealized axial pullout curve shown as a dashed line in the figure. A well-defined break in the slope of these curves occurs at 0.51 mm

(0.02 in.), after which there is variation in the normalized force vs. displacement relationships.

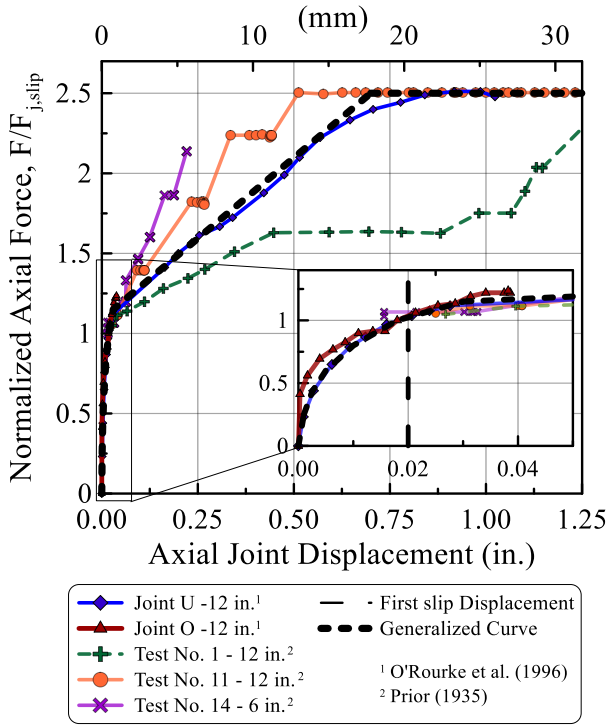

Figure 4.3. Normalized joint pullout force vs. axial displacement for lead-caulked CI joints

The inset diagram in the figure shows an expanded view of the normalized force vs. axial displacement plots at low levels of movement. There is a clear transition to a flatter slope at about 0.51 mm (0.02 in.). This displacement occurs at the onset of leakage and corresponds to a notable change in the rate at which resistance is mobilized against pullout. This slip between the lead and CI surface generates leakage paths. As discussed by O'Rourke et al. (1996), lead is both malleable and subject to creep that can actually close off leakage paths with additional sustained deformation. Thus, the slip at the onset of leakage can be identified, but a clear and consistent leakage level and trend in leakage cannot be quantified with the current experimental evidence.

4.2.3 Moment vs. Rotation of CI Joints

Harris & O'Rourke (1983) explored the relationship among moment, rotation, and leakage with four point load tests of CI joints with nominal diameters of 100, 150, and 200 mm (6, 4, and 8 in.) under nitrogen pressures of 3.0 kPa (0.43 psi) consistent with the operation of low pressure gas mains. These joints were sampled from the field after 50-80 years of operation. Figure 4.4 shows a schematic of the four-point bending setup. Figure 4.5 presents the data from 19 tests on lead-caulked pit CI joints expressed as leakage vs. joint rotation for 10% through 90% exceedance limits. Each plot represents the leakage at which a particular percentage of the test specimens exceeded the leakage rate shown. The total number of specimens involved in the testing is also plotted with respect to rotation. As the rotation increased, some of the tests were discontinued because the loads exceeded levels consistent with safety standards adopted during the tests and a number of pipes fractured, thereby reducing the number of specimens. Detailed information about the moment vs. rotation tests and tabulation of experimental data are provided in Appendix B.

There are several aspects of the figure worth noting. First, the onset of leakage occurs at approximately 0.2°, with maximum leakage at approximately 0.5°. There was actually a decline in leakage at all exceedance levels after 0.5°, similar to the reduction in leakage observed in the pullout tests in response to additional deformation of the lead caulking. Leakage eventually increased at large rotations exceeding 3-4° (not shown in the figure) in those joints that did not fail. No bell failures were observed until about

0.5°, after which there was a steady increase in the number of failures as rotation increased.

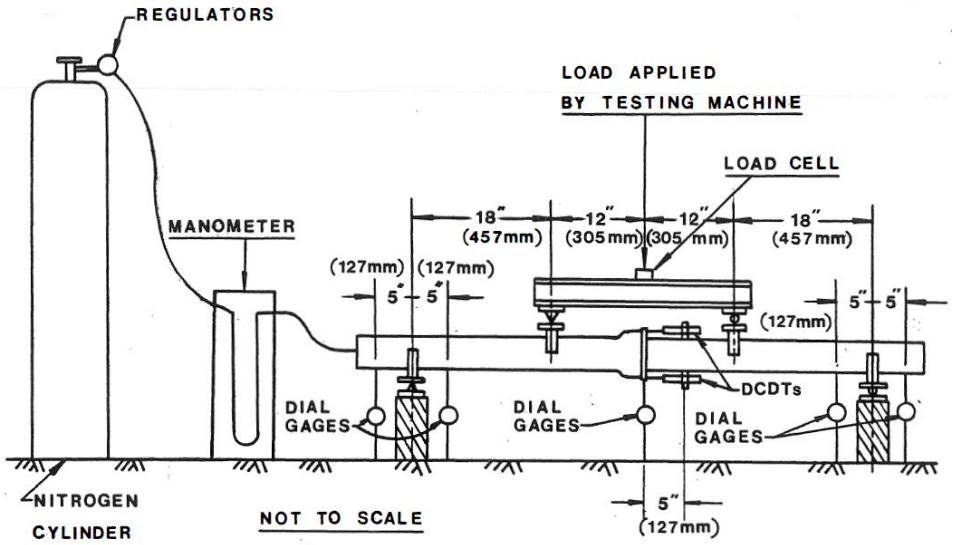

Figure 4.4. Illustration of four-point bending test setup (Harris & O'Rourke, 1983)

O'Rourke & Trautmann (1980) proposed an equation for the moment at first slip between the lead and CI surface, $M_{J,slip}$, in which C_A, d_L, and D_{os} are as defined for Eqn. 4.1, as follows

$$M_{J,slip} = \frac{3}{8}\pi D_{os}^2 C_A d_L \qquad (4.2)$$

Using Eqn. 4.2 with the mean C_A from Figure 4.2 and d_L = 57 mm (2.25 in.) as a normalizing parameter, moment vs. rotation plots were developed from four bending tests on nominal 500-mm-diameter CI joints with no internal pressure (Prior, 1935) and nominal 150-mm-diameter CI joints under 3 kPa (0.43 psi) gas pressure (Harris & O'Rourke, 1983), and are shown in Figure 4.6. In Figure 4.6(a) a change in the normalized moment vs. rotation plots can be identified at about 0.2°. Both O'Rourke

& Trautmann (1980) and Rajani & Abdel-Akher (2013) attribute this change in slope to deformation of the lead caulking, related to first slip between the lead and CI surface, that generates leakage.

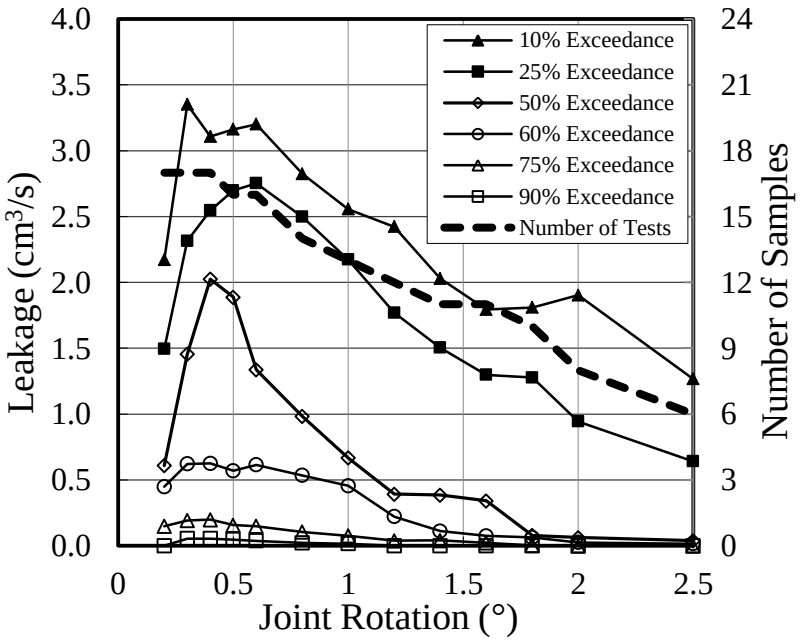

Figure 4.5. Sample size and leakage rate exceedance levels for 100, 150, and 200-mm (4, 6, and 8-in.) diameter CI joint specimens (adapted from Harris & O'Rourke, 1983)

Figure 4.6(b) is an expanded view of the normalized moment vs. rotation plots to 0.6° rotation. The rotation corresponding to a slope reduction in the plots varies between 0.1 and 0.4°. The dashed lines show the trilinear moment vs. rotation relationships for 150 and 500-mm (6 and 20-in.) diameter joints adopted in this work for FE analyses. Initial joint stiffness is given by $k_1 = M_{j,slip}/\theta_1$ where $M_{j,slip}$ is calculated from Eqn. 4.2 assuming a mean C_A and d_L = 57 mm (2.25 in.), and θ_1 = 0.2°, the rotation at first slip. As recommended by Rajani & Abdel-Akher (2013), beyond 0.2° of rotation the initial joint stiffness is reduced by 75% for diameters less than 400 mm (16 in.), and 65% for

larger diameters. Based on the available test data, this study introduces a third change at 1.0°, reducing the stiffness of the curve to 20% and 12% of the initial stiffness for 500 and 150-mm (20 and 6-in.)-diameter joints, respectively.

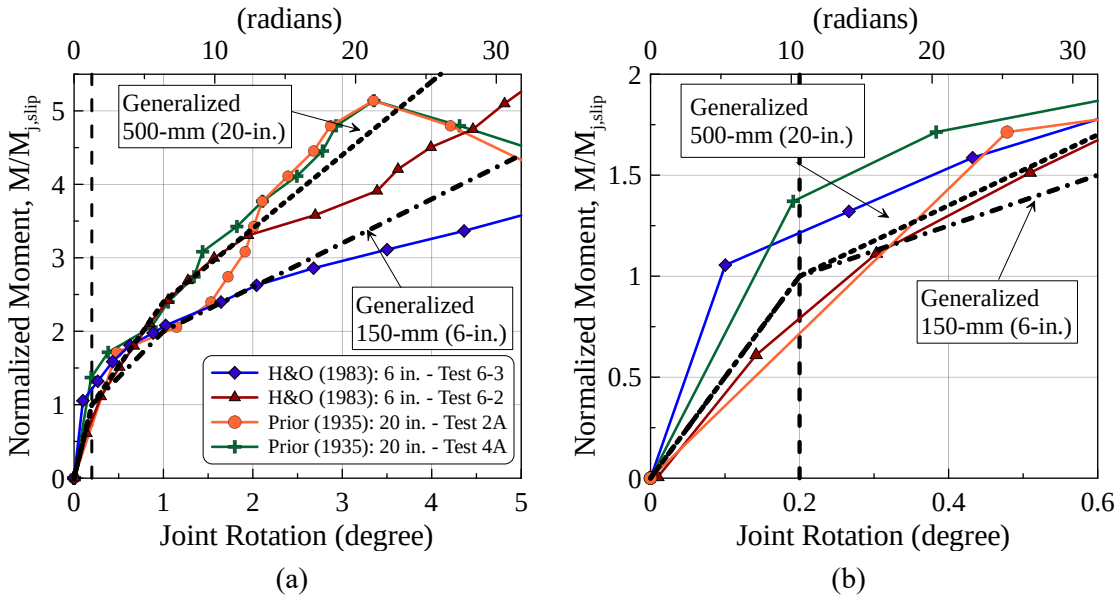

Figure 4.6. (a) Normalized moment-rotation relationships for 150 and 500-mm (6 and 20-in.) diameter CI joints and (b) expanded view of rotation at first slip

4.3 Ductile Iron Pipelines

Ductile iron pipe in U.S. practice conforms to ANSI/AWWA C151/A21.51 (AWWA, 2009). Typical stress vs. strain data from direct tension tests on pipe specimens of commercial grade DI are reported by Wham & O'Rourke (2015) and used in this work. The average ultimate strength of 460 MPa (66.7 ksi), yield strength of 311 MPa (45.1 ksi), and strain at failure of 10.4% associated with those tests exceed the minimum standard requirements. The average elastic modulus of 186,000 MPa (27,000 ksi) compares well with industry recommendations.

The DI pipelines most frequently used in water distribution systems are equipped with push-on joints for ease of installation. A typical 150-mm (6-in.) DI joint, which connects the spigot and bell ends of adjoining pipes, is shown in Figure 4.7. An elastomeric gasket provides a watertight seal. As illustrated in the figure, the maximum joint rotation before metal to metal contact, or metal binding, is nominally 5° when the spigot is inserted into the full depth of the bell. The limits of joint rotation have been recommended simply as the rotation until metal binding for full spigot insertion in the bell (e.g., Attewell et al., 1986; U.S. Pipe, 2015; American, 2015). This type of characterization is overly conservative.

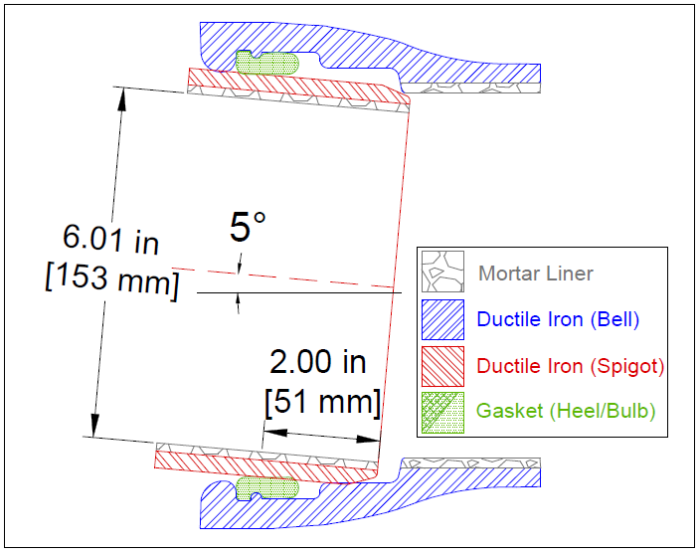

Figure 4.7. Typical 150-mm (6-in.) DI Joint cross-section with 5° rotation

Wham and O'Rourke (2015) developed a relationship among leakage, rotation, and moment at various levels of axial displacement from the results of 22 tests on DI joints with a nominal diameter of 150 mm (6 in.) under 380 kPa (55 psi) of internal water pressure. The relationship at first leakage is shown in Figure 4.8 as normalized joint

rotation (rotation divided by rotation at metal binding, 5°) vs. normalized pullout (axial displacement from the position of a fully inserted spigot divided by the maximum pullout, 51 mm (2 in.)). The experimental results are plotted for two combinations of normalized rotation and pullout at which there is metal binding and first leakage. Simplified, approximate limit states for metal binding and leakage are shown by the continuous and dashed lines, respectively.

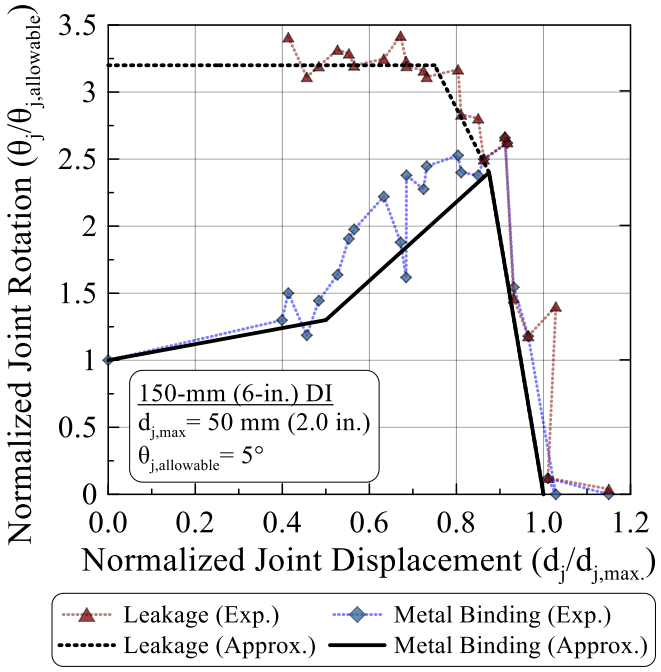

Figure 4.8. Pressure boundary for leakage of 150-mm (6-in.) diameter DI joint as a function of normalized joint rotation and axial displacement (adapted from Wham & O'Rourke, 2015)

The dashed line represents the pressure boundary for DI joints included in this study. Any combination of normalized rotation and pullout on and above this line coincides with joint leakage. Wham and O'Rourke (2015) show that the pressure boundary is

independent of load path and can be used for many different conditions of evolving rotation and pullout associated with complex ground deformation patterns.

Although Figure 4.8 is presented in terms of normalizing parameters, it is not intended for the 150 mm (6 in.) joint pressure boundary to be used for all DI pipe diameters and commercially available configurations. Similarly proportioned key dimensions for 100, 150, and 200 mm (4, 6, and 8 in.) DI push-on joints provide some justification for inferring comparable behavior. However, additional experimental testing or 3D FE analysis, as outlined by Wham & O'Rourke (2015), is necessary to confirm small diameter ($D \leq 200$ mm) behavior beyond metal binding, and to establish larger diameter joint response to combinations of joint pullout and rotation.

4.4 Soil Pipeline Interaction Model

The FE modeling used in this work follows procedures recommended for analyzing pipeline response to earthquake induced ground deformation (ASCE, 1984; Honegger & Nyman, 2004; O'Rourke et al., 2008). These procedures represent the standards currently adopted for design and ground movement risk assessment. Figure 4.9 illustrates the basic concept of the modeling process in which soil-pipe interaction relationships orthogonal and parallel to the pipeline longitudinal axis are modeled by spring-slider elements to simulate elasto-plastic response. This model has been enhanced in the current work to reflect improved characterization of soil-pipe interaction (e.g., Jung, 2010; Jung et al., 2013a and b) as well as more complex moment

vs. rotation and force vs. axial displacement relationships that govern the behavior of pipeline joints.

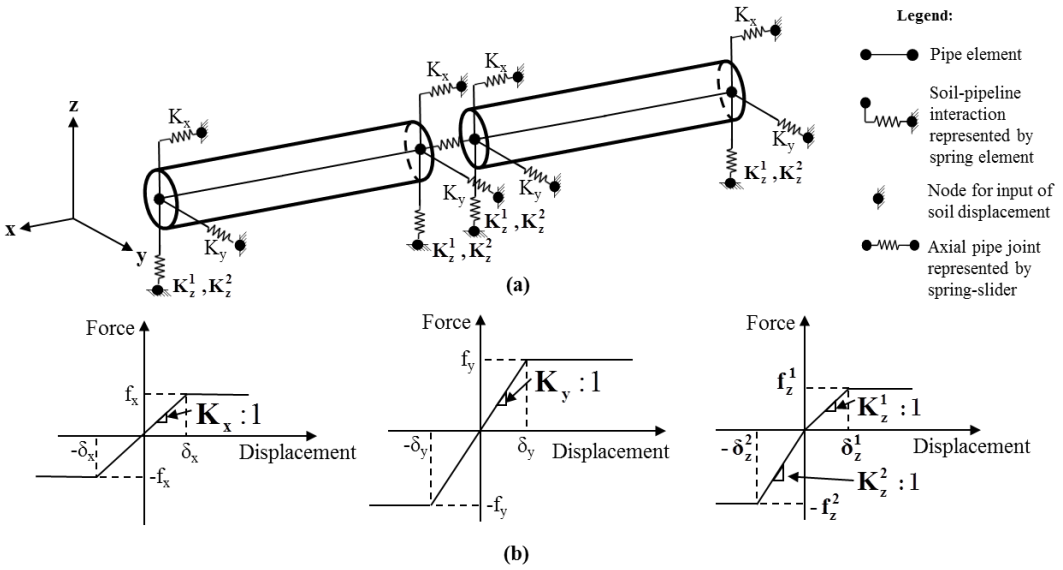

Figure 4.9. (a) Schematic of FE model and (b) bilinear force vs. displacement relationships at pipe-soil interface based on the elasto-plastic models recommended by ASCE (1984) and Honegger and Nyman (2004) [after Bouziou, 2015]

Figure 4.10 presents a schematic of the enhanced soil-pipeline interaction model with pipe elements, joints, and connection to a 90° tee. Displacements representing greenfield vertical and lateral soil movements caused by tunneling are conveyed to the nodes at the far sides of the gap and spring elements, thus simulating soil interaction with the pipe.

The model accounts for the coupled interaction between soil forces normal and parallel to the longitudinal axis. O'Rourke et al. (2015) and Argyrou (2016) provide a detailed description of coupled interaction modeling, and only its salient features are described herein.

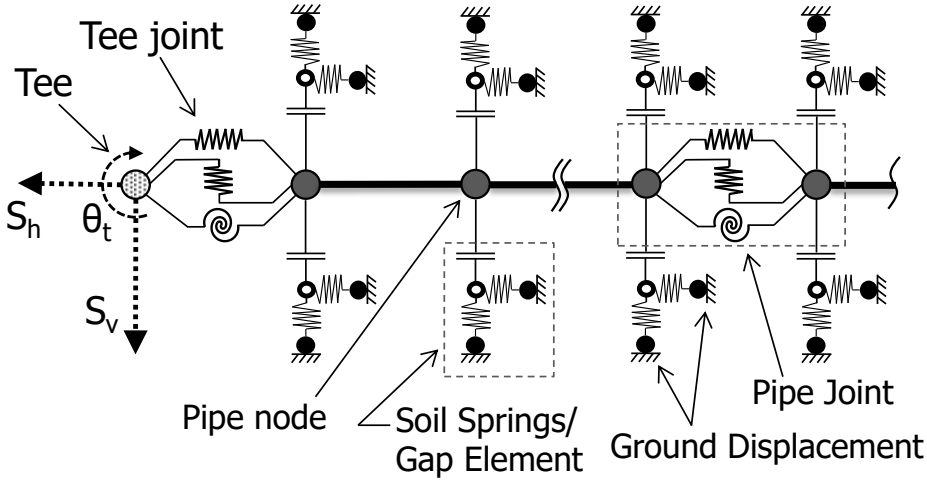

Figure 4.10. Schematic of enhanced 2D FE model including tee joint

The pipeline is composed of one-dimensional beam-column elements with elastic or elasto-plastic properties. The beam-column elements are able to accommodate geometric as well as material nonlinearity. The pipeline joints are modeled by rotational, transverse, and axial springs with linear, multi-linear, or non-linear characteristics developed from large-scale laboratory test results. The transverse spring stiffness is set to a very high value, which simulates the contact between the spigot and bell that governs the shear behavior of joints in the field. Soil reaction forces perpendicular to the longitudinal axis are modeled by springs or spring-like relationships that account for linear, multi-linear, or non-linear interaction with the pipe. As described below, soil shear forces conveyed to the pipe, which are parallel to the pipeline longitudinal axis, are modeled with gap elements that reflect either rigid plastic or elasto-plastic interaction along the soil-pipe interface.

There are several advantages to this modeling approach. It accounts simultaneously for axial and flexural pipe response as well as rotation and axial movement at the pipeline joints. The force-displacement relationship both normal and parallel to the pipeline longitudinal axis are developed from large-scale and centrifuge soil-pipeline test results (e.g., O'Rourke et al., 2008; Ha et al., 2008) and validated against the results of large-scale tests of pipeline response to ground rupture performance at the Cornell Large-Scale Lifelines Testing Facility (e.g., O'Rourke et al., 2015). The large-scale test validation applies to continuous steel and high density polyethylene pipelines in response to differential lateral ground movements as large as 1.2 m (4.0 ft). It also applies to DI pipelines with push-on joints in response to differential lateral ground movements on the order of 100 mm (4.0 in.), similar to the differential movements associated with tunneling simulated in this work.

The 2D FE model uses the analysis software ABAQUS (2014) in which the pipeline is represented by beam elements (type b33) and the soil resistance normal to the pipeline axis by nonlinear springs (type spring2). The springs are connected to the pipeline with uniaxial gap elements (type gapuni) that transfer forces parallel and perpendicular to their axes only when the corresponding normal springs carry compressive forces. This is achieved by allowing separation of the gap elements when tensile normal forces are activated in response to load relaxation and separation between soil and pipe.

The normal force per unit distance, p_N, transferred through the gap element parallel to the pipeline longitudinal axis is controlled by the Coulomb friction law, $p_N \tan\delta$, so it is proportional to the normal force acting on the pipeline at each level of deformation.

As an initial step, the displacements required to activate the normal forces for at-rest conditions are imposed on the transverse springs. With this adjustment, longitudinal frictional forces are activated to reflect at-rest conditions in the absence of normal forces triggered by relative soil displacement normal to the pipeline longitudinal axis. During simulation, incremental parallel and normal soil movements are applied simultaneously at the longitudinal and transverse spring nodes on each side of the pipeline elements.

4.5 Ground Movement Characterization

There has been substantial research focused on tunneling induced ground deformation and mathematical methods to describe the shape of the settlement profile (e.g., Peck, 1969; O'Reilly & New, 1982; Mair et al., 1993; Mair & Taylor, 1997; Marshall et al., 2012). Martos (1958) first proposed that the shape of the subsidence trough above mining excavations could be well represented by a Gaussian or normal distribution curve. Peck (1969) analyzed field measurements that showed the transverse surface settlement trough induced by tunneling followed a similar form. Based on settlement data from a variety of tunneling sites in the U.K. O'Reilly & New (1982) showed that the greenfield soil settlement trough above a tunnel may be reasonably represented by a Gaussian curve of the form

$$S_v(y) = S_{v,\max} \exp\left[\frac{-y^2}{2i^2}\right] \qquad (4.3)$$

defined by the maximum settlement at the tunnel centerline, $S_{v,max}$, and the horizontal distance to the inflection point, i, as a function of the horizontal distance from the tunnel

centerline, y. Figure 4.11 illustrates a transverse view of the tunnel and ground surface in which an enlarged view of the greenfield settlement profile is presented with $S_{v,max}$ and i_z located and labeled. The horizontal displacement profile, S_h, is also shown.

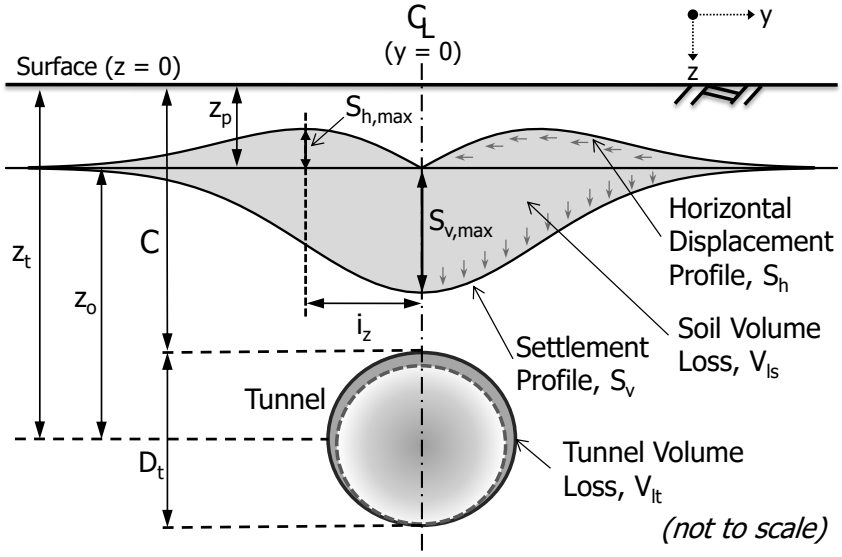

Figure 4.11. Transverse view of tunnel with settlement and horizontal movement distributions at depth of pipeline

O'Reilly & New (1982) showed by integration of Equation 4.3 that the volume of the settlement profile per unit advance, V_{ls}, is related to the maximum vertical settlement given by

$$V_{ls} = S_{v,\max} i \sqrt{2\pi} \qquad (4.4)$$

For constant volume materials, such as undrained clays, the volume V_{ls} is equivalent to the volume of soil lost as a result of tunneling, including soil excavated in excess of the intended tunnel cross-section as well as deformation of the tunnel lining. This volume loss is often expressed as a percentage, $V_{l\%}$, of the intended cross-sectional area of the tunnel.

4.5.1 Profile Width Parameter

Several authors (O'Reilly & New, 1982; Mair et al., 1993; Mair & Talyor, 1997) have noted that the value of i is related to the relative vertical distance between the tunnel axis and depth of interest. An empirical profile, or trough, width parameter, K, was recommended by O'Reilly & New (1982), and adopted by others, to relate trough width to ground conditions. Assuming constant volume deformation, the width of the zone of deformed ground decreases linearly with depth below the ground surface such that

$$i_z = Kz_o \qquad (4.5)$$

where i_z is the horizontal distance from the tunnel centerline to the inflection point of the Gaussian distribution of settlement at a depth z_o above the tunnel centerline, and K is an empirical constant related to ground conditions.

Based on centrifuge and field measurement data, Mair et al. (1993) note that, nearer to the depth of the tunnel, K=0.5 underestimates the width of the settlement trough, and hence significantly over estimates the maximum vertical settlement. To account for decreasing i with depth, Mair et al. (1993) proposed an equation that was expressed by Marshall et al. (2012) as

$$K = \frac{K_s + (\partial i / \partial z)(z_p / z_t)}{1 - z_p / z_t} \qquad (4.6)$$

where the trough width parameter is defined relative to K at the surface, K_s; the slope of i in relation to depth, $\partial i/\partial z$; distance from the ground surface to depth of interest, z_p; and distance from the ground surface to the depth of the tunnel axis, z_t. Mair et al. (1993) recommended $K_s = 0.5$ and $\partial i/\partial z = -0.325$ for clays, while Mair & Taylor (1997) show that K_s ranges typically from 0.25 to 0.45 for sands and gravels based on field measurements.

Field measurements and centrifuge test results (e.g., Lake et al., 1996; Mair & Taylor, 1997; Osman et al., 2006) show that the Gaussian settlement profile is well represented for tunneling in clays, even for high volume losses in excess of 20% of the tunnel cross-section. Because of constant volume deformation in clay, the short-term settlement profile volume, V_{ls}, remains equal to volume loss at the tunnel. A notable exception pertains to consolidation-induced volume loss caused by increased effective stresses resulting from long-term drainage into the tunnel (Lake et al., 1996; Mair & Taylor, 1997).

Tunneling induced volume losses in sand are considerably more complex that those for clay. Field measurements (e.g., Cording & Hansmire, 1975; Cording, 1991) and centrifuge test results (Marshall, 2009; Marshall et al., 2012, and Zhou, 2014) show that volume changes in sand affected by tunneling are influenced by depth, tunnel cover to depth ratio, volume loss at the tunnel, and soil density. Although the Gaussian distribution provides in general a good fit to measurement data for relatively low volume losses in sand ($\leq$ 2-3% of tunnel cross-section), other profile functions have been shown to provide a better representation (e.g., Vorster, 2005; Marshall et al., 2012). In contrast

to clay, the assumption of constant volume loss in sands will lead to an under estimation of V_{ls} for $V_{lt} \leq 1\%$ and an overestimation at high V_{lt} ($\geq$2-3%) [Marshall et al., 2012; Zhou, 2014].

4.5.2 Horizontal Ground Displacements

The horizontal component of ground movement, S_h, is more difficult to predict due to lack of case history data and the difference in behavior between cohesive and cohesionless soils (O'Reilly & New, 1982). To conform to the plane strain constant volume assumption, the magnitude of horizontal ground movement, S_h, is commonly expressed by the following relationship

$$S_h = \frac{y}{z_R} S_v \qquad (4.7)$$

where y is the horizontal distance from tunnel centerline and z_R is the distance from the depth of interest to the radial focal point of ground movement vectors. Consistent with case studies presented by several authors (e.g., Cording & Hansmire, 1975; Attewell et al., 1978; O'Reilly & New, 1982) the maximum horizontal displacement, $S_{h,max}$, occurs at the settlement trough inflection point, i_z, as illustrated in Figure 4.11.

To characterize ground movement in clay under constant volume conditions, O'Reilly & New (1982) set $z_R = z_o$, which implies that vectors of ground movement are directed toward the tunnel axis. The few available case studies that accurately measure S_h indicate that the focal point of the ground vectors varies, and for constant volume conditions, may be below the tunnel axis (e.g., Cording, 1991; Hong & Bae, 1995). Assuming that K is given by Eqn. 4.6, Taylor (1995) showed that ground movement

vectors are directed to a point $(0.175/0.325)z_t$ below the tunnel axis to preserve equal and opposite vertical and horizontal strains.

Combining Equations 4.3, 4.4, 4.5, and 4.7 provides expressions representing the vertical, $S_v(y,z)$, and horizontal, $S_h(y,z)$, components of ground displacement across the transverse cross-section of the tunnel, as follows

$$S_v(y,z) = \frac{V_{ls}}{i_z\sqrt{2\pi}} \exp\left[\frac{-y^2}{2i_z^{\,2}}\right] \qquad (4.8)$$

$$S_h(y,z) = \frac{y}{z_R}\frac{V_{ls}}{i_z\sqrt{2\pi}} \exp\left[\frac{-y^2}{2i_z^{\,2}}\right] \qquad (4.9)$$

To obtain a better fit to measured sand settlements Vorster et al. (2005) introduced a modified Gaussian profile that allows the settlement distribution to be altered in accordance with three parameters: $S_{v,max}$, i, and α. The modified Gaussian curve is given by

$$S_v(y) = \frac{n\,S_{v,\max}}{(n-1)+\exp\left[\alpha\left(y/i\right)^2\right]} \qquad (4.10)$$

$$n = e^{\alpha}\frac{2\alpha-1}{2\alpha+1}+1$$

where α is the parameter to ensure i remains constant and n is the shape function parameter defining the width of the profile.

As discussed previously, complex volume losses in sand create conditions in which the relationship between V_{ls} and V_{lt} is constantly changing, thereby affecting the distribution of vertical and horizontal movements at all levels above the tunnel. Marshall (2009) showed that the depth to the radial focal point of ground movement

vectors changes for a given sand as V_{lt} increases. Moreover, Zhou (2014) demonstrated that relative sand density has a strong influence on ground movement patterns. It appears, therefore, that there is no simple model for horizontal displacements in sand, given the spatial distribution of the displacement vectors that have been observed and measured in centrifuge tests (Marshall, 2009).

4.5.3 Selection of Vertical and Lateral Displacement Profiles

In this work settlement and lateral displacement profiles were selected to represent relatively high levels of ground deformation for tunnels with a low soil cover to tunnel diameter ratio, C/D, which is defined as the distance from ground surface to tunnel crown divided by the nominal tunnel diameter. Soil movement profiles were chosen for C/D = 1.15 and a 6.1 m (20 ft) tunnel diameter in clay and sand, consistent in size to a rapid transit tunnel. A pipeline depth, z_p, of 0.9 m was chosen to represent typical burial conditions for pressurized pipelines with $D_p \leq 300$ mm (12 in.). The intention is to subject CI and DI pipelines to upper bound deformation so that trends in performance can be delineated for joint pullout and rotation as well as tensile strain limit states. The evaluation of pipeline response on this basis allows for generalizations that guide design and risk assessment and help to identify potential difficulties regarding pipeline integrity.

The tunnel volume loss, V_{lt}, in clay was limited to 5% of the tunnel cross-section as a practical upper bound associated with undesirable tunneling performance. As discussed previously, a Gaussian distribution for no volume change provides a suitable model for greenfield movement under these conditions.

The tunnel volume loss in sand was limited to 3%. Field measurements and centrifuge test results (e.g., Marshall et al., 2012; Zhou, 2014) for tunneling induced ground movements in sand show equality between V_{ls} and $V_{lt,}$ for $V_{l\%}$ between approximately 2 and 3%, depending on soil relative density. For sands of medium to high relative density the percentage variation in V_{ls} generally increases from +10% to -10% of V_{lt} as $V_{l\%}$ increases from 1 to 3%. Given the small variation within these bounds, a Gaussian distribution model with no volume change was selected to simulate both the vertical and lateral distribution of movement at pipeline depth. Pipeline response to the modified Gaussian distribution was also analyzed to assess the sensitivity of pipeline response as a function of the profile function used for ground deformation.

The depth to focal point of radial ground movement vectors, z_R, was set to the tunnel centerline depth, z_o, for a conservative estimate of lateral movements. Field measurements and centrifuge test results show that z_R is typically less than z_o, which would lead to a lower estimate of horizontal displacement.

Table 4.1 summarizes the input parameters for the Gaussian and modified Gaussian distribution function used for clay and sand. The inflection points, i, for the Gaussian distributions were chosen from $i=Kz_o$ (Eqn. 4.5) and Eqn. 4.6 where K=0.52 for clay, based on parameters suggested by Mair et al., (1993), and K=0.28 for sand, using parameters and the equations derived from centrifuge tests in dense sand provided by Marshall et al. (2012). The relatively small K results in i for sand approximately one-half i for clay. This means that the sand settlement profile is narrower and deeper than

the one for clay, given equivalent geometry and V_{ls}. To evaluate the effects of using a Gaussian vs. modified Gaussian distribution, α was varied for fixed $S_{v,max}$ and i in both distributions, resulting in ±10% change in $V_{l\%}$ relative to the Gaussian distribution. Figure 4.12 shows the distribution of vertical and horizontal soil displacements associated with the profile functions used in the soil-pipeline interaction simulations. The vertical and lateral soil displacements for sand are concentrated closer to the tunnel centerline than those for clay. Variations in the vertical and lateral movements for Gaussian and modified Gaussian distributions in sand are greatest beyond the inflection point at the edges of the settlement trough.

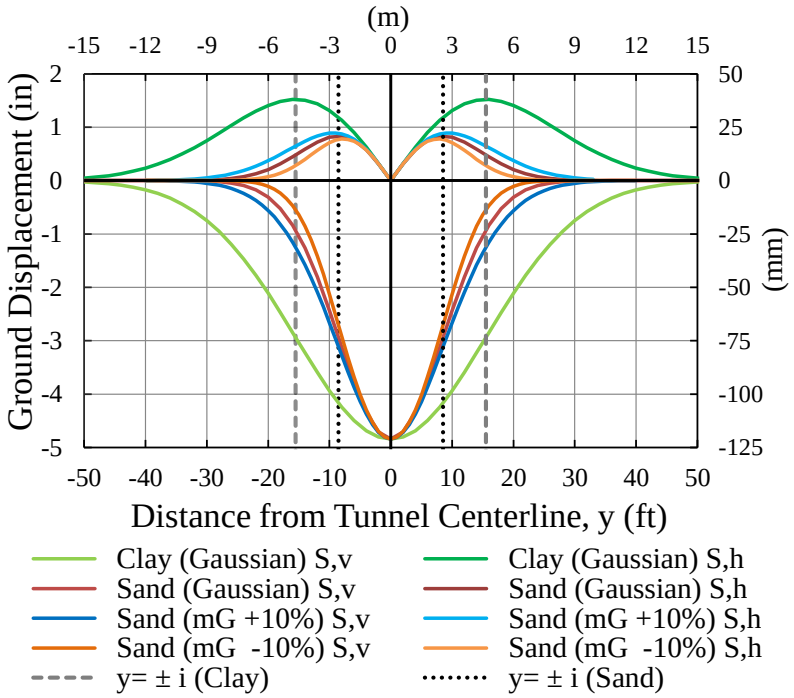

Figure 4.12. Vertical and horizontal ground settlement profiles (lateral displacements directed toward tunnel centerline)

Table 4.1. Input parameters for soil settlement profiles

Soil	Profile Function	α	n	K	i (ft) [m]	$V_{l\%,max}$ (%)	$S_{v,max}$ (in) [mm]	$S_{h,max}$ (in) [mm]
clay	(Gaussian)	0.50	1	0.52	15.5 [4.7]	5.0%	4.84 [123]	1.52 [39]
sand	(Gaussian)	0.50	1	0.28	8.5 [2.6]	2.7%	4.84 [123]	0.83 [21]
sand	(mG -10%)	0.73	1.38	0.28	8.5 [2.6]	2.5%	4.84 [123]	0.78 [20]
sand	(mG +10%)	0.33	0.72	0.28	8.5 [2.6]	3.0%	4.84 [123]	0.89 [23]

[1]Consistent parameters: D_t= 6.1 m (20 ft); z_o= 9.1 m (30 ft); z_p= 0.9 m (3 ft); z_t= 10.1 m (33 ft); z_R= 9.1 m (30 ft); C= 7.0 m (23 ft); C/D_t= 1.15

4.6 Tunneling Ground Movement Interaction Results for Continuous Jointed Pipeline

The analytical results from FE soil/pipeline interaction simulations are presented and discussed for two cases involving jointed pipelines perpendicular to the tunnel centerline axis that (1) extend well beyond the width of the settlement profile and (2) connect through 90° tees with a pipeline parallel to the tunnel centerline axis. The former case involves a continuous jointed pipeline and the latter case involves a tee. The latter case is important because it can result in pullout and leakage at the tee in response to lateral soil movements. The analytical results are presented under the forthcoming headings, first for pipelines spanning the settlement profile and then for pipelines that connect with tees.

The analytical results for tunneling movement interaction with continuous jointed pipelines are presented for nominal 150-mm (6-in.) and 300-mm (12-in.)-diameter CI and 150-mm (6-in.) DI pipe. Analyzes were performed for a CI pipeline with 3.6-m (12-ft)-long segments connected by lead-caulked joints with axial behavior and rotational stiffness as defined in Figures 4.3 and 4.6, respectfully. As illustrated in

Figure 4.13, both joint centered (JC) and pipe centered (PC) locations of the pipelines relative to the profile centerline were analyzed. The maximum joint rotations occur at the tunnel centerline for the JC configuration, and the maximum pipe bending occurs at the tunnel centerline for the PC configuration. These two configurations set bounding conditions on the most severe joint rotations and bending strains.

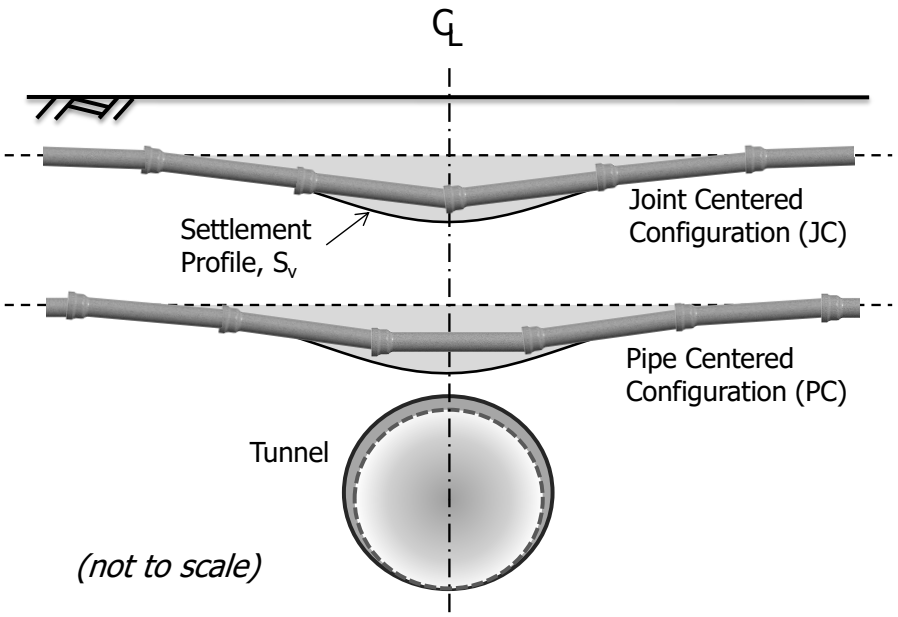

Figure 4.13. Illustration of joint centered and pipe centered pipeline configurations

The FE simulations were performed according to the methods described in Sections 3.4. In all cases, it was assumed that the pipelines were buried in granular backfill with elasto-plastic force vs. displacement characteristics typical of dense sand (Jung et al., 2013a and b; O'Rourke et al., 2015). The sensitivity of the analytical results in relation to the size of the FE mesh was investigated by varying the size of the pipe elements and length of the pipeline across the settlement profile. For the tunneling ground deformation characteristics used in this work, it was found that the analytical results

converged for element lengths ≤ 75 mm (3 in.) and total number of 3.7-m (12-ft)-CI or 5.5-m (18-ft)-DI pipe lengths between 10 and 14, depending on the pipeline configuration. The total number of beam, spring, and gap elements varied from 4,815 to 7,167 depending on type of iron and pipeline configuration.

4.6.1 Cast Iron Pipelines in Clay

The FE simulation results for CI pipeline response to tunneling in clay are presented in Fig. 4.14. As discussed in Section 3.2, leakage initiates in lead-caulked CI joints at joint pullout and rotation of 0.5 mm (0.02 in.) and 0.2°, respectively. Maximum leakage in CI joints occurs at a rotation of approximately 0.5°. The maximum allowable tensile strain is taken as 600 με.

In Figures 4.14(a), (c), and (d) and Fig. 4.14 (b) the maximum joint rotation and tensile strain, respectively, are plotted relative to the centerline settlement, $S_{v,max}$. The maximum tensile strain was determined from the addition of the axial and bending strains at all locations along the pipeline. All settlements shown in the figure are for V_{ls} ≤ 5% volume loss.

Figure 4.14(a) shows maximum joint rotation vs. centerline settlement for 150-mm (6-in) and 300-mm (12-in.)-diameter pipelines with JC and PC configurations. For a given settlement and pipe diameter, the maximum joint rotation for a JC configuration always exceeds that for a PC configuration. For the same settlement, the rotations of the 300-mm-diamter pipelines more than double those of the 150-mm-diameter pipelines. The initiation of joint leakage at 0.2° rotation in 150-mm-diamter pipelines

occurs between 100 and 125 mm (4 and 5 in.) of centerline settlement. Joint leakage initiation in 300-mm-diameter pipelines occurs between 50 and 75 mm (2 and 3 in.) of centerline settlement. Only the 300-mm-diameter JC pipeline exceeds the 0.5° maximum leakage threshold.

Figure 4.14(b) shows the maximum tensile strain vs. centerline settlement. In all cases the tensile strains are below the allowable limit. Similarly, the pullout displacement in all cases is below the axial movement associated with initial joint leakage. Typical pullout displacements are shown for CI pipelines in sand under the next heading.

Figure 4.14(c) demonstrates the sensitivity of joint rotation to the modulus of the CI pipe. As the modulus increases from 76 to 128 GPa (11,000 to 18,500 ksi), the maximum joint rotation increases for the same $S_{v,max}$. Figure 4.14(b) shows little change in tensile strain in the 150-mm-diameter pipeline for a given settlement, reflecting nearly constant bending moment for the range of E pertaining to pit and centrifugally cast iron. For small strains, the pipe curvature $\kappa = M/EI$ where M, E, and I are the moment, modulus, and moment of inertia of the pipe. Since M does not change with E, the curvature, κ, decreases as E increases. Less pipe curvature results in increased joint rotation, as illustrated in the figure.

Figure 4.14(d) shows maximum joint rotation vs. centerline settlement for a 150-mm-diameter pipeline with a JC configuration. The different plots correspond to the mean, 10%, and 90% exceedance levels associated with the normal cumulative distribution of the CI-lead adhesion, C_A, plotted in Fig. 4.2. The 10% and 90% exceedance levels

define a statistical range that helps to quantify the uncertainty associated with the effect of C_A on joint rotation. For a given level of settlement, the strongest and stiffest joints with 90% exceedance levels for C_A reduce rotation by about one third relative to the weakest joints with 10% exceedance levels. The figure also shows the rotations for joints with no rotational stiffness, thus setting an upper bound for rotation. The moment mobilized in CI joints reduces rotation to about half the value associated with zero-moment, or pinned, connections.

4.6.2 Cast Iron Pipelines in Sand

Figure 4.15 shows plots similar to those in Fig. 4.14 for CI pipelines in sand. As previously discussed and depicted in Fig. 4.12, tunneling in sand results in a narrower settlement profile with i = 2.6 m (8.5 ft), nearly one-half i = 4.73 m (15.5 ft) for clay. All settlements shown in the figure are for $V_{ls} \leq 3\%$ volume loss. The figure also presents results for Gaussian and modified Gaussian distributions to explore pipeline response to different mathematical representations of the settlement profile.

As expected for a narrower settlement profile, CI joint rotations are larger than those for the same centerline settlement in clay for similar size pipe and joint configuration (i.e., JC and PC conditions). Figure 4.15(a) shows that, for a given settlement and pipe diameter, the maximum joint rotation for a JC configuration always exceeds that for a PC configuration. The same trend is shown in Fig. 4.14. Of particular note, the centerline settlements decrease for limit state rotations of 0.2° and 0.5°. The centerline settlements, which trigger maximum leakage at 0.5°, are as low as 30 and 60 mm (1.2 and 2.4 in.) for 300-mm and 150-mm-diameter pipelines, respectively.

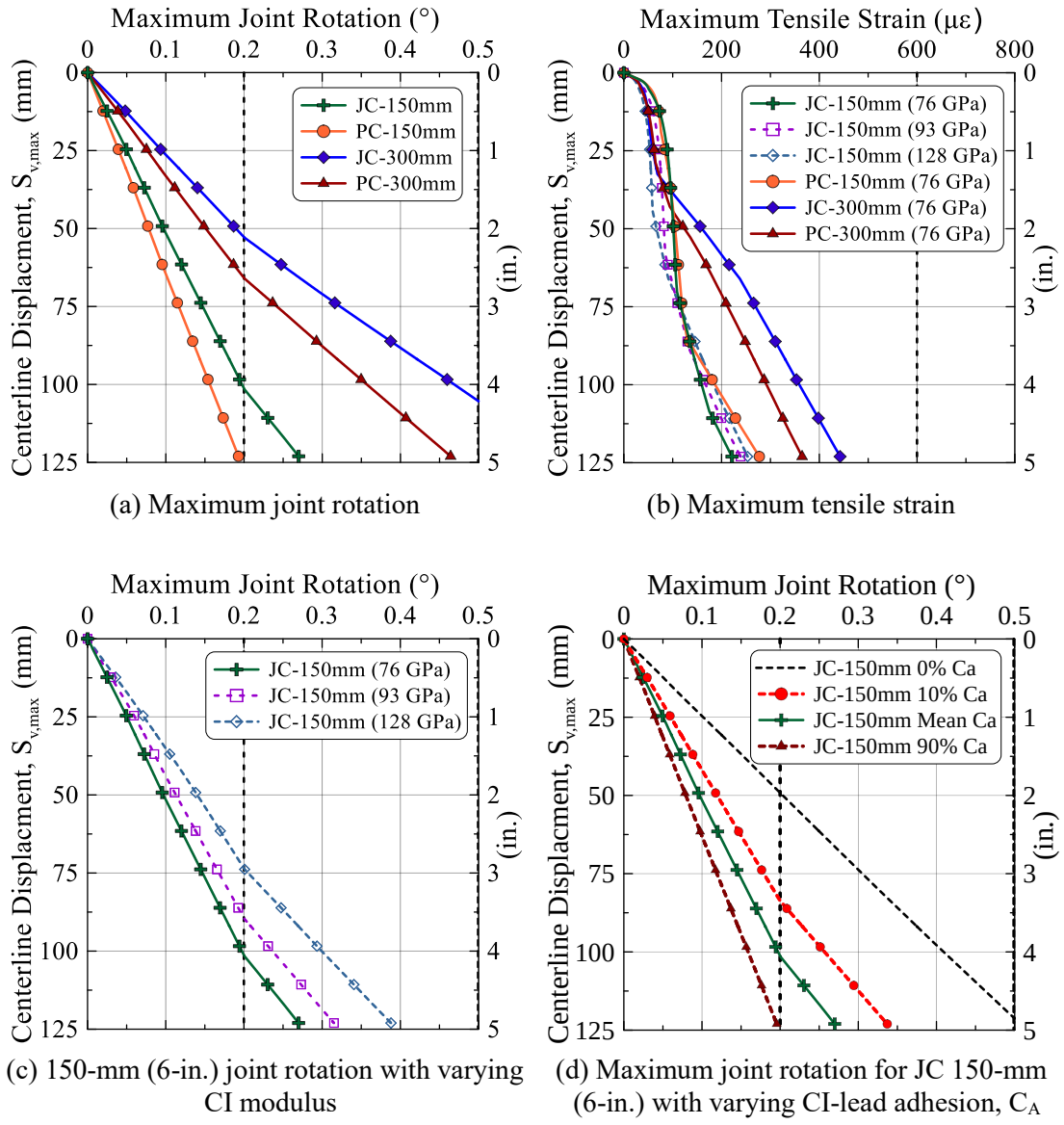

(a) Maximum joint rotation

(b) Maximum tensile strain

(c) 150-mm (6-in.) joint rotation with varying CI modulus

(d) Maximum joint rotation for JC 150-mm (6-in.) with varying CI-lead adhesion, C_A

Figure 4.14. Continuous jointed CI pipeline results for clay settlement profile

Figure 4.15(b) shows the maximum tensile strains vs. centerline settlement. Consistent with the trends in Fig. 4.14, maximum tensile strains are larger than those for the same centerline settlements in clay for similar size pipe and joint configurations. The allowable tensile strain of 600 με is exceeded for PC configurations at approximately 55 and 60 mm (2.2 and 2.5 in.) centerline settlement for 150-mm and

300-mm-diameter pipelines, respectively. Hence, the limit states for both rotation at maximum leakage and allowable strain are exceeded at similar levels of centerline settlement.

Similar to the results for clay, the pullout displacement in all cases is below the axial movement associated with initial joint leakage. Figure 4.15(c) presents the maximum joint pullout vs. centerline settlement, which shows that pullout in most instances was less than 0.25 mm (0.02 in.), and therefore marginal. Similar trends were obtained for clay.

Figures 4.15(a) and (d) compare the maximum joint rotations and tensile strains, respectively, vs. centerline settlement for the Gaussian and modified Gaussian distributions in relation to a 300-mm-diameter pipeline. As described previously, the modified Gaussian distribution results were generated for constant $S_{v,max}$ and i by varying the α parameter to produce ±10% V_{ls} of the Gaussian distribution. Such variability should be expected when characterizing complex movement patterns, and the results help to assess the consequences of such variability. Figure 4.15(a) shows that the use of the two distributions does not result in significantly different maximum joint rotation vs. $S_{v,max}$. The maximum tensile strains, however, show significant sensitivity to the choice of distribution.

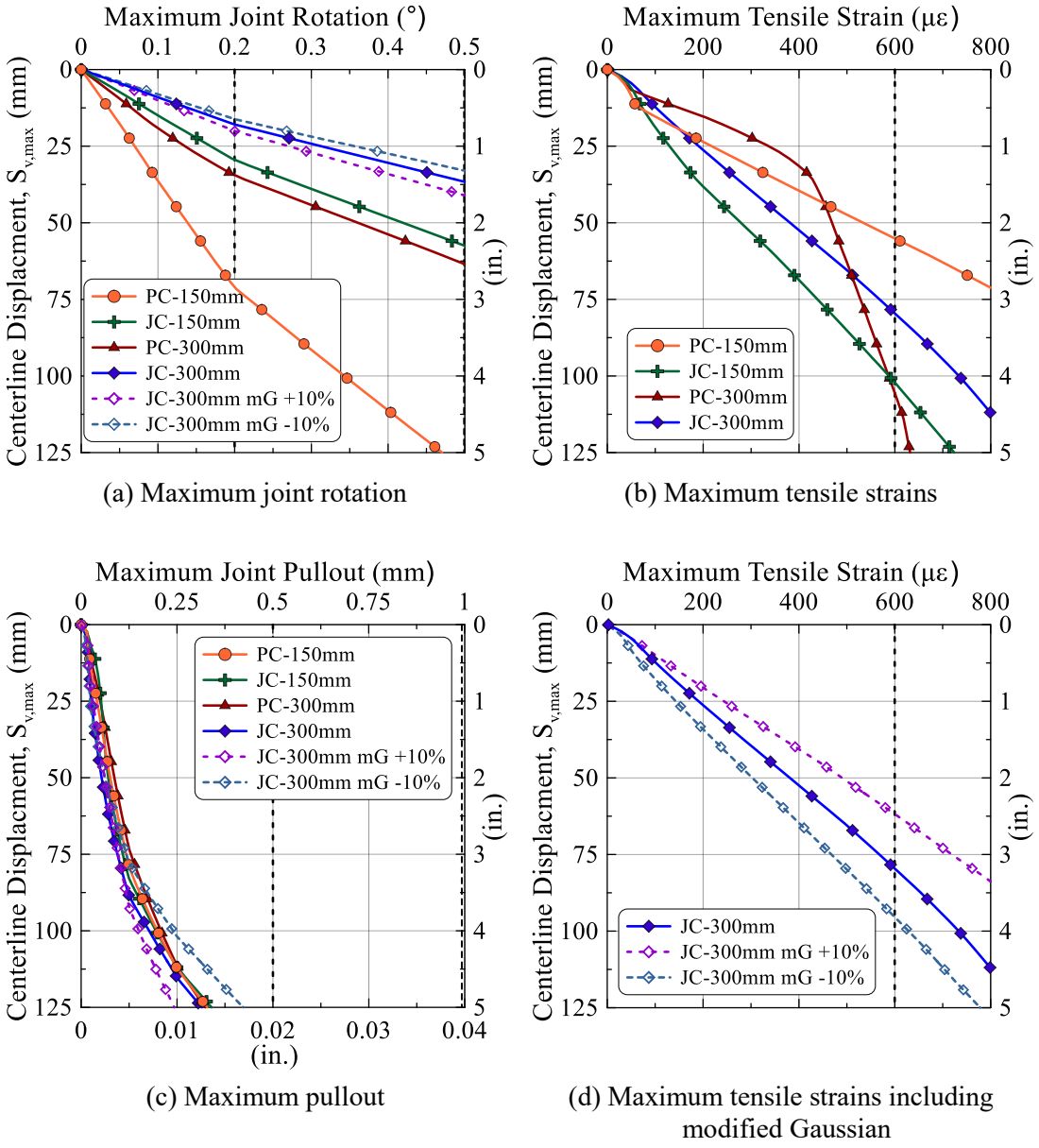

Figure 4.15. Continuous jointed CI pipeline results for Gaussian and modified Gaussian sand settlement profiles

Centerline settlements required to exceed the allowable tensile strain vary from approximately 60 to 95 mm (2.5 to 3.8 in.). As shown in Figure 4.12, the settlement profile for Gaussian and modified Gaussian distributions are in close agreement inside a horizontal distance of i from the centerline where maximum rotation is generated for

a JC configuration. Thus, the rotations are in close agreement. Outside the distance i, the curvature associated with the distributions differ, resulting in bending strain variations that affect the maximum tensile strain.

4.6.3 Ductile Iron Pipeline in Sand

Figure 4.16 presents the maximum joint rotations and tensile strains for 150-mm-diameter DI pipelines in sand vs. centerline settlements. Given the high capacity for rotation, high yield strength, and ductility of DI pipelines, the more severe ground deformation associated with sand was selected for analysis. Three joint configurations were evaluated, including JC, PC, and an intermediate case where the DI joint is offset one quarter of the 5.5-m (18 ft) pipe length from the tunnel centerline. All settlements shown in the figure are for $V_{ls} \leq 3\%$.

In all cases, joint rotations are well under the limits for metal binding and far less than the rotational capacity at first leakage. The maximum joint pullout (not shown) was less than 5 mm (0.2 in.), well below the 50 mm (2 in.) allowable pullout for joint leakage. Likewise, the tensile strains are well below the 3500με yield strain defined according to ASTM (2015) standards. For the 125-mm maximum settlement, the maximum bending strain is less than the 1500με proportional limit of DI (maximum strain for constant E).

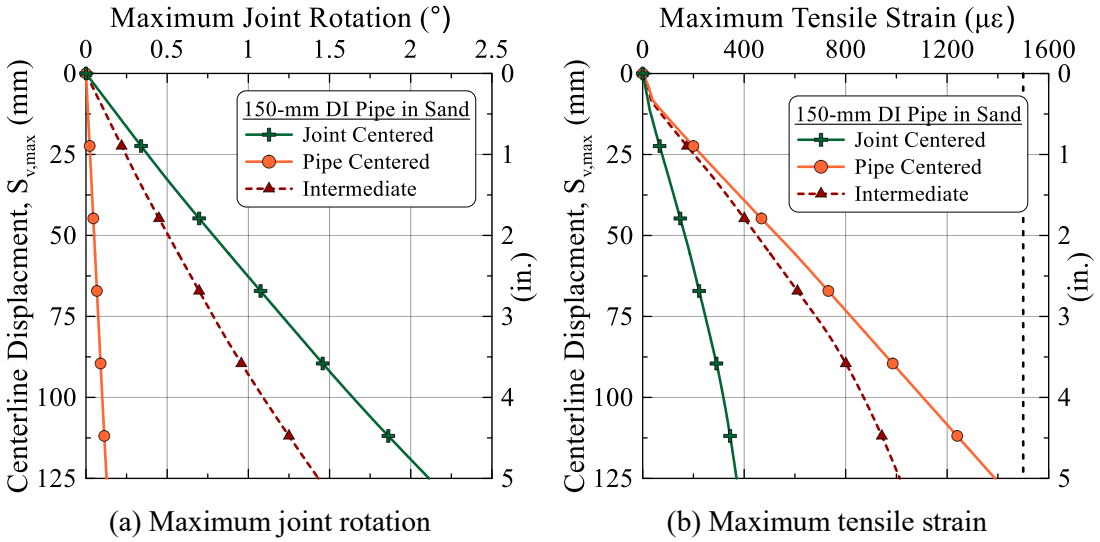

(a) Maximum joint rotation

(b) Maximum tensile strain

Figure 4.16. Results for 150-mm (6-in.) continuous DI pipe for joint and pipe centered configurations in sand profile

4.7 Pipelines with Tees

Figure 4.17 shows a transverse cross-section of a tunnel and settlement profile affecting a branch pipeline connected through a 90° tee to another pipeline parallel to the longitudinal axis of the tunnel. A plan view of the tee and interconnecting parallel and branch pipelines is also shown. This case is important because tunneling induced ground movements can induce pullout and large rotation between the tee and branch pipeline.

Figure 4.18 presents a simplified 3D view of the tee. A concrete thrust clock is often placed adjacent to the tee to resist unbalanced force from internal water pressure. For CI pipelines and tees the thrust block and torque combined from the two joints connecting with the parallel pipeline will resist the overturning moment at the joint induced by differential settlement of the branch pipeline. The evaluation of relative

rotation in Appendix C shows that the tee tends to settle without rotation for both CI and DI pipelines and tees. Thus, no rotation of the tee was assumed in the FE simulations.

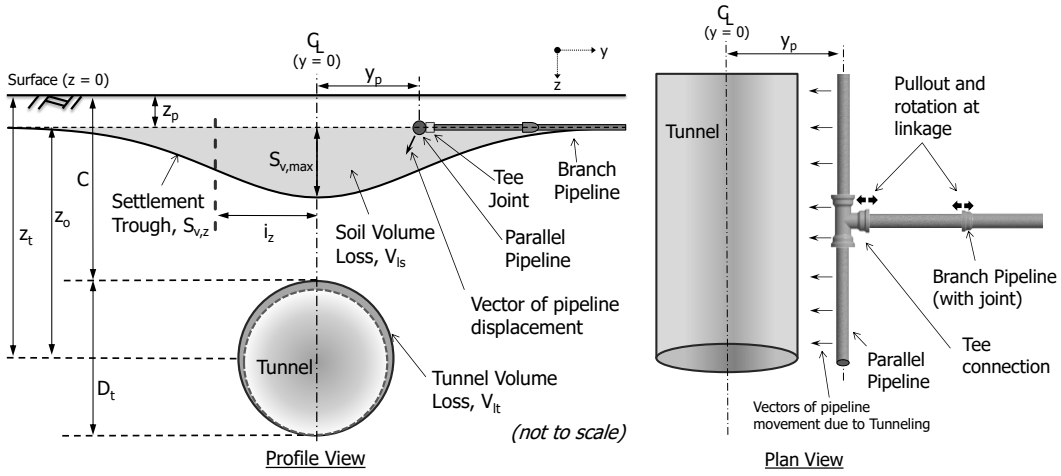

Figure 4.17. Illustration of tunnel cross-section, settlement trough and parallel pipeline with tee connection

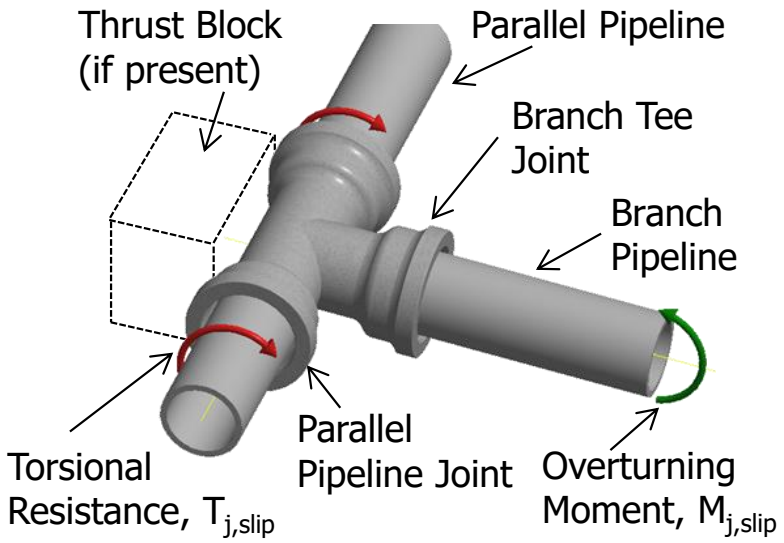

Figure 4.18. 3D illustration of typical CI tee joint

4.7.1 Cast Iron Tees

Figure 4.19 shows the analytical results of joint pullout and rotation associated with a CI tee connected to a 150-mm (6-in.)-diameter branch pipeline for a centerline settlement of 28 mm (1.1 in.). The joint pullout and rotation for each joint of the branch pipeline are plotted for analyses with tee locations of 0, 1.5, 4.7, 7.6, and 10.7 m (0, 5, 15.5, 25, and 35 ft) from the tunnel centerline.

Figure 4.19(a) and (b) show that a maximum pullout and rotation of 3.3 mm (0.13 in.) and 0.20°, respectively, occur when the tee is located at the inflection point of the clay settlement profile, 4.7 m (15.5 ft) from the tunnel centerline. For each tee position the maximum rotation occurs at the tee joint while only joints beyond the settlement profile inflection point, defined by the range y = i to 3i, experience pullout greater than the threshold value of 0.5 mm (0.02 in.). When the tee is located at the tunnel centerline (y=0), joint pullout and rotation are minimal. As the tee is positioned further from the tunnel centerline, the second and third branch joints experience maximum pullout. At tee locations ≥ 7.6 m (25 ft) the maximum pullout occurs at the tee.

By extracting the maximum pullout and rotation from multiple simulations at different tee distances with respect to the tunnel centerline, unique relationships between maximum joint pullout and rotation, as well as maximum pipe tensile strain, with respect to the tee location were generated. From each of these relationships, the maximum settlement associated with levels of pipeline deformation exceeding joint pullout and rotation limit states were identified and plotted as a function of the tee location in Figs. 4.20(a) and (b) for tunneling conditions in clay and sand, respectively,

as well as allowable tensile strain in Fig. 4.21 for both soil conditions. Thus, a unique relationship between maximum settlement and various limit states can be defined for each location of the tee.

Figures 4.20(a) and (b) show the centerline settlement for clay and sand, respectfully, with pullout and rotational limit states for 150 and 300-mm-(6 and 12-in.) diameter pipelines as a function of tee location. A range of 0.5 to 1.0mm (0.02 to 0.04 in.) is used to bracket the axial slip at first leakage. For both clay and sand, the CI tees are susceptible to pullout-related leakage at low settlements of approximately 10-15 mm (0.4-0.6 in.) when the tee is located between a horizontal distance of 0.5i to 2i from the tunnel centerline. Low settlements of about 15 mm (0.6 in.) are associated with rotation at first leakage in sand when the tee is located a horizontal distance i from the tunnel centerline.

Figure 4.21 provides a similar plot for centerline settlements vs. tee location at which allowable tensile strain is exceeded for 150-mm and 300-mm-diameter tees in clay and sand. In all cases the settlements associated with allowable strain are well above those that exceed the pullout and rotational limit states.

Figure 4.20 shows high susceptibility to leakage from pullout when CI tees are located between 0.5i and 2i from the tunnel centerline. The maximum tunnel settlements associated with the initiation of leakage are sufficiently low that tee locations within the width of the settlement trough ($\cong$ 2.5i) should be regarded as a potentially high risk situation.

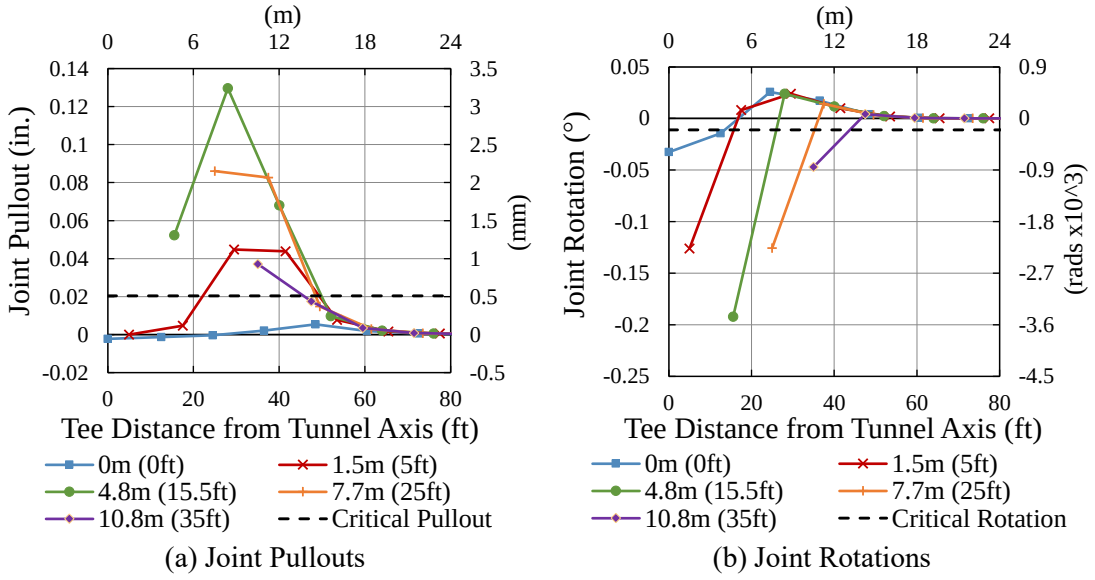

Figure 4.19. Joint pullout and rotation for 150-mm (6-in.)-diameter CI tee in clay at 28 mm (1.1 in.) of centerline displacement for varying tee locations

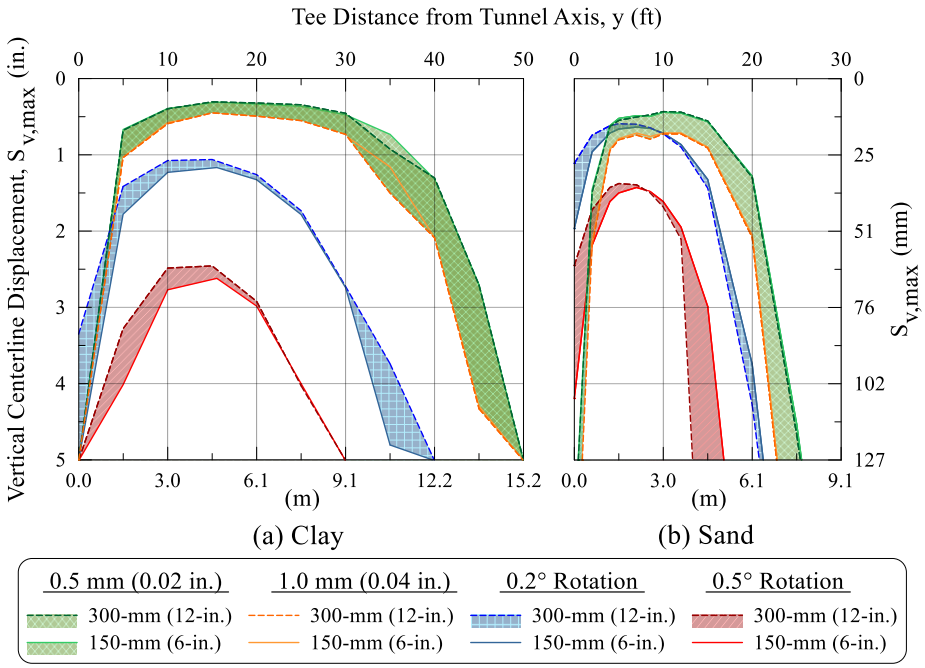

Figure 4.20. Relationships between CI tee location and centerline settlement for pullout and joint rotation limit states

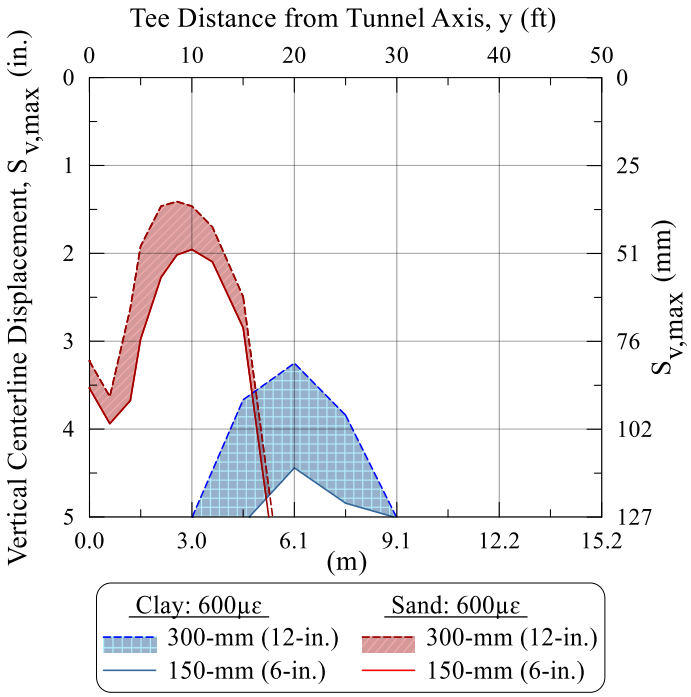

Figure 4.21. Relationships between CI tee location and centerline settlement for allowable pit cast iron tensile strain

4.7.2 Ductile Iron Tees

As demonstrated in Figure 4.16, DI joints have high capacity for rotation without leakage. This capacity exceeds the rotational deformation imposed by tunneling induced ground movements when DI pipelines span the settlement profile. This resistance to settlement also applies for DI tees in clay and sand.

To explore the susceptibility of DI tees to pullout, the analytical results for maximum pullout at 120-mm (4.8-in.) of centerline settlement is plotted with respect to tee location in Fig. 4.22. The tee location is expressed in terms of horizontal distance from the tunnel centerline normalized by i for clay and sand. Both an unrestrained tee and a tee

restrained from pullout at its connection with a 150-mm-diameter branch pipeline were modeled.

Figure 4.22 shows that maximum pullout occurs when the tee is at or near the inflection point, i, in all cases simulated. At all tee locations the maximum pullout is slightly higher in sand than clay. The largest pullouts occur for restrained tees at the next joint of the branch pipeline. Restraining the tee from pullout actually reduces the degrees of freedom available in the branch pipeline to accommodate lateral ground movement. Thus, more separation is induced in the branch pipeline joints for a restrained vs. an unrestrained tee.

All analytical results for DI tees were examined for combined joint pullout and rotation and compared with the metal binding and pressure boundaries presented in Fig. 4.8. Although some limited cases show pullout and rotation on the order of 70 to 80% and 60 to 70%, respectively, of push-on joint pullout capacity, all combinations of pullout and rotation were below the metal binding boundary and well below the pressure boundary.

While the worst case conditions may require some special precautions, the analytical results indicate that pullout will not be a major risk for the great majority of cases involving tunneling beneath DI tees. Given the absence of pullout resistance in push-on joints, tees should always be checked as a potential risk tunneling induced ground deformation.

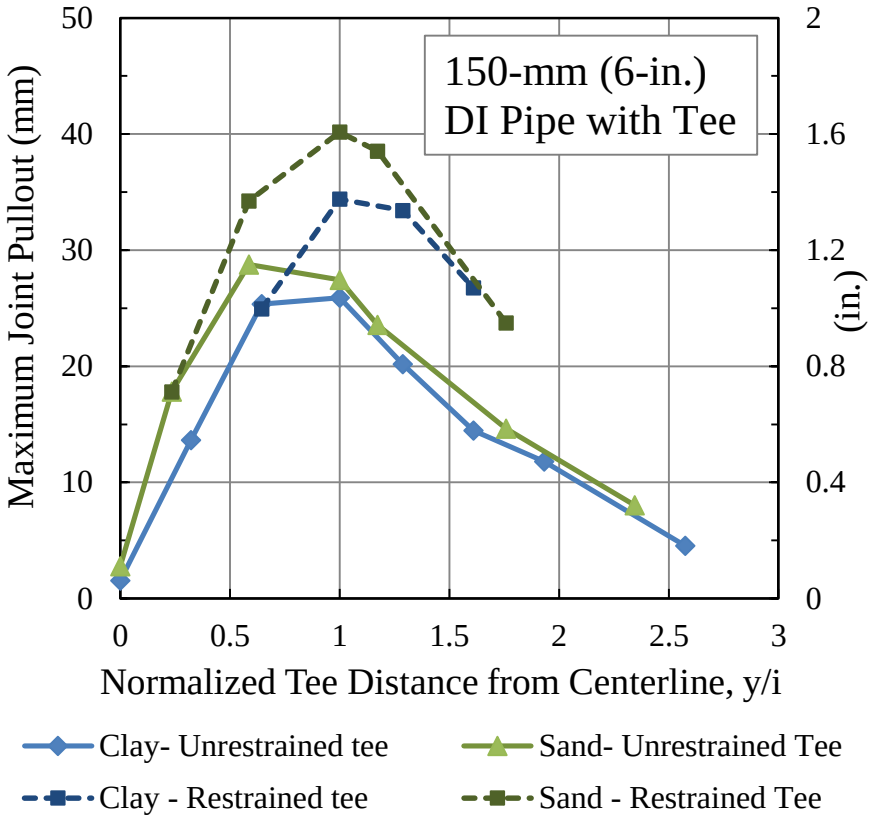

Figure 4.22. Maximum DI joint pullout in sand as a function of normalized tee location

4.8 Conclusions

Soil/pipeline interaction modeling for vertical and horizontal ground movements caused by tunneling was performed for two cases involving jointed CI and DI pipelines perpendicular to the tunnel centerline that (1) extend beyond the width of the settlement profile and (2) connect through 90° tees with a pipeline parallel to the tunnel. The modeling incorporates the results of large-scale laboratory tests to characterize the axial force vs. displacement and moment vs. rotation relationships of DI and CI joints commonly encountered in practice. Tunneling induced soil displacement profiles were modeled for a 6.1-m (20-ft)-diameter tunnel in clay and sand with a cover to depth ratio,

C/D, of 1.15 affecting 150-mm and 300-mm (6 and 12-in.)-diameter CI and DI pipelines. The analytical results are reported for volume losses confined to 5% and 3% of the tunnel cross-section in clay and sand, respectively, to allow for the assumption of no volume loss deformation when modeling of soil settlement and horizontal movement. The evaluation of pipeline response on this basis allows for generalizations that guide design and risk assessment and help to identify potential difficulties regarding pipeline integrity

With respect to jointed CI and DI pipeline performance, the principal observations and conclusions are:

- The limit states for first leakage in lead-caulked CI joints are related to measured deformation, or slip, between the lead and CI surfaces within the joints at 0.5 mm (0.02 in.) of axial pullout and approximately 0.2° of joint rotation. Moment vs. rotation test results for 100-mm, 150-mm, and 200-mm (4-in., 6-in. and 8-in,)-diameter lead-caulked CI joints taken from the field after 50 to 80 years of operation show that leakage under typical operating pressure peaks initially at about 0.5° rotation and declines thereafter until leakage again increases at rotations in the range of 3 to 4°.
- Equations for evaluating the CI pullout force and moment at first leakage are provided, which are related to the CI-lead adhesion, C_A. Data for C_A from large-scale pullout tests are shown to follow a normal distribution, thus allowing for the quantification of uncertainty in pullout force and moment to initiate leakage.

- The joints display complex behavior in which additional slip and creep of the lead can close off leakage paths that are reopened with further increase in deformation. Thus, the slip and rotation at incipient leakage can be identified, but a clear and consistent trend in leakage after its initiation cannot be quantified with the available experimental evidence.
- In contrast to CI pipelines, DI pipelines with push-on joints can sustain without leakage rotations well above 5° at which metal binding occurs within the joints. Push-on joints, however, are susceptible to pullout at approximately 50 mm (2 in.), which represents their greatest vulnerability with respect to ground movement.

For jointed CI and DI pipelines that extend beyond the width of the settlement profile, the principal observations and conclusions drawn from the analytical results are:

- For the same tunnel diameter and C/D, the response to tunneling in sand is accompanied by joint rotations and maximum tensile strains that exceed those in clay by a factor as high as two to three for the same centerline settlement and pipe diameter. This difference is related to the narrower settlement profile in sand that generates larger differential settlements and curvatures.
- For the tunneling conditions examined in this work, CI joint rotation at first leakage in clay occurs between 50 and 120 mm (2.0 and 4.8 in.) of centerline settlement, and depends on both the pipe diameter and location of the joints with respect to tunnel centerline. For sand the threshold of incipient leakage is exceeded at centerline settlements on the order of 25 mm (1 in.). These levels

of settlement pertain to relatively severe conditions of tunneling with low C/D and apply only for the initiation of leakage, which may involve very small losses.

- Allowable tensile strain levels for pit cast iron pipe were not exceeded for centerline settlements in clay as high as 120 mm (4.8 in.), but were exceeded at centerline settlements in sand of approximately 50-100 mm (2-4 in.). Pullout displacements for all cases in clay and sand were below the axial movement associated with initial joint leakage.
- For DI pipelines joint rotations were well under the limits for metal binding and far less than the rotational capacity at first leakage. Joint pullout was minimal, and maximum tensile strains were below yield conditions.

For jointed pipelines, which connect through 90° tees with a pipeline parallel to the tunnel, the principal observations and conclusions drawn from the analytical results are:

- There is high susceptibility to leakage from pullout when CI tees are located between 0.5i and 2i from the tunnel centerline (where i is the location of the settlement profile inflection point). The maximum tunnel settlements associated with the initiation of leaks are sufficiently low that tee locations within the width of the settlement trough ($\cong$ 2.5i) should be regarded as a potentially high risk situation with respect to the effects of tunneling.
- The largest pullouts for DI pipelines with unrestrained and restrained tees occur at a distance close to the inflection point, i, from the tunnel centerline. Moreover, the largest pullouts occur for restrained tees. Restraining the tee from

pullout actually reduces the degrees of freedom available in the branch pipeline to accommodate lateral soil movement.

- The DI tees were examined for combined joint pullout and rotation and compared with the metal binding and pressure boundaries applicable for push-on joints. In every case the combinations of pullout and rotation were below both the metal binding and pressure boundaries, indicating satisfactory performance.
- Pullout will not be a major risk for the great majority of cases involving tunneling beneath DI tees. Some limited cases, however, show pullout on the order of 70 to 80% of push-on joint pullout capacity. Given the absence of pullout resistance in push-on joints, tees should always be checked as a potential risk with respect to tunneling induced ground deformation.

The observations and conclusions apply for CI and DI pipelines without significant corrosion and material defects. The effects of corrosion and defects are beyond the scope of this work, but should be considered in practical situations. In some cases, water or gas operations personnel are able to identify areas susceptible to corrosion. In all cases the mechanical performance of pipelines without defects provides an essential framework for design and risk assessment.

REFERENCES

ABAQUS 6.13. (2014). [Computer software]. Providence, RI, ABAQUS.

American. (2015). “American Pipe Manual.” American Cast Iron Pipe Company. Birmingham, AL.

Argyrou, C. (2016). *Response of Pipeline with CIPP Linings to Permanent Ground Deformation.* PhD Thesis, Cornell University, Ithaca, NY. In progress.

ASCE. (1984). *Guidelines for the seismic design of oil and gas pipeline systems*. Committee on Gas and Liquid Fuel Lifelines, American Society of Civil Engineers: Reston, VA.

ASTM. (2015). “Standard Test Methods for Tension Testing of Metallic Material.” *E8/E8M-15a,* West Conshohocken, PA.

Attewell, P. B., Glossop, N. H. and Farmer, I. W. (1978). “Ground deformations caused by tunnelling in a silty alluvial clay.” *Ground Engineering*, **2**(8), 32-41.

Attewell, P. B., Yeates, J., & Selby, A. R. (1986). *Soil movements induced by tunnelling and their effects on pipelines and structures*, Chapman & Hall, New York.

AWWA. (2009). “Ductile iron pipe, centrifugally cast, for water.” *American Water Works Association Standard: ANSI/AWWA C151/A21.51-09,* Denver, CO.

Bouziou, D. (2014). *Earthquake-induced ground deformation effects on buried pipelines*. PhD Thesis. Cornel University, Ithaca, NY.

Bracegirdle, A., Mair, R. J., Nyren, R. J., & Taylor, R. N. (1996). “A methodology for evaluating potential damage to cast iron pipes induced by tunneling.” *Proc. Geotechnical Aspects of Underground Construction in Soft Ground*. London: Balkema, 659-664.

Cooper, M. L., Chapman, D. N., Rogers, C. D. F. & Chan, A. H. C. (2002). “Movements in the Piccadilly Line tunnels due to Heathrow Express construction.” *Géotechnique* **52**(4), 243–257.

Cording, E. J. & Hansmire, W. H. (1975). “Displacements around soft ground tunnels.” *General Report 5th Pan American Conference on Soil Mechanics and Foundation Engineering*, Buenos Aires, Session IV 571-632.

Cording, E. J. (1991). “Control of ground movements around tunnels in soil.” *Proc. 9th Pan-American Conf. Soil Mech. Found. Engng, Valparaiso*, 2195–2244.

Davis, C. (2015). Resilience Manager, Los Angeles Department of Water and Power, personal communication.

Ha. D., Abdoun, T., O’Rourke, M.J., Symans, M.D. ,O’Rourke, T.D., Palmer, M.C., & Stewart, H.E. (2008). “Buried high-density polyethylene pipelines subjected to normal and strike-slip faulting – a centrifuge investigation.” *Can. Geotech. J.*, **45**(12), 1733-1742.

Harris, C. W., & O’Rourke, T. D. (1983). “Response of jointed cast iron pipelines to parallel trench construction.” *Geotechnical Engineering Rep. 83-5,* School of Civil and Environmental Engineering, Cornell Univ., Ithaca, NY.

Honegger, D. & Nyman, D. J. (2004). *Guidelines for the Seismic Design and Assessment of Natural Gas and Liquid Hydrocarbon Pipelines*. Pipeline Research Council International; Catalog No. L51927.

Hong, S. W. and Bae, G. J. (1995). “Ground movements associated with subway tunnelling in Korea.” *Proc. Underground Construction in Soft Ground*. Rotterdam: AA Balkema, 229-232.

Johnson, J. B. (1890). “Cast-Iron-Strength, Resilience, Tests and Specifications.” *Trans. Am. Soc. Civil Eng.*, XXII(1), 91–120.

Jung, J. K. (2010). *Soil-pipe interaction under plane strain conditions*. PhD Thesis, Cornell University, Ithaca, NY.

Jung, J. K., O'Rourke, T. D., & Olson, N. A. (2013a). "Uplift soil–pipe interaction in granular soil." *Can. Geotech. J.* **50**(7), 744-753.

Jung, J. K., O'Rourke, T. D., & Olson, N. A. (2013b). "Lateral soil-pipe interaction in dry and partially saturated sand." *J. of Geotech. Geoenviron. Engng ASCE.* **139**(12), 2028-2036.

Klar, A., Vorster, T. E. B., Soga, K. & Mair, R. J. (2005). "Soil–pipe interaction due to tunnelling: comparison between Winkler and elastic continuum solutions." *Géotechnique.* **55**(6), 461–466.

Klar, A., Marshall, A. M., Soga, K. & Mair, R. J. (2008). "Tunneling effects on jointed pipelines." *Can. Geotech. J.*, **45**(1), 131–139.

Lilliefors, H. W. (1967). "On the Kolmogorov-Smirnov test for normality with mean and variance unknown." *Journal of the American Statistical Association*, **62(**318), 399-402.

Lake, L. M., Rankin, W. J., & Hawley, J. (1996). *Prediction and effects of ground movements caused by tunnelling in soft ground beneath urban areas*. CIRIA.

Mair, R. J., Taylor, R. N. & Bracegirdle, A. (1993). Subsurface settlement profiles above tunnels in clays." *Géotechnique.* **43**(2), 315-320.

Mair, R. J. & Taylor, R. N. (1997). Bored tunnelling in the urban environment. *Proc. 14th Int. Conf. Soil Mech. Found. Engng, Hamburg*, **4**, 2353–2385.

Marshall, A. (2009). *Tunnelling in sand and its effect on pipelines and piles.* PhD Thesis, Engineering Department, University of Cambridge, UK.

Marshall, A., Farrell, R., Klar, A., & Mair, R. (2012). "Tunnels in sands: the effect of size, depth and volume loss on Greenfield displacements." *Géotechnique*. **62**(5), 385–399.

Martos, F. (1958). “Concerning an approximate equation of the subsidence trough and its time factors.” *Proc. International Strata Control Congress,* Leipzig, 191-205.

O’Reilly, M. P. & New, B. M. (1982). “Settlements above tunnels in the United Kingdom: their magnitude and prediction*.” Proc. Tunnelling ’82, Brighton*, 173–181.

O’Rourke, T. D. (1984). “Manual for assessing the influence of excavations on parallel cast iron gas mains.” *Geotechnical Engineering Rep. 84-3*, School of Civil and Environmental Engineering, Cornell Univ., Ithaca, NY.

O’Rouke, T. D., Jung, J. K. & Argyrou, C. (2015). “Underground Infrastructure Response to Earthquake-Induced Ground Deformation.” *Proc. 6th Int. Conf. on Earthquake Geotech. Eng.* Christchurch.

O'Rourke, T. D. & Kumbhojkar, A. S. (1984). *Field Testing of Cast Iron Pipeline Response to Shallow Trench Construction*. Cornell University.

O’Rourke, T. D., Netravali, A. N., Pendharkar, S. M., Toprak, S., Tonkinson, A., & Chaudhuri, D. (1996). “Evaluating service life of anaerobic joint sealing products and techniques.” *Final Rep. 96/0318,* Gas Research Institute, Chicago.

O’Rourke, T. D., Jezerski, J. M., Olson, N. A., Bonneau, A. L., Palmer, M. C., Stewart, H. E., O’Rourke, M. J., & Abdoun T. (2008). “Geotechnics of pipeline system response to earthquakes*.” Geotech. Earthquake Engng. and Soil Dynamics IV (GEESD),* Sacramento, CA.

O’Rourke, T. D., and Trautmann, C. H. (1980). “Analytical modeling of buried pipeline response to permanent earthquake displacements.” *Rep. 80-4, School of Civil and Environmental Engineering*, Cornell Univ., Ithaca, NY.

Osman, A. S., Mair, R. J., & Bolton, M. D. (2006). “On the kinematics of 2D tunnel collapse in undrained clay.” *Géotechnique*. **56**(9), 585-595.

Peck, R. B. (1969). “Deep excavations and tunnelling in soft ground.” *Proc. 7th Int. Conf. Soil Mech. Found. Engng., Mexico City,* 225–290.

Pipeline Safety and Hazardous Materials Administration [PHMSA]. (2015). Data and Statistics http://www.phmsa.dot.gov/pipeline/library/data-stats (accessed 30 Nov. 2015).

Prior, J. C. (1935). *Investigation of bell and spigot joints in cast-iron water pipes. Part I-Pullout strength. Part II-Bell strength. Part III-Harness strength*, College of Engineering, Ohio State Univ., Columbus, OI.

Rajani (2012) "Nonlinear stress-strain characterization of cast iron used to manufacture pipes for water supply." *J. Eng. Materials and Tech. ASME* **134**(4), 041005.

Rajani, B. & Abdel-Akher, A. (2013). “Performance of cast-iron-pipe bell-spigot joints subjected to overburden pressure and ground movement.” *J. Pipeline Syst. Eng. Pract. ASCE* **4**(2), 98-114.

Schlick, W. J. & Moore, B. A. (1936). “Strength and elastic properties of cast iron in tension, compression, flexure, and combined tension and flexure,” *Bulletin 127*, Iowa Engineering Experiment Station, Ames, IA.

Stewart, H. E., O’Rourke, B. J., O’Rourke, T. D., & New, B.M. (1989). “Evaluation of cast iron pipeline response at excavation crossings.” *Geotechnical Engineering Rep. 89-1*, School of Civil and Environmental Engineering, Cornell Univ., Ithaca, NY.

Taki, H., & O’Rourke, T. D. (1984). “Factors affecting the performance of cast iron pipe.” *Geotechnical Engineering Rep. 84-1*, School of Civil and Environmental Engineering, Cornell Univ., Ithaca, NY.

Taylor, R. N. (1995). “Tunnelling in soft ground in the UK.” *Underground Construction in Soft Ground,* K. Fujita and O. Kusakabe (eds.), Balkema, 123-126.

U.S. Pipe. (2015). *TYTON JOINT pipe-ductile iron*, Birmingham, AL.

Vorster, T. E. B. (2005). *The effects of tunnelling on buried pipes*. PhD thesis, Engineering Department, University of Cambridge, UK.

Vorster, T. E. B., Klar, A., Soga, K. & Mair, R. J. (2005). “Estimating the effects of tunneling on existing pipelines.” *J. Geotech. Geoenviron. Engng* **131(**11), 1399–1410.

Wham, B. P. & O’Rourke, T. D. (2015). “Jointed Pipeline Response to Large Ground Deformation.” *J. Pipeline Syst. Eng. Pract.*, 04015009.

Wham, B. P., Argyrou, C., Bouziou, D., O’Rourke, T. D., Stewart, H. E., and Bond, T. K. (2014). “Jointed pipeline response to Earthquake induced ground deformation.” *Proc., 10th National Conf. on Earthquake Engineering*, Earthquake Engineering Research Institute, Anchorage, AK.

Zhou, B. (2014). *Tunelling-induced ground displacements in sand*. PhD Thesis, Department of Engineering, University of Nottingham, Nottingham, UK.

CHAPTER 5

CONCLUSIONS

This thesis presents research intended to improve the characterization of jointed pipeline response to ground deformation caused by extreme events, such as earthquakes, and by adjacent underground construction with emphasis on tunneling. Whereas previous studies of pipeline response to ground deformation use simplified joint limit states, a distinctive feature of this work is the detailed characterization of pipeline joint response in terms of axial force vs. pullout and moment vs. rotation relationships as well as the identification of limits states for axial and rotational deformation at the joints. The results of full-scale laboratory tests are used to understand in detail jointed pipeline limits states with respect to joint pullout and rotation as well as allowable tensile strains. This thesis reports on three separate, but interrelated research investigations to evaluate the (1) response of jointed DI pipelines commonly used in practice to the effects of large permanent ground movements, (2) performance of biaxially oriented PVCO pipelines under earthquake-induced ground deformation, and (3) performance of CI and DI pipelines subjected to tunneling induced ground movements. The findings of each of these studies are summarized briefly under the subheadings that follow.

5.1.1 Ductile Iron Pipeline Response to Large Ground Deformation

Chapter 2 presents results from 22 pressurized joint rotation tests on 150-mm (6-in.)-diameter DI pipeline specimens with push-on joints that show the relationship among

joint leakage, rotation, and applied moment at various levels of axial displacement. This relationship establishes a pressure boundary for the onset of leakage in DI pipe joints, providing an upper bound on mechanical joint behavior in response to faulting, liquefaction, landslides, mining, dewatering, and construction activities including tunneling.

The test program shows that the mechanical behavior of even a simple push-on joint requires resolution of leakage as a function of both axial pullout and rotation to characterize performance under extreme deformation. In the past, joint behavior has been characterized simply as rotation until metal binding, independent of axial pullout. This type of characterization is overly simplistic, and will yield markedly conservative results.

Although DI push-on joints have limited capacity to accommodate pullout, they have considerable capacity for rotation without leakage, even for axial displacements as high as 70% of the maximum insertion depth. The DI joint is expected to leak at rotations greater than approximately 16° when displaced axially 21 to 41 mm (0.83 to 1.62 in.), providing three times more rotational capacity than the manufacturer's guidelines (e.g., 5° for 150-mm (6-in.) joints). Beyond 38 mm (1.62 in.), the DI joint becomes increasingly more susceptible to deflection-induced leakage, with straight axial pullout occurring at 58 mm (2.3 in.).

When the spigot is fully seated in the bell, the DI push-on joint has substantial capacity to accommodate rotation without leaking. For joint rotation exceeding 16°, however, experimental and FE results show high levels of irrecoverable local

deformation of the spigot. Therefore, a rotational limit of 16° is recommended for joint pullouts between 0 and 20 mm (0.8 in.) to reduce the risk of additional degradation and future leakage.

This study also shows that the pressure boundary is independent of load path. This finding has important practical ramifications because one pressure boundary can be used for many different conditions of ground deformation, thus reducing analytical demand and computational requirements when modeling soil-pipeline interaction.

5.1.2 PVCO Pipeline Performance under Large Ground Deformation

Chapter 3 presents results from an experimental program evaluating material properties and mechanical characteristics of 150-mm (6-in.)-diameter Bionax PVCO water distribution pipelines fitted with mechanical pipe joint restraints. Full-scale tests were conducted to assess the pipeline's ability to accommodate severe ground deformation. Stress-strain characteristics of the PVCO pipe were derived from tensile coupon and internal pressure tests. Axial tensile and compression tests for joints with and without mechanical joint restraints provide axial force-displacement relationships for the joints and predictions of joint failure under extreme loading conditions. Moment-rotation relationships are derived from four-point bending test results offering a characterization of the bending behavior of the pipe and restrained joint.

During a full-scale fault rupture simulation the PVCO pipeline was able to accommodate significant fault movement through axial tensile and bending strains in the pipe in combination with modest levels of axial slip at the restrained joints.

Although the pipeline failed because of stress concentration where the pipe restraint clamps were fastened to the pipe, the axial stress in the pipeline was sufficient to induce relatively large levels of strain (between 1 and 2% at failure) in the low modulus PVCO material.

Overall the pipeline was able to accommodate 206 mm (8.1 in.) of axial extension, corresponding to an average tensile strain of 1.67% along the pipeline. Such extension is large enough to accommodate the great majority of liquefaction-induced lateral ground strains measured by high resolution LiDAR after each of four major earthquakes during the Canterbury Earthquake Sequence in Christchurch, NZ (O'Rourke et al., 2012).

The testing provides a characterization of restrained joint behavior in response to deformations imposed by faulting, liquefaction, landslides, mining, dewatering, and construction activities. The findings are useful in practice for the design and risk assessment of PVCO pipelines subjected to large ground deformation.

5.1.3 Jointed Pipeline Response to Tunneling Induced Ground Deformation

Chapter 4 reports the results of soil/pipeline interaction modeling for vertical and horizontal ground movements caused by tunneling for two cases involving jointed CI and DI pipelines perpendicular to the tunnel centerline that (1) extend beyond the width of the settlement profile and (2) connect through 90° tees with a pipeline parallel to the tunnel. The modeling incorporates the results of large-scale laboratory tests to characterize the axial force vs. displacement and moment vs. rotation relationships of

DI and CI joints commonly encountered in practice. Tunneling induced soil displacement profiles were modeled for a 6.1-m (20-ft) diameter tunnel in clay and sand affecting 150 and 300-mm (6 and 12-in.) diameter CI and 150-mm (6-in.)-diameter DI pipelines. The analytical results are reported for volume losses confined to 5% and 3% of the tunnel cross-section in clay and sand, respectively, to allow for the assumption of no volume loss deformation when modeling soil settlement and horizontal movement. The evaluation of pipeline response on this basis allows for generalizations that guide design and risk assessment and help to identify potential difficulties regarding pipeline integrity.

The limit states for first leakage in lead-caulked CI joints are related to measured deformation, or slip, between the lead and CI surfaces within the joints at approximately 0.5 mm (0.02 in.) of axial pullout and 0.2° of joint rotation, with maximum incipient leakage corresponding to 0.5°. Data for the CI-lead adhesion, C_A, from large-scale pullout tests are shown to follow a normal distribution, thus allowing for the quantification of uncertainty in pullout force and moment to initiate leakage.

The joints display complex behavior in which additional slip and creep of the lead can close off leakage paths that are reopened with further increase in deformation. Thus, the slip and rotation at incipient leakage can be identified, but a clear and consistent trend in leakage after its initiation cannot be quantified with the available experimental evidence.

For jointed CI and DI pipelines that extend beyond the width of the settlement profile, the principal observations and conclusions drawn from the analytical results are:

- For the same tunnel diameter and C/D, the response to tunneling in sand is accompanied by joint rotations and maximum tensile strains that exceed those in clay by a factor as high as two to three for the same centerline settlement and pipe diameter. This difference is related to the narrower settlement profile in sand that generates larger differential settlement and curvatures.
- For the tunneling conditions examined in this work, CI joint rotation at first leakage in clay occurs between 50 and 120 mm (2.0 and 4.8 in.) of centerline settlement, and depends on both the pipe diameter and location of the joints with respect to tunnel centerline. For sand the threshold of incipient leakage is exceeded at centerline settlements on the order of 25 mm (1 in.). These levels of settlement pertain to relatively severe conditions of tunneling with low C/D and apply only for the initiation of leakage, which may involve very small levels losses.
- Allowable tensile strain levels for pit cast iron pipe were not exceeded for centerline settlements in clay as high as 120 mm (4.8 in.), but were exceeded at centerline settlements in sand of approximately 50-100 mm (2-4 in.). Pullout displacements for all cases in clay and sand were below the axial movement associated with initial joint leakage.

- For DI pipelines joint rotations were well under the limits for metal binding and far less than the rotational capacity at first leakage. Joint pullout was minimal, and maximum tensile strains were below yield conditions.

For jointed pipelines, which connect through 90° tees with a pipeline parallel to the tunnel, the principal observations and conclusions drawn from the analytical results are:

- There is high susceptibility to leakage from pullout when CI tees are located between 0.5i and 2i from the tunnel centerline. The maximum tunnel settlements associated with the initiation of leaks are sufficiently low that tee locations within the width of the settlement trough ($\cong$ 2.5i) should be regarded as a potentially high risk situation with respect to the effects of tunneling.
- The largest pullouts for DI pipelines with unrestrained and restrained tees occur at a distance close to the inflection point, i, from the tunnel centerline. Moreover, the largest pullouts occur for restrained tees. Restraining the tee from pullout actually reduces the degrees of freedom available in the branch pipeline to accommodate lateral soil movement.
- The DI tees were examined for combined joint pullout and rotation and compared with the metal binding and pressure boundaries applicable for push-on joints. In every case the combinations of pullout and rotation were below both the metal binding and pressure boundaries, indicating satisfactory performance.
- Pullout will not be a major risk for the great majority of cases involving tunneling beneath DI tees. Some limited cases, however, show pullout on the

order of 70 to 80% of push-on joint pullout capacity. Given the absence of pullout resistance in push-on joints, tees should always be checked as a potential risk with respect to tunneling induced ground deformation.

The observations and conclusions apply for CI and DI pipelines without significant corrosion and material defects. The effects of corrosion and defects are beyond the scope of this work, but should be considered in practical situations. In many cases, water or gas operations personnel are able to identify areas susceptible to corrosion. In all cases the mechanical performance of pipelines without defects provides an essential framework for design and risk assessment.

APPENDIX A

CAST IRON PIPE PULLOUT TEST RESULTS

Estimating CI-lead adhesion strength

Cast iron joint performance has been addressed by several authors through full-scale experiments (CCIJ, 1915; Prior, 1935; Harris & O'Rourke, 1983; O'Rourke et al., 1996) as well as through interpretation of full-scale test results (e.g., Attewell et al., 1986; Finno, 2003; El Hmadi & O'Rourke, 1989; O'Rourke & Trautmann, 1980; Rajani & Adbel-Akher, 2013).

Figure A.1 shows a profile view of a typical CI joint, which connects the spigot and bell ends of adjoining pipes. The annular space between the spigot and bell is packed with hemp or jute yarn, also referred to as oakum, and caulking. Lead and cement are the caulking materials in the great majority of CI joints, with lead used substantially more often than cement. Prior (1935) indicates that the lead caulking depth is typically 57 mm (2.25 in.), while Attewell et al. (1986) suggest depths of 44 to 57 mm (1.75 to 2.5 in.), depending on diameter.

Full-scale experimental results suggest that the axial displacement associated with first slip ranges from about 0.5 to 1.0 mm (0.02 to 0.04 in.), and is representative of the axial pullout necessary to initiate joint leakage for CI joints of both water and gas distribution pipelines (O'Rourke et al., 1996). The expression for joint pullout force at first slip, $F_{j,slip}$, is

$$F_{J,slip} = \pi D_{os} d_L C_A \qquad (A.1)$$

where C_A is the CI-lead adhesion, D_{os} is the outer spigot diameter, and d_L is the lead caulking depth as illustrated in Figure A.1. Through Eqn. A.1 the C_A corresponding to first leakage was calculated from the results of pullout tests under internal water pressure ranging from 140 to 2500 kPa (20 to 360 psi) on 15 specimens of lead caulked CI joints ranging from 150 to 1500 mm (6 to 60 in.) in nominal diameter (Prior, 1935), and two similar specimens of nominal 300-mm (12-in.) diameter CI joints tested under nitrogen pressure of 2.0 kPa (0.29 psi) (O'Rourke et al., 1996). In both sets of tests the lead caulking depth was approximately 57 mm (2.25 in.).

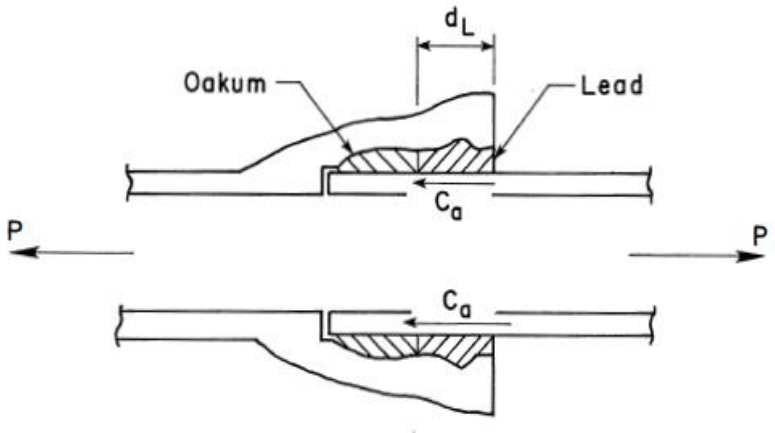

Figure A.1. Lead caulked joint subject to pullout (O'Rourke & Trautmann, 1980)

Figure A.2 shows the data for CI-lead adhesion strength as a function of nominal pipe diameter originally published by O'Rourke & Trautmann (1980) for joint pullout tests performed by Committee on Cast Iron Joints [CCIJ] (1915) and Prior (1935). Figure A.3 shows the same test results interpreted by Rajani and Abdel-Akher (2013) assuming a variable depth of lead caulking. Rajani and Abdel-Akher (2013) suggest

that C_A is a function of pipe diameter, decreasing linearly from 2 to 1.2 MPa (290 to 174 psi) for pipe diameters between 18 and 60 in. due to difficulties in pouring a uniform caulking depth around the circumference of larger diameter pipes.

Figure A.4 shows the CI-lead adhesion, C_A, as a function of pipe diameter for pullout test results used in this study. Pullout tests results reported by CCIJ (1915) were used by O'Rourke & Trautmann (1980) and Rajani and Abdel-Akher (2013), but omitted in this work due to limitations in the presentation of their data and measurement techniques. In addition to the tests reported by Prior (1935), the figure includes two pullout test results reported by O'Rourke et al. (1996) on lead caulked CI joints. Linear regression analysis shows $r^2 = 0.02$, which indicates there is no significant correlation of C_A with pipe diameter. The mean value of C_A=1.63 MPa (0.236 ksi) is indicated in the plot, and represents the best estimate of C_A on average.

Table A.1 provides a summary of the pullout test data from Prior (1935) and O'Rourke et al. (1996) that was used to estimate CI-lead adhesion strength. To address uncertainty in the experimental data the CI-lead adhesion, C_A, is presented in a cumulative frequency plot in Figure A.5. A normal cumulative probability curve, developed from the mean and standard deviation of the data, is also shown in Figure A.5. The Lilliefors (1967) goodness of fit test shows that a normal distribution is verified at the 5% significance level, and thus represents a good fit of the data.

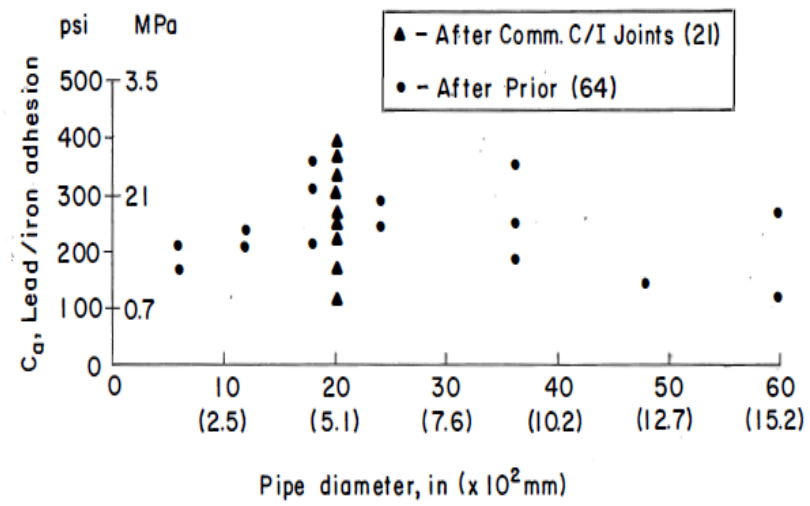

Figure 3.5 Lead-iron adhesion as a function of pipe diameter.

Figure A.2. CI-lead adhesion as a function of pipe diameter (O'Rourke & Trautmann, 1980)

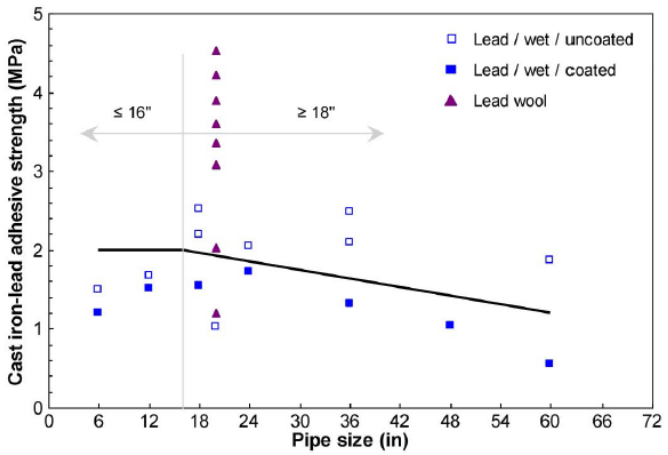

Fig. 8. Variation of cast-iron–lead adhesive strength with pipe size (data from O'Rourke and Trautmann 1980)

Figure A.3. CI-lead adhesive strength, CA, as a function of pipe size [Rajani & Abdel-Akher (2013) with data from O'Rourke & Trautmann (1980)]

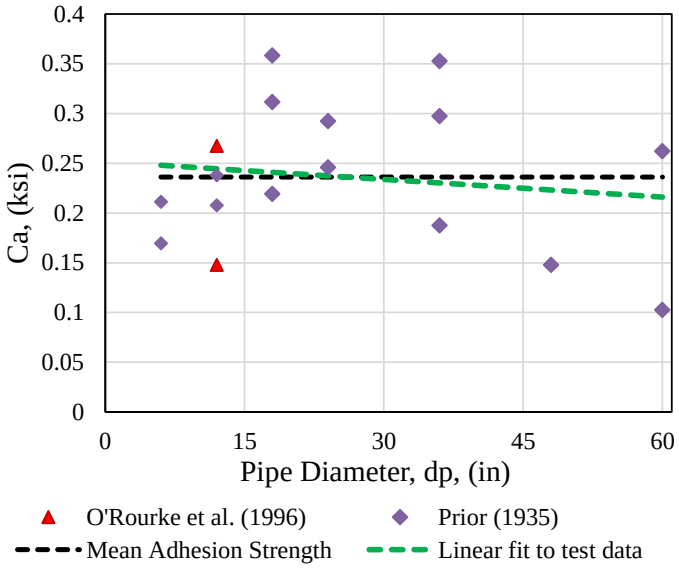

Figure A.4. Summary of cast-iron-lead adhesive strength vs. pipe diameter used in this study

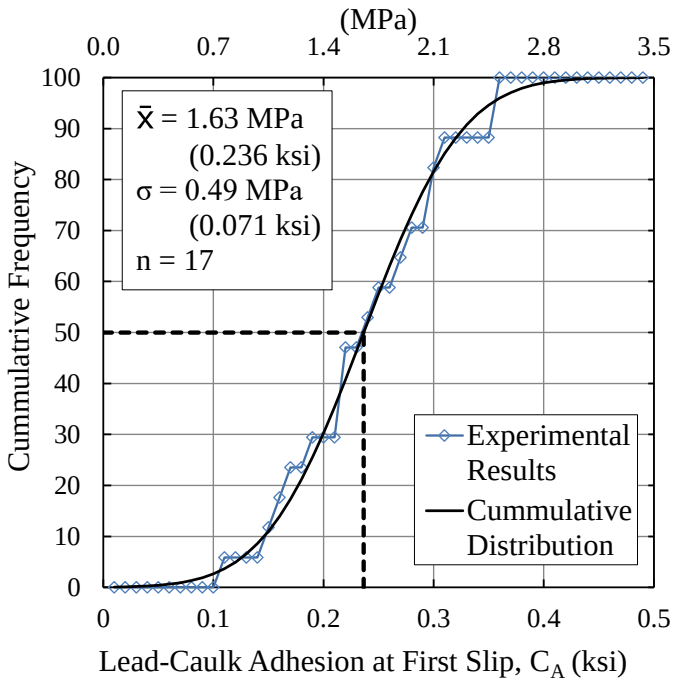

Figure A.5. Summary of available pullout data comparing the cumulative probability of joint slippage relative to force at first joint slippage normalized by pipe circumference.

Table A.1. Summary of joint pullout test results

Nominal Pipe Diameter		Outer Pipe Diameter, D_{os}		Pull Force at First Slip, $F_{j,slip}$		Lead Caulk Adhesive Strength, C_A		Reference
mm	[in.]	mm	[in.]	kN	[kips]	MPa	[ksi]	
150	[6]	180	[7.1]	38	[8.5]	1.17	[0.169]	Prior (1935)
150	[6]	180	[7.1]	47	[10.6]	1.46	[0.211]	Prior (1935)
300	[12]	343	[13.5]	101	[22.7]	1.64	[0.238]	Prior (1935)
300	[12]	343	[13.5]	88	[19.8]	1.43	[0.207]	Prior (1935)
300	[12]	343	[13.5]	63	[14.1]	1.02	[0.148]	O'Rourke et al. (1996)
300	[12]	343	[13.5]	113	[25.5]	1.84	[0.267]	O'Rourke et al. (1996)
450	[18]	505	[19.9]	224	[50.4]	2.47	[0.358]	Prior (1935)
450	[18]	505	[19.9]	195	[43.8]	2.15	[0.311]	Prior (1935)
450	[18]	505	[19.9]	137	[30.8]	1.51	[0.219]	Prior (1935)
600	[24]	668	[26.3]	203	[45.7]	1.69	[0.246]	Prior (1935)
600	[24]	668	[26.3]	242	[54.3]	2.01	[0.292]	Prior (1935)
900	[36]	996	[39.2]	231	[51.9]	1.29	[0.187]	Prior (1935)
900	[36]	996	[39.2]	435	[97.7]	2.43	[0.353]	Prior (1935)
900	[36]	996	[39.2]	367	[82.4]	2.05	[0.297]	Prior (1935)
1200	[48]	1321	[52]	242	[54.3]	1.02	[0.148]	Prior (1935)
1500	[60]	1646	[64.8]	534	[120]	1.81	[0.262]	Prior (1935)
1500	[60]	1646	[64.8]	209	[47]	0.71	[0.103]	Prior (1935)

Cast iron joint pullout characterization

Figure A.6 shows the normalized force vs. displacement plots for five typical pullout tests, including two with internal gas pressure (O'Rourke et al., 1996) and three with internal water pressure (Prior, 1935). The measured axial force is normalized with respect to the pullout force at first slip. Due to limitations of the measuring methods used by Prior (1935), initial joint stiffness data at displacements less than 0.79 mm (0.031 in.) are not reliable. The O'Rourke et al. (1996) pull-out tests offer the most detailed data available for assessing initial joint stiffness and provide the basis for the idealized axial pullout curve shown as a dashed line in the figure. A well-defined break

in the slope of these curves occurs at 0.51 mm (0.02 in.), after which there is variation in the normalized force vs. displacement relationships.

The inset diagram in the figure shows an expanded view of the normalized force vs. axial displacement plots at low levels of movement. There is a clear transition to a flatter slope at about 0.51 mm (0.02 in.). This displacement occurs at the onset of leakage and corresponds to a notable change in the rate at which resistance is mobilized against pullout. This slip between the lead and CI surface generates leakage paths.

Using C_A for various exceedance levels from Figure A.5 and joint geometric characteristics, $F_{j,slip}$ can be determined from Eqn. A.1. Table A.2 summarizes normalized force and axial pullout at CI joints from the most reliable test data identified in this study. These values can be used to define a generalized curve representing axial joint response.

Figure A.7 shows select force-displacement test results for 300-mm (12-in.) CI joints. The dashed lines were developed using Table A.2, and correspond to the mean, 10%, and 90% exceedance levels associated with the normal cumulative distribution of the CI-lead adhesion, C_A, plotted in Figure A.5. The 10% and 90% exceedance levels define a statistical range that helps to quantify the uncertainty associated with the effect of C_A on joint pullout.

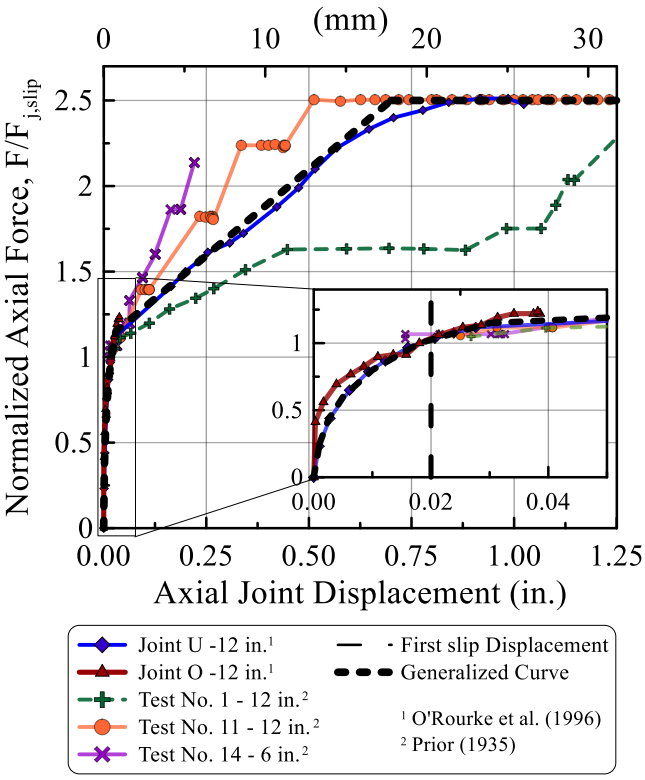

Figure A.6. Normalized joint pullout force vs. axial displacement for lead-caulked CI joints

Table A.2. Summary of normalized pullout force and joint displacement

Force/$F_{j,slip}$		0	0.25	0.43	0.6	0.8	1	1.15	2.5	2.5
Joint displacement	(in)	0	0.001	0.0025	0.005	0.01	0.018	0.03	0.7	2
	(mm)	0	0.025	0.064	0.127	0.25	0.46	0.76	17.78	50.80

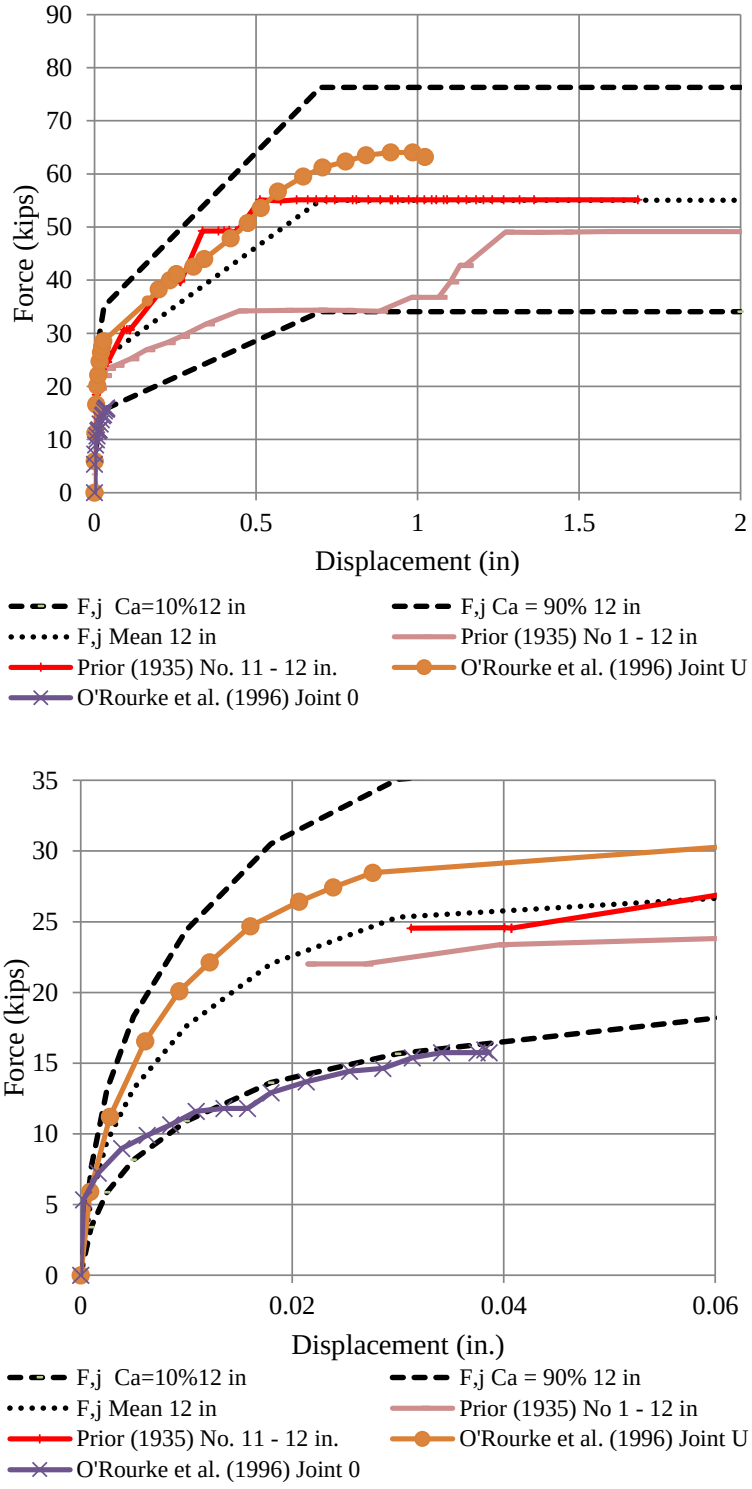

Figure A.7. Force-displacement for 300-mm (12-in.) CI joints including bounding idealized curves

APPENDIX B

CAST IRON PIPE MOMENT-ROTATION TEST RESULTS

Harris and O'Rourke (1983) conducted bending tests on 23 CI joints of 100, 150, and 200 mm (4, 6, and 8 in.) diameter pit-cast grey iron gas mains installed in New York between 1878 and 1914. Figure 4.4 shows a schematic of the four-point bending setup. Figure B.9 shows digitized moment-rotation data from 19 bending tests on CI joints.

Figure 4.5 presents the data from 19 tests on lead-caulked pit CI joints expressed as leakage vs. joint rotation for 10% through 90% exceedance limits. Each plot represents the leakage at which a particular percentage of the test specimens exceeded the leakage rate shown. The total number of specimens involved in the testing is also plotted with respect to rotation. As the rotation increased, some of the tests were discontinued because the loads exceeded levels consistent with safety standards adopted during the tests and a number of pipes fractured, thereby reducing the number of specimens. Figure B.11 plots the raw leakage rate data from individual bending tests relative to joint rotation. The figure indicates the rotation level at which each bending test was discontinued or failed.

Figure B.12 shows the percentage of specimens that failed relative to joint rotation. The total number of specimens involved in the testing is also plotted with respect to rotation. The reduction in sample size reflects experiments that were discontinued prior to failure due to test safety standards. The percentage of failed specimens in the figure

represents the number of CI joints that failed relative to the sample size at different levels of rotation.

There are several aspects of the figures worth noting. First, the onset of leakage occurs at approximately 0.2°, with maximum leakage at approximately 0.5°. There was actually a decline in leakage at all exceedance levels after 0.5°, similar to the reduction in leakage observed in the pullout tests in response to additional deformation of the lead caulking. Leakage eventually increased at large rotations exceeding 3-4° in some of the joints that did not fail. No bell failures were observed until about 0.5°, after which there was a steady increase in the number of failures as rotation increased.

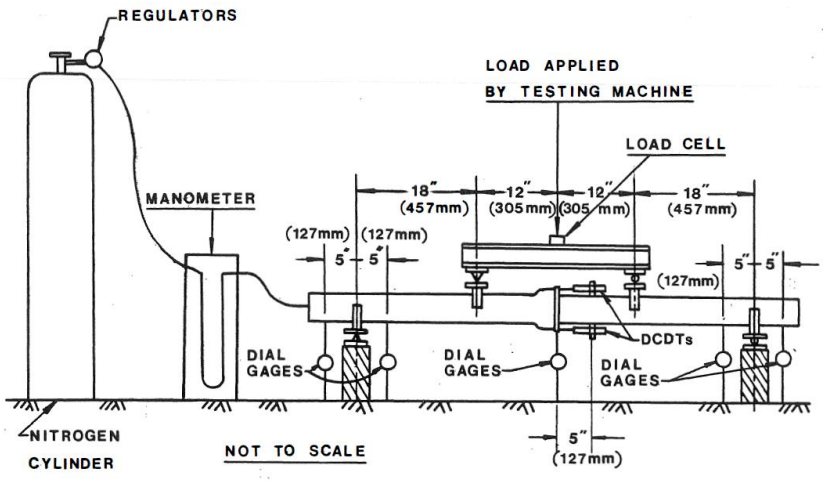

Figure B.8. Illustration of four-point bending test setup (adapted from Harris & O'Rourke, 1983)

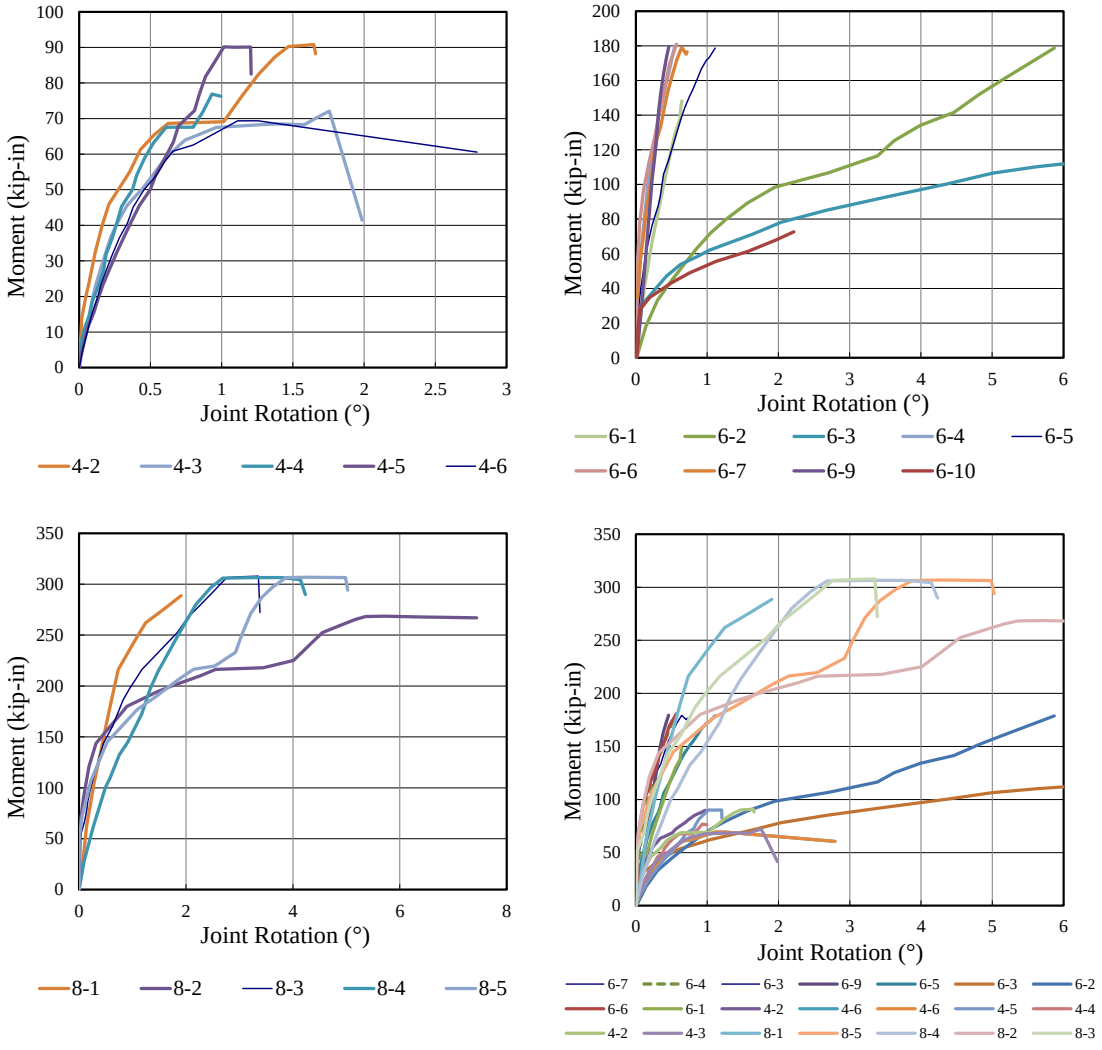

Figure B.9. Moment vs. rotation plots for 100, 150, and 200 mm (4, 6, and 8 in.) CI joints (Harris & O'Rourke, 1983)

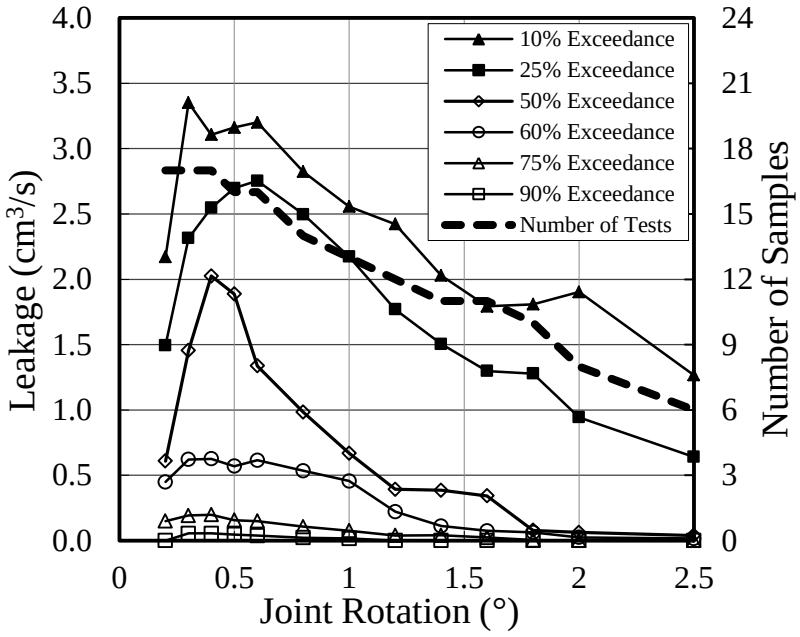

Figure B.10. Leakage rate exceedance levels for 100, 150, and 200-mm (4, 6, and 8-in.) diameter specimens relative to imposed joint rotation

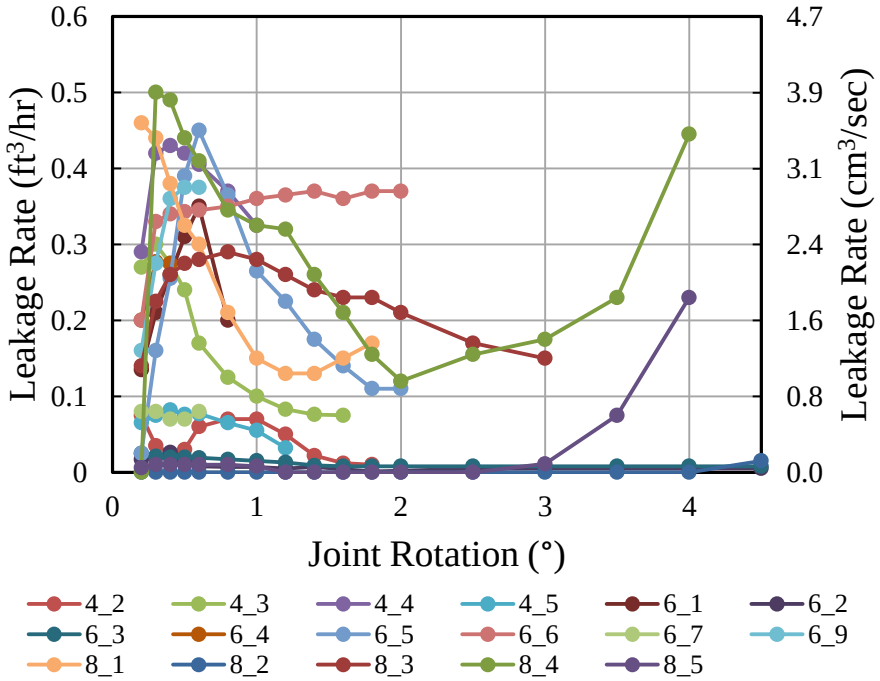

Figure B.11. Leakage rate vs. joint rotation for Harris & O'Rourke (1983) joint bending tests

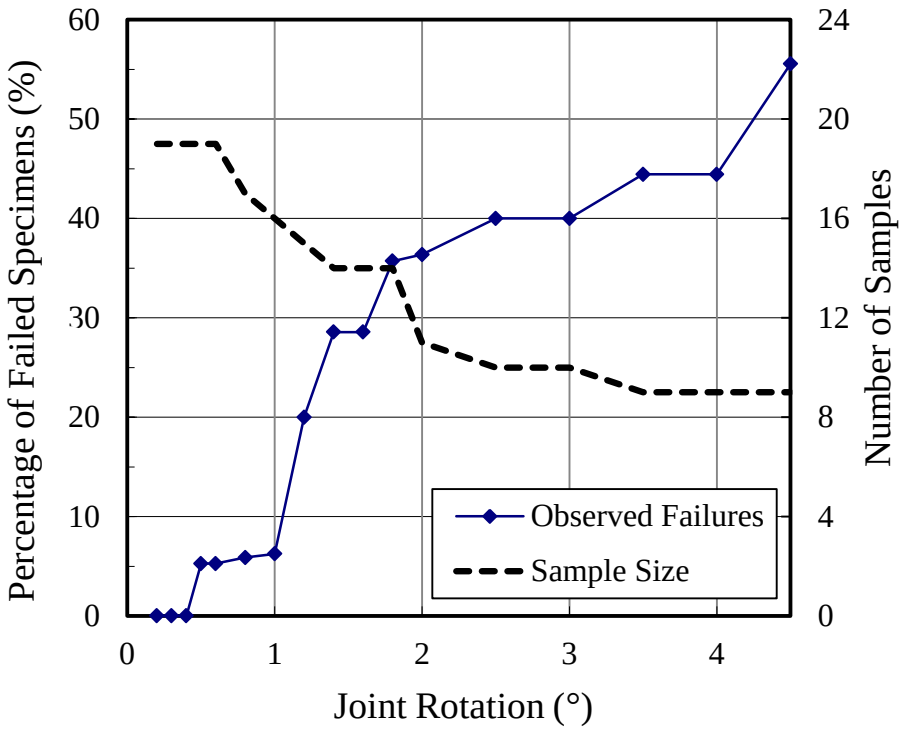

Figure B.12. Observed failure probability of Harris & O'Rourke four-point bending tests

Cast Iron Generalized Moment Rotation

Prior (1935) performed a series of joint rotation tests on AWWA standard Class B, 500-mm (20-in.) diameter CI pipe joints. These test results, along with the Harris & O'Rourke (1983) data, were used by previous authors (e.g., Attewell et al., 1986; Rajani & Abdel-Akher, 2013) to develop generalized, bilinear moment-rotation models for lead-caulked CI joints of various diameters and joint conditions.

O'Rourke & Trautmann (1980) proposed an equation for the moment at first slip between the lead and CI surface, $M_{J,slip}$, in which C_A, d_L, and D_{os} are as defined for Eqn. A.1, as follows

$$M_{J,slip} = \frac{3}{8}\pi D_{os}^2 C_A d_L \qquad (B.2)$$

Using Eqn. B.2 with the mean C_A from Figure A.5 and d_L = 57 mm (2.25 in.), moment vs. rotation plots were developed from four bending tests on nominal 500-mm-diameter CI joints with no internal pressure (Prior, 1935) and nominal 150-mm-diameter CI joints under 3 kPa (0.43 psi) gas pressure (Harris & O'Rourke, 1983), and are shown in Figure B.13. In Figure B.13(a) a change in the normalized moment vs. rotation plots can be identified at about 0.2°. Both O'Rourke & Trautmann (1980) and Rajani & Abdel-Akher (2013) attribute this change in slope to deformation of the lead caulking, related to first slip between the lead and CI surface, that generates leakage.

Figure B.13(b) is an expanded view of the normalized moment vs. rotation plots to 0.6° rotation. The rotation corresponding to a slope reduction in the plots varies between 0.1° and 0.4°. The dashed lines show the trilinear moment vs. rotation relationships for 150 and 500-mm (6 and 20-in.) diameter joints adopted in this work for FE analyses. Initial joint stiffness is given by $k_1 = M_{j,slip}/\theta_1$ where $M_{j,slip}$ is calculated from Eqn. B.2 assuming a mean C_A and d_L = 57 mm (2.25 in.), and θ_1 = 0.2°, the rotation at first slip. As recommended by Rajani & Abdel-Akher (2013), beyond 0.2° of rotation the initial joint stiffness is reduced by 75% for diameters less than 400 mm (16 in.), and 65% for larger diameters. Based on the available test data, this study introduces a third change at 1.0°, reducing the stiffness of the curve to 20% and 12% of the initial stiffness for 500 and 150-mm (20 and 6-in.) diameter joints, respectively.

Figure B.14 shows select force-displacement test results for 150-mm (6-in.) CI joints. Similar to Figure A.7, the dashed lines in the figure correspond to the mean, 10%, and

90% exceedance levels associated with the normal cumulative distribution of the CI-lead adhesion, C_A, plotted in Figure A.5. The 10% and 90% exceedance levels define a statistical range that helps to quantify the uncertainty associated with the effect of C_A on joint pullout.

It should be noted that lead caulked CI joints have a tendency to self-heal after initial leakage. This phenomenon is well documented (CCIPJ, 1915; Maynard & O'Rourke, 1977) and O'Rourke & Trautmann (1980) suggest that it is related, in part, to the oakum behavior. While not likely to occur in dry natural gas lines, in water mains the wet oakum can adjust to change within the annual space between the spigot and bell during deformation, plugging leakage paths. Attewell et al. (1986) pointed out that the laboratory test results were obtained at loading rates that may be substantially faster than occur during tunneling. Thus, the results of the large-scale tests should be regarded as providing a conservative estimate.

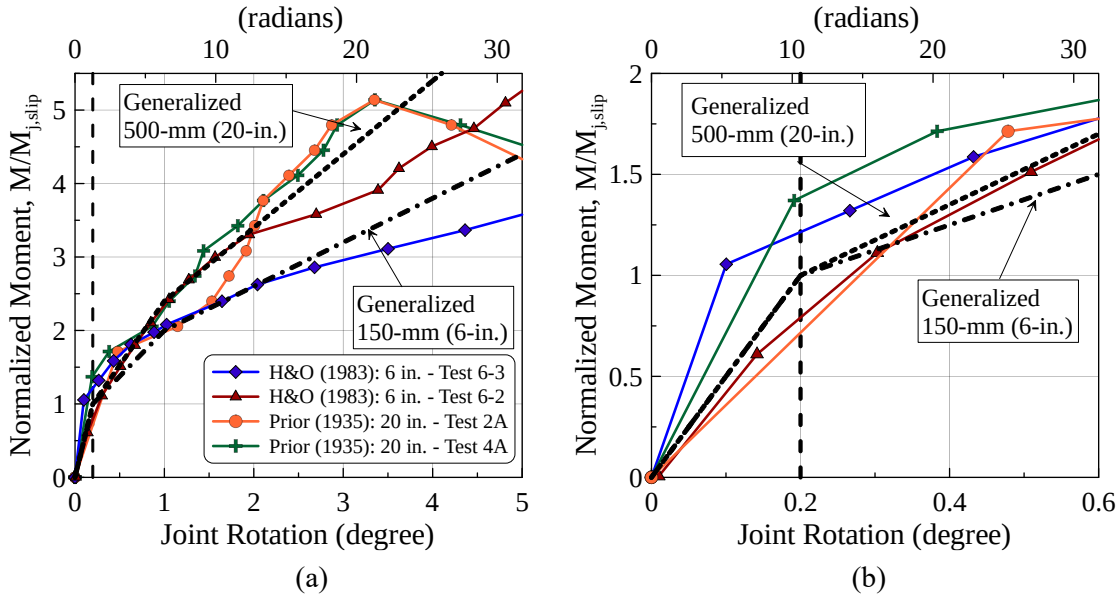

Figure B.13. (a) Normalized moment-rotation relationships for 150 and 500-mm (6 and 20-in.) diameter CI joints and (b) expanded view of rotation at first slip

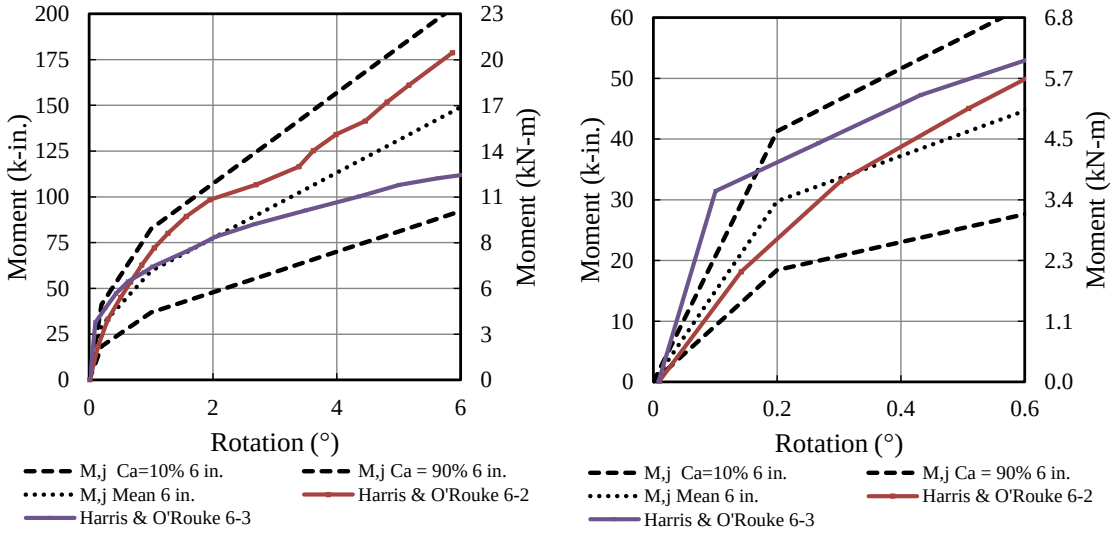

Figure B.14. Moment-rotation results from select 150-mm (6-in.) tests and generalized curves

APPENDIX C

PIPELINE TEES

Various tees, bends, and dead ends are present in water and gas distribution systems. Tees and bends are used to avoid obstacles, change vertical and horizontal position, and make branch connections. Figure C.15 illustrates a branch pipeline that connects through a 90° tee with a pipeline parallel to the longitudinal axis of an underlying tunnel. The parallel pipeline will move with the ground settlement profile, displacing vertically and laterally toward the tunnel centerline. The branch pipeline deformation depends on the settlement profile and lateral soil displacement as well as the pipe and pipe joint characteristics. The interaction between the soil and intersecting pipelines will affect the tee joint (shown in Figure C.15 and Figure C.16) rotation and lateral pullout.

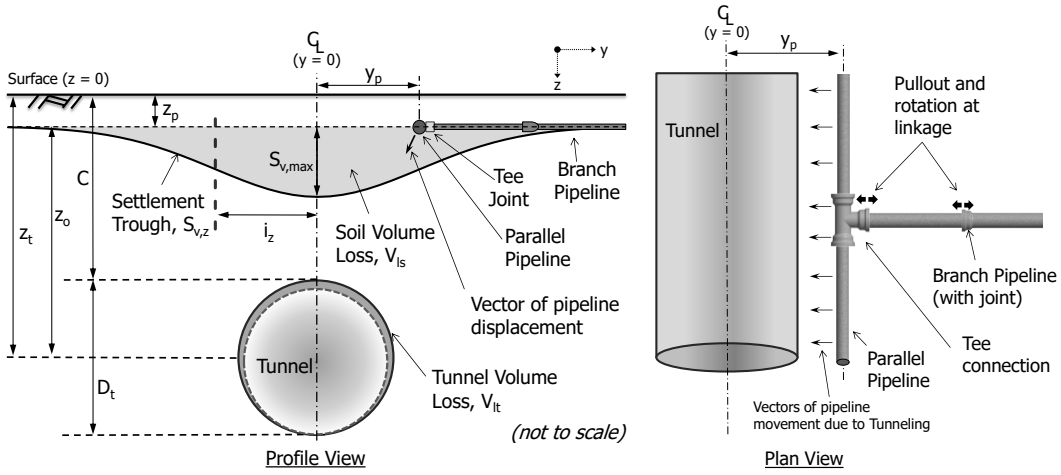

Figure C.15. Illustration of tunnel cross-section, settlement trough and parallel pipeline with tee connection

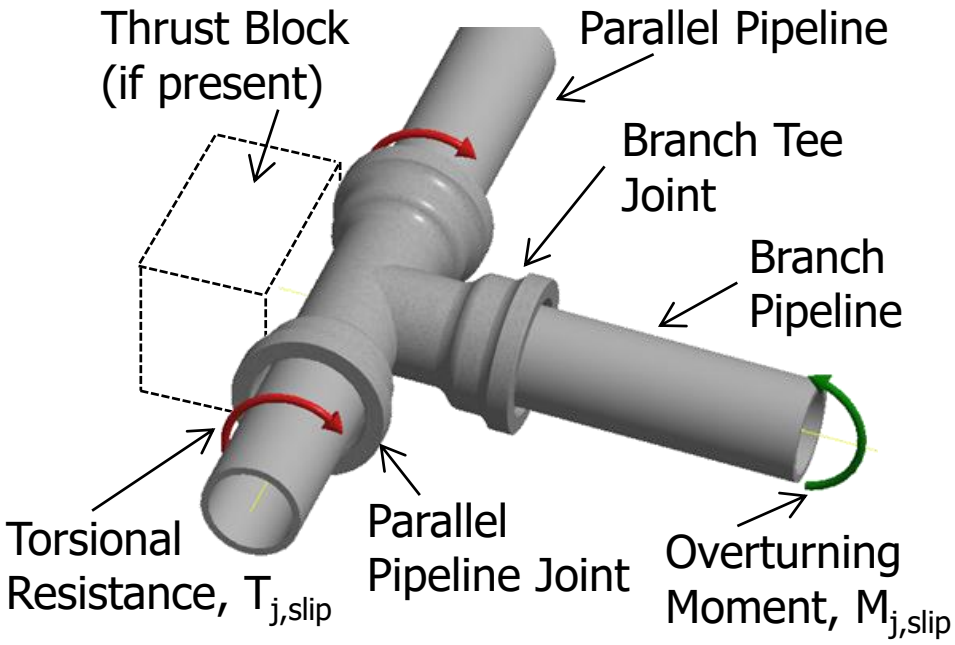

Figure C.16. 3D view of typical CI tee joint

Restrained vs. Unrestrained

To limit joint pullout at these connections due to unbalanced forces from internal pipe pressure, municipalities typically install thrust blocks at the back side of the tee as illustrated in Figure C.17, which is taken from construction drawings used by the Los Angeles Department of Water and Power (LADWP, 2015). A thrust block is commonly constructed of concrete poured into the excavation, filling the distance between the tee and undisturbed soil. When a thrust block and adjoining tee are affected by externally imposed ground deformation, the block will constrain movement of the tee. In particular, the ability of the tee to rotate with respect to branch pipeline will be resisted. Thrust blocks are used in most CI and many DI pipeline networks.

For CI pipelines the tee joints are typically lead or cement caulked. For DI pipelines the tee joints are either push-on or restrained joints. Restrained joints are used for the connection of the branch pipeline, and may or may not be accompanied by a thrust block at the tee. Restrained joints for DI pipe employ insertions and mechanical locking or gripping mechanisms to resist pullout. The details of such joints will vary depending on the pipe manufacturer. These joints provide substantial pullout resistance (Meis et al., 2005) while allowing for rotation to approximately 5° before metal binding (e.g., U.S. Pipe, 2008).

Design guidelines (e.g., DIPRA, 2015) provide procedures for calculating the length of restrained joints or length of pipe imbedded in soil necessary to generate longitudinal friction to resist unbalance pressurization loads. Branch joints lying with in this distance must be restrained from pullout. The number of restrained joints can be calculated based on pipe characteristics (e.g., segment length, size, type, fitting type, and test pressure), ground parameters (e.g., depth of burial, soil type, and trench type), and a selected safely factor. Normally, for pipelines with diameters ≤ 300 mm (12 in.) restrained joints would be used at the tee connection and in some instances at the next joint along the branch pipeline, depending on size and available length of pipeline.

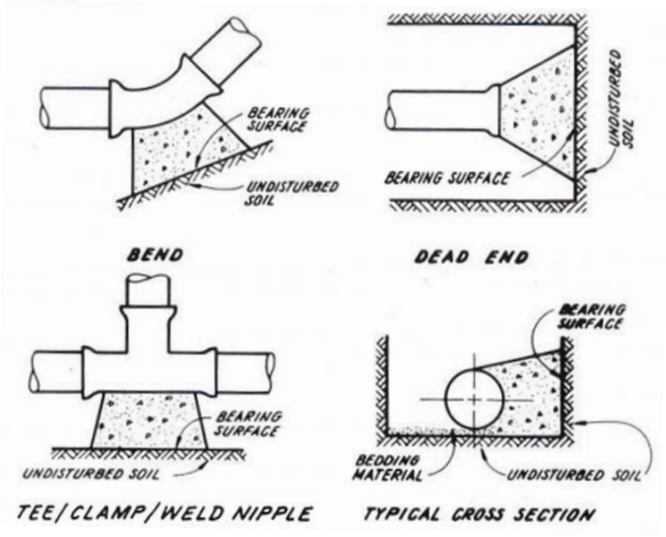

Figure C.17. Examples of thrust blocks (provided by LADWP, 2015)

Tee Rotation

The magnitude of relative rotation between the branch pipeline and tee joint is dependent on the rotational stiffness of the tee joint as well as the capacity of the parallel pipeline tee joints to provide torsional resistance. Figure C.16 illustrates the torsional resistance and overturning moment imposed on the tee in response to tunneling induced ground deformation. Differential settlement of the tee relative to the branch pipeline imposes counter-clock-wise rotation at the tee joint, depicted by the green arrow, activating the rotational stiffness of the joint tee. Torsional stiffness of the parallel pipeline tee joints, shown as red arrows in the figure, provides resistance to tee rotation.

For the CI pipeline the torque necessary to initiate slippage of the two parallel pipeline joints can be estimated based on the lead-cast iron adhesive strength, C_A, and joint geometry as

$$T_{j,slip} = 2\left[\tfrac{1}{2} D_{os} A_j C_A \right] = \pi D_{os}^2 d_L C_A \qquad (C.3)$$

The moment resistance at the tee joint assuming a standard lead-caulk joint can be estimated by

$$M_{J,slip} = \tfrac{3}{8} \pi D_{os}^2 C_A d_L \qquad (C.4)$$

Manipulation of Eqns. C.3 and C.4 shows that $M_{j,slip} = 3/8\ T_{j,slip}$. The calculated torque resistance for the two parallel pipeline tee joints will in general be significantly greater than the tee joint's bending moment at first leakage, suggesting that the tee joint is likely to leak due to rotation prior to rotation of the parallel pipeline joints. Based on this assessment, the CI tee was assumed to remain in a vertical orientation with respect to the adjoining branch connection for the FE simulations. In the FE models, it was assumed that the tee translates vertically and laterally with the soil displacements, but does not rotate during soil-pipeline interaction.

For DI tees there will generally be little torsional or rotational stiffness available at the joints. Given the rotational flexibility of the branch pipeline joint, with little resistance before metal binding at rotation approaching 5°, overturning moments from the branch connection will be very low or absent, and will be resisted by the thrust block when present. The tee, therefore, tends to remain in its initial orientation during tunneling induced ground deformations, thus justifying the assumption that the tee translates vertically and laterally with the soil displacements, but does not rotate during soil-pipeline interaction.

REFERENCES

Ductile Iron Pipe Research Association [DIPRA]. (2015). *Thrust restraint design for ductile iron pipe*. Golden, CO.

Meis, R., Maragakis, M. & Siddharthan, R. (2005). "Dynamic axial stiffness of typical restrained and unrestrained underground pipe joints." *J. of Testing and Evaluation*, 33(6).

U.S. Pipe. (2008). *Restrained joint ductile iron pipe and fittings*, Birmingham, AL.